Proton-Proton Intersecting Storage Accelerator Facility ISABELLE

at the Brookhaven National Laboratory[*]

H. Hahn, M. Month, and R. R. Rau

Brookhaven National Laboratory

Upton, New York 11973

Proton-Proton Intersecting Storage Accelerator Facility ISABELLE

at the Brookhaven National Laboratory

H. Hahn, M. Month, and R. R. Rau

Brookhaven National Laboratory

Upton, New York 11973

ABSTRACT

The intersecting storage accelerator facility ISABELLE which
is proposed for construction at the Brookhaven National Laboratory
is reviewed. ISABELLE would permit the exploration of proton-
proton collisions at center-of-mass energies continuously variable
from 60 to 400 GeV and with luminosities of 10^{32} to 10^{33} $cm^{-2}sec^{-1}$
over the entire energy range. The facility would consist of two
interlaced rings of superconducting magnets, operating at 40 kilo-
gauss, in a common tunnel about 3 km in circumference. The proton
beams would collide at eight intersection regions where particle
detecting systems would be located. Protons of about 30 GeV from
the AGS will be accumulated in each ring to obtain the design cur-
rent of 10 A prior to their acceleration to the final energy. In

this paper the design philosophy underlying the principal design choices, as well as a brief description of the major accelerator systems and the conventional structures, is presented. An overview of the physics potential provided by ISABELLE is then given. The large extension of the center-of-mass energy range combined with the very high luminosity would provide unique possibilities for the investigation of the questions of greatest current interest in particle physics. Arguments, based on the available data and reasonable theoretical concepts, are presented which suggest strongly that the intermediate vector bosons required for a unified weak and electromagnetic field theory should be discovered. They would be studied in detail. The hadron production at high transverse momentum, the energy dependence of the strong interactions and the possible search for new, massive particles is also discussed. The paper concludes with a detailed beam analysis, the various limitations on beam current, the procedures followed in optimizing the luminosity, and a justification of the projected performance levels.

I. INTRODUCTION

In particle physics the parameter of greatest interest is the center of mass (c.m.) energy. This follows naturally from the fact that as higher energies were made available by the ingenuity of the accelerator scientists, new discoveries have tumbled forth in profusion. Around the 1 GeV level experiments at the large synchrocyclotrons showed that the proton-proton total cross section decreased to a minimum, then sharply began to increase. Shortly, a totally new and rich spectroscopy revealed itself when the πp, I=3/2 resonance at 1232 MeV was discovered. At the 3-GeV Brookhaven National Laboratory Cosmotron associated production of strange particles was discovered, and antiprotons were produced at the 6-GeV Bevatron at the Lawrence Berkeley Laboratory. The Brookhaven Alternating Gradient Synchrotron (AGS) and the CERN Proton Synchrotron (PS) continued the line of fundamental discoveries, which in turn called for the larger energies now available at the 400-GeV synchrotron at Fermi National Accelerator Laboratory (FNAL), the 31 x 31 GeV proton-proton Intersecting Storage Rings (ISR) at CERN, and the 400-GeV synchrotron at CERN. The energy "frontier" is of primary interest to experimentalists and theorists alike. The proposal for the construction of a 200 x 200 GeV proton-proton Intersecting Storage Accelerator (ISABELLE, 1976) at the Brookhaven National Laboratory provides a significant step in the c.m. energy beyond that which is presently available.

The concept of colliding beams represents the only practical method of significantly extending the available c.m. energy in man-made proton-proton collisions. The highest energy in the c.m. presently available from an accelerator is provided by the CERN ISR, where the top energy of 31 GeV per beam

produces a total c.m. energy of 62 GeV. For accelerators with stationary targets, the total available energy in the c.m. varies only as the square root of the accelerator energy. On the other hand, for two identical particles colliding head on, the total energy of both particles is available in the reaction: $E_{cm} \simeq 2E$. The importance of colliding beams in providing extremely high c.m. energies can be illustrated by the following numerical comparison. The 400 GeV proton beam at FNAL provides about 28 GeV c.m. energy while head-on collisions of protons each of 200 GeV give 400 GeV c.m. energy. A c.m. energy of 400 GeV would require an 85 TeV fixed target accelerator, clearly beyond the realm of current financial possibility.

Colliding beam devices do have important limitations. They produce far fewer interactions per second than are achieved by a regular accelerator because the particle density in the beams is necessarily far less than that of a stationary target. With colliding beams the luminosity $L(cm^{-2}sec^{-1})$ is the machine parameter which determines the interaction rate as follows: R (interactions/sec) $= \sigma(cm^2) \ L(cm^{-2}sec^{-1})$; σ is the relevant cross section. For comparison note that the luminosity of the CERN ISR has reached $2 \times 10^{31} \ cm^{-2}sec^{-1}$, while a proton beam of the order of 2×10^{12} particles/sec striking a 1-meter liquid hydrogen target has an equivalent luminosity of about $10^{37} \ cm^{-2}sec^{-1}$. Thus the essential features distinguishing colliding beam machines from fixed target accelerators are that the former are optimized for c.m. energy, the latter for the production of secondary particle beams.

Fixed target accelerators and intersecting storage rings differ in other respects as well. In order to be effective in performing colliding beam experiments, a storage ring should not only have good luminosity but also a beam lifetime much longer than the time required to store the beams. In practice, a lifetime of several hours is required, while in a usual accelerator the beam

need live for at most a few seconds. Another important difference is the
close interrelationship required between the design of each experiment and
the storage rings themselves. Since collisions between the circulating beams
occur inside the vacuum chamber, experiments become an integral part of the
machine and must be designed with regard for the specific properties of the beams
and their geometry at the collision points.   Nevertheless, the ex-
tremely large c.m. energy possible with intersecting storage rings remains
an overriding argument in their favor and they must be part of a well-balanced
high energy physics program. Burhop (1963) stated it rather well: "...storage
rings have to be considered as a window on the future..."

The questions of greatest current interest in particle physics demand
the high c.m. energy of ISABELLE. Do the predicted charged and neutral inter-
mediate vector bosons required for a unified weak and electromagnetic field
theory exist? Estimated masses for these particles are in the 40-100 GeV/c^2
range. The consequences for our understanding of particle physics resulting
from either the discovery of these particles or their non-existence in the
mass range below 150 GeV/c^2 will be enormous. Can the strong interaction
also be melded with the other two? Are there new unpredicted heavy particles,
perhaps similar in some way to the J/ψ charm particle family, now being un-
tangled? Does the pp total cross section continue to rise as now seen in
the data from the ISR and FNAL, or does its behavior again change at the
higher ISABELLE energies? These fundamental questions, plus scores of other
less dramatic questions, can be studied. Finally, research at ISABELLE
energies may well pose new questions and find unexpected answers about the
fundamentals of particle physics.

A. Storage Rings - Historical Notes (O'Neill, 1966)

Wideröe (1943) in a patent application in the early 1940's explicitly recognized the advantage of colliding beams to achieve higher c.m. energies. Naturally many physicists understood the simple relativistic fact that with stationary targets and relativistic particles as projectiles the available c.m. energy increases slowly as the square root of the laboratory energy of the particle. At least in principle, colliding beams thus were a simple method of achieving very high c.m. energies. However, two technical problems prevented their realization until the early 1960's. The primary problem was to produce beams with large currents and high particle densities so that a usable reaction rate could be obtained. Second was the need for a very good vacuum so that particle-gas nucleus interactions would not mask particle-particle collisions.

The practical beginning of colliding beam work was in 1956 in the United States when D. W. Kerst (1956a) and the MURA (Midwestern Universities Research Association) group suggested a system of two intersecting fixed field alternating gradient (FFAG) accelerators. Symon and Sessler (1956) proposed a radiofrequency system for "stacking" particles in circular accelerators. Also in 1956, O'Neill suggested storing particles in separate fixed field storage rings for colliding beam experiments.[1] Designs for intersecting FFAG machines were studied in detail by the MURA and CERN groups who concluded that it would be too complex and costly to obtain high energies. The separate storage rings then became the focus for colliding beam physics.

_____

[1]According to O'Neill (1966), W. M. Brobeck of the University of California at Berkeley and D. B. Lichtenberg, R. Newton, and M. Ross of MURA had the idea almost simultaneously with himself.

The first successful demonstration of collisions in storage rings involved electrons and positrons and occurred in 1963. These collisions were between counterrotating 250 MeV positrons and electrons in a single small ring, ADA, built by a group (Touscheck, 1963) from the National Laboratory at Frascati, and the University of Rome. They transported the ring to Orsay, near Paris, in order to use the French 1-GeV electron linear accelerator as an injector. ADA was used solely to demonstrate collisions. A year or so later at Stanford and then at Novosibirsk, U.S.S.R., high energy physics experiments began using dual storage rings with electrons in each ring (O'Neill, 1966). In the following years the single ring electron-positron colliding beam machines multiplied rapidly at several centers -- Frascati, Orsay, Novosibirsk, CEA (Cambridge Electron Accelerator), DESY (Hamburg), and SLAC (Stanford). Currently the highest energy machines are located at SLAC (SPEAR) and at DESY (DORIS) which have a maximum of about 4.5 GeV in each beam. Authorized and under construction are two larger electron-positron storage rings ($\sim$15 x 15 GeV), one at SLAC (PEP), the other at DESY (PETRA). Present plans expect beams in 1979-1980.

In 1960 the CERN group began studying two intersecting storage rings, into which 28 GeV protons from the CERN PS would be injected. After extensive study and research on a model electron ring, the ISR project began construction in 1966 and came into operation in early 1971 (Johnsen, 1973). The ISR remains the only existing proton-proton storage ring facility. The design of ISABELLE has drawn very heavily on the ISR experience and on the expertise of the ISR staff.

B. Origins of ISABELLE

For over five years a strong design and development effort has been underway at Brookhaven directed toward the construction of a 200 x 200 GeV proton-proton intersecting storage accelerator facility, designated ISABELLE (ISABELLE, 1976). Protons of 30 GeV from the presently operating AGS would be accumulated in two interlaced rings (accelerators) prior to their acceleration to 200 GeV. Therefore all c.m. energies from 60 GeV to 400 GeV would be available in eight crossing or intersecting points at very large luminosities, up to 10^{33} $cm^{-2}sec^{-1}$ at top energy. The new technology of superconducting magnets will provide magnetic fields of at least 40 kG, and is crucially important to the performance and cost of ISABELLE.

The 1963 Brookhaven Summer Study (Proceedings, 1963) considered the feasibility of storage rings which were to use the AGS as their injector. Jones (1963) worked out a first parameter list for these colliding beams and pointed out that storage rings of two or three times the circumference of the AGS could be used to accelerate the stacked beams to higher energies.

In late 1970, John Blewett (1971) .revived the idea of building storage rings at Brookhaven. In 1971 an AUI (Associated Universities, Inc.) High Energy Study Committee, chaired by V. L. Fitch of Princeton, recommended that Brookhaven proceed to develop an intersecting storage accelerator with maximum energy around 200 GeV in each ring and based upon superconducting magnet technology. Detailed work on the ISABELLE design began at Brookhaven in May 1971. In addition to the Brookhaven staff efforts, two summer studies and numerous smaller workshops have been held. Scientists from outside the Laboratory have made important contributions to the current mature design. Prototype full-size superconducting magnets have been tested and meet the stringent demands of a proton storage accelerator ring. A proposal

(ISABELLE, 1976) for construction of ISABELLE has been submitted to ERDA

(Energy Research and Development Administration).

In 1974 and 1975 the AEC, then ERDA, through its High Energy Physics

Advisory Panel (HEPAP) formed Subpanels on New Facilities. The 1975 sub-

panel updated the recommendation of the 1974 subpanel and recommended a

national program (Report, 1975) including construction of the positron-

electron colliding beam facility (PEP) at SLAC (Stanford Linear Accelerator

Center) beginning in Fiscal Year 1976, the funding of ISABELLE starting in

FY 1977, and the strong support at FNAL directed toward the long-term goal

of fixed target and/or colliding beam systems of energy in the range of

1000 GeV and higher.

This paper reviews the status of the design for ISABELLE, and the physics

potential opened up by the proposed machine. Since the ongoing research and

development effort is apt to result in improvements on the engineering and

hardware level of the machine, emphasis will be placed here on the underlying

conceptual basis. A general overview is obtained by reading Sections II and

III containing the design philosophy and a brief description of the machine.

The physics potential covering the production of charged and neutral inter-

mediate vector bosons, the hadron production at high transverse momentum,

searches for new, massive particles, and the energy dependence of the strong

interactions is discussed in Section IV. Finally, the dynamics of the proton

beams during the various phases of injection, stacking, acceleration, storing,

and the justification for the performance levels predicted are presented in

Section V.

II. DESIGN PHILOSOPHY

A. Basic Design Criteria

Although a dozen or so electron-positron and electron-electron storage rings have been built or are presently under construction, only one proton-proton colliding beam machine, the CERN ISR, has been constructed and used successfully for experiments. The conceptual design adopted for the proposed proton-proton storage accelerator facility ISABELLE, therefore, draws extensively upon the ISR experience in order to improve the performance potential with due regard to minimizing the construction and operating costs. The basic design criteria for pp colliding beam machines are the available energy, the event rate or luminosity, the signal-to-noise ratio or radiation background, adequate space for detecting equipment, and flexibility of the experimental insertion layout. Essential to the ISABELLE design is the application of superconducting magnets.

Extending the colliding beam principle in proton machines to higher energies is not expected to encounter fundamental limitations. Roughly, for a given magnetic field strength the circumference of the rings scales linearly with laboratory energy and the construction cost increases correspondingly. The strong expectation for the existence of the intermediate vector boson, W, with a mass of 40 to 100 GeV/c^2 suggests a threshold c.m. energy which the next generation of accelerators must exceed. With at least 400 GeV ISABELLE is comfortably above this predicted threshold and stays within the financial scope for the projected national high-energy physics program. Clearly, not all significant experiments would demand the highest energies, and in fact, it is of considerable importance that a new machine has an energy band which overlaps those of existing machines. ISABELLE has been designed so as to be

capable of covering the entire energy range from 60 GeV available at the ISR to 400 GeV in the c.m. system with high interaction rates.

It was recognized very early in accelerator history that head-on collisions of particles are more efficient in yielding high c.m. energies than particles bombarding a target at rest. The square of the c.m. energy, $s = E_{cm}^2$, is in general expressed by

$$s = (E_1 + E_2)^2 - (\underset{\sim}{p}_1 + \underset{\sim}{p}_2)^2 \tag{2.1}$$

with E the total energy and $\underset{\sim}{p}$ the momentum vector of the particle in the laboratory system. Introducing the rest mass m of the particle and the usual kinematic variables $\gamma = E/mc^2$ and $\beta = v/c$ one obtains

$$s = m_1^2 c^4 + m_2^2 c^4 + 2m_1 m_2 \gamma_1 \gamma_2 c^4 (1 + \beta_1 \beta_2 \cos \alpha) \tag{2.2}$$

where α is the crossing angle between the beams. Considering the relativistic limit only, one finds for the case of one particle at rest $(\gamma_2 = 1)$,

$$E_{cm} \approx (2E_1 m_2 c^2)^{\frac{1}{2}} \tag{2.3}$$

whereas for both particles in motion

$$E_{cm} \approx 2 (E_1 E_2)^{\frac{1}{2}} \cos \tfrac{1}{2} \alpha . \tag{2.4}$$

In colliding beams, the available energy increases linearly with the energy of the particles rather than with the square root. A fixed target accelerator with 100 GeV c.m. energy would be in the multi-TeV range and probably represents the practical limit of what can be achieved. The energy range beyond this is the domain of colliding beam devices.

Acceleration of the stacked high-current beam is an essential part of the ISABELLE concept. Availability of the AGS as an injector is the historical reason for this solution. However, in the course of the design study it became clear that low-energy injection and acceleration to higher energies results in several advantages which render this approach technically superior to direct stacking at the desired high energy. Since ISABELLE is designed to accommodate the full current throughout the entire energy range from 30 to 200 GeV, the luminosity varies only with the effective beam height and thus the square root of energy, permitting comparatively high luminosities at lower energies. In contrast, the luminosity

of an aperture-limited machine, that is, one designed for stacking at full energy, is $\gamma^{5/2}$. A further argument in favor of accelerating the proton beam stems from the operating characteristics of superconducting magnets which need a safety margin against quenching.[2] Heating of the superconducting coil reduces the critical current and can lead to a transition to the normal state. The margin against quenching is several degrees (or roughly 10 mJ/cm^3) at 30 GeV, whereas at 200 GeV it is about one degree (or about 1 mJ/cm^3). If low energy stacking is used, it is clear that significantly larger beam losses are tolerable during injection, where losses are most likely.

In the field of particle physics, the available c.m. energy is of foremost importance, but the luminosity and thus the interaction rate is of crucial importance. At the CERN ISR a luminosity of over 2×10^{31} cm^{-2}sec^{-1} has been reached (Gourber, 1975) and plans for further improvements using a special insertion region with near-zero crossing angle, low-beta and vanishing momentum

---

[2] Quenching is the transition from the superconducting to the normal (non-superconducting) state.

dispersion at the intersection point have been formulated (Montague, 1974).
Employing similar concepts for the experimental insertions would permit
luminosities in the range from 10^{32} to 10^{33} $cm^{-2}sec^{-1}$ in ISABELLE at each
crossing region. With the total pp cross section of about 40 mb, a lumin-
osity of 10^{33} $cm^{-2}sec^{-1}$ results in a total event rate of 40 MHz.

Performing experiments on a storage ring must take into account the close
interrelationship between the design of each experiment and the constraints
imposed by the machine. Since collisions between the circulating protons
occur inside the vacuum chamber, experiments essentially become an integral part
of the machine. They must take into consideration the detailed characteristics
as well as the constraints imposed by the geometry of the machine. Of
paramount concern to the experimenter is the length of the free space around the
crossing region available for the particle detecting apparatus. The CERN ISR
provides 17 m of field-free straight sections around the crossing point. More
space is needed with the higher energies at ISABELLE and 40 m was adopted.
Inherent to the experimental insertion design is the considerable flexibility
in changing the beam optics in order to accommodate different experimental requirements
However, it was thought prudent to retain initially the option of operating with high
symmetry which is characteristic of the operating synchrotrons, and also the CERN
ISR until recently (Gourber, 1975). Each of the two ISABELLE rings has the con-
figuration of a circle divided into octants by eight geometrically equal inser-
tions. Simplicity of the insertion design is assured by an arrangement with the
two rings in the same horizontal plane, as at the CERN ISR.

The AGS is an ideal source of protons for injection into ISABELLE. It
is capable of delivering 10^{13} protons per pulse at an energy of up to 30 GeV.
When used as an injector, the AGS would be tuned for the greatest beam bright-
ness, which is achieved by operating the AGS at lower than peak intensity,

about 5×10^{12} protons per pulse. In order to accumulate the desired current of 10 A in ISABELLE, beam stacking in momentum phase space (Symon, 1956) as used at the CERN ISR is undoubtedly the most efficient procedure. Stacking can be done in the rings directly or in a separate intermediate storage ring (Schnell, 1975a; Month, 1977). The latter suggestion has many advantages, including a large reduction in the impedance constraints on the main ring imposed by longitudinal instabilities. A third ring could be part of a future improvement program.

In order to be effective in performing colliding beam experiments, a storage ring should have a long beam lifetime. In practice, the beams should last for several hours. Fundamentally, the lifetime will be limited by the desired beam-beam interaction in the crossing regions. In ISABELLE, for example, with seven insertions each having a luminosity of 10^{32} $cm^{-2}sec^{-1}$ and one a luminosity of 10^{33} $cm^{-2}sec^{-1}$ the beam-beam interaction rate causes $\dot{I}/I \approx 10^{-5}$ min^{-1} which is a lifetime of more than 1000 hours. However, the beam lifetime in a real machine will be shortened by various scattering processes, especially the multiple Coulomb scattering of particles off each other (intrabeam scattering). In addition, anomalous beam loss from nonlinear resonance excitation due to beam-beam space charge forces (Bryant, 1974) and from electron-proton transverse instabilities (Schnell, 1975b) have been observed at the CERN ISR. Such beam losses provide background particles, some of which reach the experimental equipment. This background represents a crucial performance parameter and every effort must be made to minimize it.

Electron storage rings are operated with bunched beams so as to continuously accelerate in order to compensate the synchrotron radiation losses. In proton storage rings, one has the option of running with bunched or unbunched beams. The CERN ISR employs coasting beams; even acceleration of the beams from 26 to 31 GeV is performed on unbunched beams using the phase displacement technique

(Henrichsen, 1974). The possibility of operating ISABELLE with bunched beams has been investigated (Month, 1974a). It became clear that coasting-beam and bunched-beam storage rings are basically different machines requiring different design criteria. The main conclusion was that it is not feasible to operate a high-luminosity, long lifetime storage facility with colliding bunched proton beams. There is also the uncertainty regarding the question of beam loss and resulting radiation background. Following the ISR, ISABELLE will provide collisions with unbunched beams.

B. Optimization of Luminosity

The performance of a storage ring is primarily equated to the luminosity at each intersection. Assuming unbunched beams which are crossing in the horizontal plane and colliding at an angle such that they are well separated at the ends of the magnet-free crossing region, the luminosity is given approximately by

$$L \approx \frac{1}{\pi^{\frac{1}{2}} e^2 c} \frac{I^2}{\sigma_v \alpha} \, , \qquad (2.5)$$

where I is the stored current in each ring, α the crossing angle, and σ_v the vertical rms beam half height at the collision point. The luminosity is a function of the beam parameters (current and transverse emittance) as well as machine parameters (crossing angle and betatron amplitude function at the collision point). The above equation suggests how to maximize the luminosity: decrease the crossing angle, decrease the vertical beam height (implying a smaller emittance and/or beta-function) and increase the circulating beam current. Naturally there are limitations on the variation of each of these parameters. The limitations may be fundamental in nature or dictated by hardware

and thus by economical considerations. An optimized design in which the more severe limits are reached simultaneously is obtained by trial and then only after many iterations. Performance optimization will be discussed in depth in Section V. Simplifying arguments are given here as an introduction to a complex subject.

The beam-beam interaction is thought to be a fundamental limitation on luminosity. When a particle of one beam crosses the other beam, it is subject to electromagnetic forces which modify its dynamical behavior. The forces are highly nonlinear; however, the linear betatron tune shift is a measure of the strength of the beam-beam interaction (Keil, 1974a),

$$\Delta \nu_{bb} \approx \frac{\sqrt{2} r_p}{\pi^{\frac{1}{2}} ec} \frac{I \beta^*}{\gamma \sigma_v \alpha} \tag{2.6}$$

where β^* is the vertical betatron amplitude function, r_p the classical proton radius.   It has been observed at the ISR that beam loss rate and experimental background increase with the beam-beam tune shift (Bryant, 1974). In a rough sense, it can be expected that an optimal mode of operation would be to maximize the luminosity for fixed beam-beam tune shift. To see the implications of this reasoning, one writes the luminosity in the form (Keil, 1974b)

$$L \approx \frac{1}{\sqrt{2} er_p} \frac{\gamma I}{\beta^*} \Delta \nu_{bb} \quad . \tag{2.7}$$

For a given current, it is clearly advantageous to operate with low-beta insertions. The smallest value of β^* that is achievable depends upon the length of the free space required for experimental equipment. In fact, it is not the

small beta itself, but the resulting high-beta value at the first insertion quadrupole which causes concern, $\beta_{max} \approx \ell^2/\beta^*$ with 2ℓ the magnet-free space around the crossing point. One factor which limits the value of β_{max} is that the beam size must be contained within the aperture of the focusing quadrupole. Another is related to the momentum aperture available for beam stacking. In general, high performance proton-proton storage rings require a large momentum aperture since large currents are built up by accumulating many small momentum bites. However, the presence of insertions with high values of β_{max} diminishes the width of the available momentum aperture. The chromaticity of the machine (i.e., the tune variation with momentum) is increased by the low-beta insertions and must be corrected by the addition of strong sextupole magnets which implies an intrinsically nonlinear machine with a limited momentum aperture (Chasman, 1975). Finally, a third limiting factor on the maximum beta value is related to the construction and placement tolerances of the quadrupoles, which become more difficult as the local beta values increase. In ISABELLE the smallest value of β^* is 1 m, which at 10 A and 200 GeV yields a beam-beam limited luminosity of 3×10^{33} $cm^{-2}sec^{-1}$, taking $\Delta\nu_{bb} \approx 5 \times 10^{-3}$, which is considered to be the maximum acceptable beam-beam tune shift in proton-proton storage rings.

Under standard operating conditions in ISABELLE, the beam-beam limit will not be reached and, at maximum current, the luminosity can be optimized by reducing the crossing angle and the vertical beam size at the crossing point.

Reduction of the crossing angle is limited for various reasons. As the crossing angle is decreased, the interaction region or effective target size becomes longer. Thus α is limited by the acceptance of the experimental apparatus. In a practical design, the natural crossing angle is determined simply by the insertion length and the separation of the rings. The standard crossing

angle in ISABELLE is about 11 mrad. A reduction of this value can be obtained at the expense of bending magnets common to both rings resulting in a shortened magnet-free space.

Reduction of the beam size is limited by two considerations. One arises from the intrinsic nature of the beam itself (the emittance ϵ), the other from the linear focusing properties of the storage ring (the betatron amplitude function β, which is a function of position along the central orbit). For a machine constructed in a horizontal plane in order to avoid vertical momentum dispersion, the rms beam half height at the crossing point may be written as

$$\sigma_v = \tfrac{1}{2}(\epsilon_v \beta^*/\pi)^{\tfrac{1}{2}} \ . \tag{2.8}$$

In an ideal machine the normalized emittance $E_{v,h} = \beta\gamma\epsilon_{v,h}$ (with β and γ the usual relativistic variables) is an invariant characteristic of the beam (Courant, 1958). This automatically implies an increase of luminosity with the square root of the energy. The transverse emittance of the beam in ISABELLE is determined by the conditions of the AGS. With proper tuning of the AGS an invariant emittance of $E_v = E_h \approx 20 \ \pi \ \mu m \cdot rad$ can be expected. The beam size at the crossing point is compressed by the use of low-beta insertions. As discussed above, one can achieve values for β^* of the order of a meter, implying beam sizes in ISABELLE of a few tenths of a millimeter at the crossing point.

Increasing the beam current is clearly the most efficient way to provide higher luminosities. In proton machines there are several limiting phenomena, none of which is clearly more important than all the others. There are limits imposed by phase-space arguments, by collective effects, and by technical considerations. For a given vacuum chamber or momentum aperture, the phase-space density of the injected beam sets an upper limit on the current that can be accumulated ,

$$I \leq ec \ \Delta p \ (N/A)_b \qquad\qquad (2.9)$$

where Δp is the available momentum aperture and $(N/A)_b$ is the number of pro-

tons divided by the longitudinal phase-space per AGS bunch. With 5×10^{11}

protons in 1 eV·sec per AGS bunch and assuming no dilution during stacking,

one can accumulate about 15 A in a momentum space of 0.7%, available in

ISABELLE at injection. This means that a dilution during stacking by a

factor of 1.5 will still allow the design current of 10 A. In principle,

it is possible to obtain higher currents by stacking in the transverse phase

space, but since this also increases the beam size and is a rather inefficient

process, potential gain from this procedure is uncertain.

A limitation on the beam current results from the single-beam space charge

forces at high beam intensities (Laslett, 1967). The space charge forces cause

a tune shift which depends on the position of the particle in the beam and thus

indirectly on its momentum. In the case of a bunched beam the periodic syn-

chrotron motion of particles results in a periodic oscillation of their tune.

This effect has been estimated for the various operational phases of the ISA-

BELLE cycle (Chao, 1975) and leads to tune migration on the order of $\sim$0.03 for

particles of largest synchrotron amplitude. With the particular choice of

operating tune, enough tune space exists so that potentially harmful nonlinear

resonances can be avoided (Gareyte, 1975). In general, a tune shift also

results from image effects in the vacuum chamber and iron shield. Although

the image effects vanish on the axis due to the circular symmetry, particles

on off-axis orbits during injection and stacking experience a tune shift which

could be appreciable for orbits near the vacuum chamber wall. This results

in a limit on the fraction of the vacuum chamber aperture which is available for

stacking. Since, however, the dominant consequences will be to alter the working

line, such effects can be corrected to some extent by the magnetic working line correction system.

Current limitations also result from coherent instabilities which arise because of the electromagnetic interaction between collective beam oscillation modes of the circulating beam with the surrounding structures. These phenomena, including, for example, the transverse resistive wall instability (Laslett, 1965), and the related brickwall effect at the CERN ISR (Month, 1973a) lead to a threshold current above which the beam becomes unstable. Fortunately coherent instabilities can be controlled in a number of ways since, in practice, it is impossible to design a machine without sources of instabilities. Landau damping resulting from a spread in frequency of the particles participating in the incipient oscillation mode is a very important stabilizing mechanism (Jackson, 1960; Hereward, 1965). Coherent oscillations which are not stabilized in this way can be controlled by external feedback loops. However, there are technical constraints imposed by the bandwidth of the feedback system which restrict this approach to the lower mode numbers. The coherent longitudinal instability in the microwave region is an example where external feedback is impractical (Schnell, 1975a). In this latter case, the appropriate stability criterion is written as a limit on the longitudinal coupling impedance. In the ISABELLE cycle the worst condition exists during the stacking of the individual AGS pulse and results in the requirement that the coupling impedance divided by mode number not exceed a few ohms, which is a severe, but manageable, design constraint on the hardware. A more detailed treatment of the instabilities limiting the current in ISABELLE will be found in Section V of this paper.

Besides the more fundamental limitations, there are technical difficulties imposing a practical design constraint on the current. One of these is given by the energy stored in the beam which must be disposed of safely in the beam dump. In emergency cases, the beams must be ejected in one turn (few microseconds) creating problems of local heating and stress. The use of a beam absorber system consisting of a sequence of materials with increasing density seems to be capable of handling the 20 MJ stored in each ISABELLE beam. In addition, particularly in superconducting machines, the beam power deposited in the magnets can represent a heat load on the cryogenic system or cause quenching of the magnets. A beam lifetime of 5 hours is equivalent to a heat load of 1 kW or a potential heat deposition in the magnets of up to 1 W/m. It is therefore essential to operate with stable beams, having lifetimes of well over one day.

Perhaps the most stringent current limitation in proton storage rings is set by the beam-induced pressure rise (Calder, 1974). Qualitatively, this effect is due to the circulating beam ionizing residual gas molecules which are then propelled to the vacuum chamber walls by the electrostatic potential of the beam. The incident ions desorb molecules from the wall surface resulting in an exponential pressure rise at a sufficiently large current. The critical current I_{cr} depends on the chamber geometry and the desorption coefficient η approximately according to

$$\eta I_{cr} = \frac{(2\pi)^{5/2} e}{3\sigma} \frac{r^3}{L^2} \left(\frac{R_G T}{M}\right)^{\frac{1}{2}} \tag{2.10}$$

where r is the radius of the circular vacuum chamber, L the distance between pumps (i.e., the magnet length in superconducting machines), M the molar mass (the critical molecule is CO), T the absolute temperature, σ the ionizing cross

section, and R_G the gas constant. The desorption coefficient depends on the energy of the incoming ion and the state of the surface. Properly cleaned and baked surfaces exhibit $\eta \leq 3$, a value tolerable in ISABELLE. The current limit imposed by the "pressure bump" phenomena translates then into a requirement on the vacuum chamber aperture, in the case of ISABELLE about 8 cm. As it turns out, this value is well matched to the other aperture requirements imposed by injection, magnetic field quality, coherent instabilities, etc. The ISABELLE design incorporates a warm vacuum chamber similar to that of the ISR. The possible advantages and problems associated with a cold vacuum chamber are not sufficiently well understood to consider it at present for a high current colliding beam machine (Halama, 1975). The impending experiments involving a cold vacuum section in the ISR will contribute significantly to the understanding of this question.

C. Superconducting Magnet Technology

The construction of the next generation of proton storage rings or accelerators will have to be based on the use of superconducting magnets. This choice is dictated by considerations of the desired performance potential as well as the economic pressure to minimize energy consumption. The preceding discussion of the current limitations indicates that most limitations due to collective effects become more stringent for a machine with a large circumference and small vacuum chamber aperture. Superconducting magnets are beneficial on both accounts. Operation at fields of at least 40 kG can be reliably assumed for superconducting dipoles as compared with the 12 kG of the CERN ISR bending magnets. The higher field reduces the machine radius by a factor of more than two as compared to a conventional machine of equal maximum energy. Superconductors allow very much higher current densities resulting in magnet designs

where the coils are smaller and close to the useful magnetic field region. This implies that the vacuum chamber diameter can be increased with a resulting linear increase in cost, whereas for conventional magnets, the cost rises more rapidly with increasing magnet gap. As a result, operation of large-gap conventional magnets is prohibitive in terms of the electric power consumption, while economically designed (narrow-gap) conventional magnets limit the luminosity of storage accelerators, otherwise comparable to ISABELLE, to values about an order of magnitude below the present design value.

The use of superconducting magnets requires a low-temperature environment. Costs for the required dewar, refrigerator and liquid helium distribution system are offset by savings due to the smaller tunnel diameter, less vacuum equipment, and other field-dependent items. A comparison of ISABELLE with a low-luminosity conventional magnet machine shows that the initial capital expenditures may be roughly equal. However, there is an economic advantage during the operation of a superconducting machine which results from the fact that the electric power consumption is lower by more than a factor of three. Thus, performance and economic considerations both dictate the use of superconducting magnets.

The magnet system providing the bending and focusing of the beam in storage rings is similar to that of a conventional synchrotron but requires control of the field with considerably higher accuracy in order to avoid beam diffusion and thus beam loss and poor performance. The use of separated-function lattices, where bending dipoles and focusing quadrupoles are distinct, is advantageous with superconducting components mainly because of the resulting symmetry of the forces, smaller iron saturation effects, and lower peak fields in the magnets. The added benefit of operational flexibility by having control over the betatron tune is essential for a storage ring, in which the insertions will be modified to accommodate varying experimental needs.

The first significant high-field superconducting magnet material was reported in 1961 (Kunzler, 1961), half a century after the discovery of the superconducting state. Three basic physical properties are required of super-conductors for high-field applications, high critical temperature T_c, high upper critical field B_{c2}, and a high critical current density J_c. The first two of these critical parameters, T_c and B_{c2}, are intrinsic properties of the atomic structure of the material, whereas the critical current is dependent on the metallurgical state of the material (Dew-Hughes, 1971). Practical superconducting materials can be divided into two groups: the ductile solid solution alloys, e.g., NbTi (Coffey, 1965) and the relatively brittle inter-metallic compounds mainly of the A15 structure, e.g., Nb_3Sn (Kunzler, 1961). The high ductility, low stress sensitivity and simple heat treatment cycles have made niobium titanium the only superconducting material commercially available and suitable for magnet design in the immediate future. The most widely used material in the United States is Nb-60 at % Ti (Strauss, 1976) having a critical temperature of $T_c = 9.3$ K and an upper critical field of $B_{c2} = 140$ kG at 0 K.

In type II superconductors subjected to strong magnetic fields, it is energetically more favorable for magnetic flux to penetrate into the bulk of the conductor giving rise to a rather complicated magnetic flux line or vor-tex structure. If, in addition to the shielding currents in the vortices, the conductor carries transport currents, then a Lorentz force on the flux lines results. Unless pinned by some mechanism, the flux lines will move causing energy dissipation and a flux flow resistance. Pinning results from any lat-tice defects such as dislocations found in heavily cold worked materials, or from impurities and second phase precipitations; "hard" superconductors are metallurgically dirty. If the pinning is sufficiently strong, vortex motion

can be made small enough so that the superconductor acts very much like a perfect superconductor. The critical current is usually defined as that current which produces a detectable voltage across the specimen (typical effective resistivity $\rho \approx 10^{-12}$ Ω cm). The variation of the critical current with temperature and magnetic field is not easily parameterized (Fig. 1). Models have been suggested which qualitatively describe the dependence (1) on magnetic field (Kim, 1963)

$$J_c(B) \approx J_o B_o/(B + B_o) \qquad (2.11)$$

where J_o is the critical density at zero field and B_o coincides approximately with the thermodynamic critical field of the material, and (2) on the temperature (Duchateau, 1975)

$$J_c(T) \approx J_{cb} \left[1 - (T - T_b)/\tau_c\right] \qquad (2.12)$$

where J_{cb} is the critical density at the helium bath temperature T_b and $\tau_c = - J_{cb}/(\partial J_c/\partial T)_b$. Modern conductors are capable of sustaining a critical current of up to 200 kA/cm^2 at 4.2 K and 40 kG in the superconducting material.

Early superconducting magnets, with few exceptions, were plagued by irregular or unstable performance characterized by "degradation" (failure to reach the current or field expected from tests on short samples of the conductor) and "training" (diminishing degradation after each successive transition to the normal state). The first of these related phenomena, premature quenching, is now largely understood and is attributed to the process of "flux jumping," i.e., sudden discontinuous field changes accompanied by rapid heating as flux moves in the conductor. Flux jumps are typically initiated by a temperature rise of the superconductor resulting from a release of mechanical stress energy, from radiation heating, or during pulsing. Stabilization

of superconductors involves various techniques which reduce magnetic diffusivity by adding high-conductivity normal materials, improve cooling of the superconductor, and provide sufficient heat capacity locally from helium in intimate contact with the superconductor (Wilson, 1976). A full understanding of training has proven more elusive, and all high field superconducting magnets will suffer from it to some extent. It is in large measure attributed to conductor motion due to electromagnetic forces, but appears to have other causes as well. Rigid clamping of the superconductor at helium temperatures is the best antidote currently available.

One of the more significant steps towards the development of stable superconducting magnets was the appearance of intrinsically stable multi-filamentary conductors, an outgrowth of the concept of adiabatic stabilization which requires the diameter of the superconductor to be smaller than a critical value given by (Wilson, 1970)

$$d \approx (\mu_o^{-1} C_s \tau_c)^{\frac{1}{2}}/J_{cb} \qquad (2.13)$$

where C_s is the heat capacity per unit volume, μ_o is the permeability of free space, and the other quantities as previously defined. A typical value for niobium titanium is $d \approx 40$ μm. Intrinsically stable multifilamentary conductors are available in the form of a twisted composite wire containing many hundreds or even thousands of superconducting filaments embedded in a high conductivity normal copper matrix. The filament diameter, however, is chosen not solely to ensure flux-jump stability, but rather to minimize power losses under pulsed conditions as well as remanent magnetization effects at low field levels (Duchateau, 1974). The filaments have to be twisted in order to avoid electrical coupling by the metal matrix in a changing magnetic field.

A practical requirement on the superconductor is imposed by the need for high currents to prevent excessive voltages during pulsing. Suitable conductors, capable of several thousand amperes, have been developed in the form of twisted cables (Thomas, 1974) or fully transposed braids containing up to one hundred multifilamentary composite wires (McInturff, 1972). An important advance was made through the discovery at Brookhaven of the exceptional stable magnet performance realized by bonding the individual uninsulated twisted multifilamentary wires in the braid (or cable) with a secondary matrix of a soft metal, such as indium or tin, through a series of metallurgical steps. Such a conductor possesses enhanced heat capacity and thermal conductivity, has excellent mechanical stability, and is quite insensitive to wire motion. It may be thought of as an "intrinsically" stable cable analogous to the multifilamentary composite wire, where now the transposed multicore wires in a soft metal matrix play the role of individual twisted filaments in a pure metal matrix.

A number of different technical solutions to building superconducting magnets have been suggested. The stable and reliable magnets for ISABELLE result from the use of cold iron and of a single layer coil, with a cos-theta current distribution. Experience with superconducting magnets points to the requirement for complete mechanical stability together with good provisions for cooling of the superconducting coils in order to assure stable and training-free operation. Cold iron and a single layer coil present a simple design for providing adequate mechanical support. Iron close to the field producing coils has the additional advantage of increasing the magnetic field at a given current and of decreasing the stored energy at operating conditions. A small stored energy is desirable in case of a magnet quench.

The single-layer coil design of the ISABELLE magnet entails a good thermal coupling between neighboring conductors and nearly isotropic quench propagation. Operation of a large system is simplified if a magnet is capable of absorbing its own stored energy. A quench protection system will have to be provided in order to prevent energy exchange between magnets during a magnet quench.

One of the most important considerations in the magnet design comes from the requirements on the quality and reproducibility of the magnetic field. Systematic errors, affecting the field quality equally in all magnets, cause nonlinear effects in the beam. In simple terms, the tolerance on the uniformity of the dipole field is given as $\Delta B/B \leq 2 \times 10^{-5}$ and of the quadrupole gradient $\Delta G/G \leq 10^{-3}$ over the good field aperture, about 8 cm, of the magnets. The cos-theta coil configuration with six blocks per quadrant in the dipole is in principle sufficient to produce the required field shape; in quadrupoles a three-block coil configuration is adequate. Errors in the magnet field shape are caused by iron saturation effects at high field levels or diamagnetic currents within the superconducting filaments at low field levels. Furthermore, eddy currents in the vacuum chamber or the superconducting braid may cause field changes during pulsing of the magnets. Precision control of the field will necessitate various correction coils. Providing complete control over the magnetic field will be one of the major functions of the computer control system.

The efficient design of superconducting magnets requires the presence of current carrying coils close to the vacuum chamber aperture. This has the effect of making the magnetic field within the magnet aperture sensitive to the errors in positioning the coil blocks (Month, 1976). Because particles

traveling on paths lying close to the error source would be subject to sub-
stantial random errors, only a fraction of the coil aperture is useful in
practice. For example, random dipole errors cause displacement of the closed
orbit, necessitating a design tolerance of $\Delta B/B \leq 2 \times 10^{-4}$ rms. These toler-
ances can be met if the position of the coil blocks is held to an accuracy
of 50 μm rms, which is attainable with suitable magnet fabrication techniques.
In practice, effective field errors resulting from misalignment of magnets
will be equally or more important than construction errors. It will be neces-
sary to position the quadrupoles to within 0.25 mm rms and the dipoles to within
0.5 mrad rms in angle. The closed orbit correction system has been designed
so as to achieve a residual error of a few mm. However, particular care will
be directed at the crossing points where the small beam size necessitates ver-
tical closed orbit control of better than 0.03 mm.

It is pointed out above that only a fraction of the full coil aperture
(12 cm in ISABELLE) exhibits the good field qualities as required for storage
rings. The vacuum chamber aperture (8 cm) covers the good field region. The
remaining space is used for correction coils and superinsulation, allowing
the stainless steel vacuum chamber to be operated at room temperature without
paying an economical penalty.

A program to develop superconducting magnets for high energy physics
applications has been going on at Brookhaven (Dahl, 1976) and other labora-
tories (Reardon, 1976) for over a decade. Although relatively new, the
superconducting magnet technology has advanced to the point where the per-
formance of magnets in regard to peak field and field quality can be predicted
with an accuracy equal to that for conventional magnets. Recently, several
full-sized ISABELLE dipole and quadrupole magnets have been fabricated and
tested. A dipole has been successfully operated using a forced circulation

refrigeration system, which produced subcooled helium at supercritical pressures as proposed for the storage accelerator. The 4¼ m-long dipole has reached a maximum central field of 49 kG (McInturff, 1976), safely above the design field of 40 kG. A quadrupole of similar design achieved a gradient of 7.1 kG/cm compared to the design value of 5.4 kG/cm. The performance of these full-size prototype magnets provides the proof that our design concept is valid for ISABELLE ring magnets.

III. DESCRIPTION OF ISABELLE

A. Overview

The proton-proton storage accelerator facility ISABELLE would consist of two interlaced magnet rings providing counterrotating proton beams, each with an energy between 30 GeV and 200 GeV, thus providing a c.m. energy of 400 GeV. The two rings are magnetically uncoupled to allow operation with unequal energies in the rings. In Fig. 2, the location of the ISABELLE AGS complex on the Brookhaven site is shown.

The configuration of ISABELLE is essentially a circle broken by eight symmetrically placed insertions where the beam lines cross. The circumference of each ring is 2.960 km, exactly 3-2/3 times the circumference of the AGS. Almost 1/3 of the circumference is contained in the eight straight sections, each of 116 m length. The beams cross horizontally at the center of the straight sections. A sketch of the ISABELLE rings, with the experimental halls, is shown in Fig. 3. The geometries and sizes of the seven experimental halls vary widely, reflecting different needs of particular classes of experiments. Sketches with dimensions of three typical halls are given in Fig. 4.

The two interlaced magnet rings are located side by side in a common tunnel. The ring separation is 80 cm from magnet center to magnet center. A cross section of the ISABELLE tunnel is shown in Fig. 5. The horseshoe-like structure has a width of 4.2 m and is 3 m high. The tunnel will be covered with 5 m of sand for the radiation shielding. In addition, a muon shield will extend 80 m radially in the plane of the rings (Stevens, 1976).

B. Beam Transfer, Stacking, and Acceleration System

The protons of about 30 GeV would be provided to the ISABELLE rings from the AGS. The method of momentum stacking used at the CERN ISR has been adopted to fill the rings because it permits optimizing AGS performance to obtain high stacking efficiency, requires no costly modifications or additions to the AGS, and imposes no excessive aperture requirements.

Preparing for injection, the peak rf voltage in the AGS is reduced from 386 kV to approximately 36 kV in order to match the AGS bunch shape to the buckets of the ISABELLE stacking rf system. The latter operates at the same frequency as the AGS (4.45 MHz, 12th harmonic in AGS, 44th harmonic in ISABELLE).

The AGS intensity is reduced from the nominal 10^{13} protons to 5.2×10^{12} in 11 bunches to optimize phase-space density. The 11 bunches are injected into one-fourth of the ISABELLE circumference and then are accelerated through about 1.8% in energy, slowly debunched, and deposited in the stacking orbit. This procedure is repeated approximately 120 times, giving a total stacked beam of 6.2×10^{14} protons or 10 A. The beam transport system from the AGS will have conventional magnets; this does not impose a large power load because the system needs to be energized only during the stacking process.

Assuming a transverse beam emittance of 20 π μrad·m (normalized) or 0.64 π μrad·m at 29.4 GeV, a longitudinal phase-space area of 1 eV·sec per bunch, a longitudinal phase-space dilution factor of 1.5 during stacking (based on extrapolation from experience at the CERN ISR), the stacked debunched beam will have a momentum spread of $\Delta p/p = 0.7\%$, and its maximum dimensions in the regular lattice structure will be 22 mm horizontally, 10 mm vertically. The aperture subdivision during the stacking process is shown in Fig. 6.

To prevent the development of instabilities during the stacking process and in the stack after it is formed, coupling impedances between the beam and the vacuum chamber and rf system must be kept low. The most severe requirements arise for the single injected pulse on its way into the stack. To prevent self-bunching and phase-space dilution, the longitudinal coupling impedance Z/n must be kept below about 5 Ω for high mode numbers n, corresponding to frequencies in the GHz region, and below about 25 Ω at the stacking rf frequency (n = 44). This will be achieved by an appropriate feedback system for the rf system and careful design to minimize discontinuities of the vacuum chamber.

Transverse coherent instabilities, induced by the resistive component in the transverse coupling impedance, can be suppressed by Landau damping if the tune spread in the 10 A stacked beam exceeds $\Delta\nu \approx 0.02$.

In order to accelerate the stacked beam, it will be rebunched by an rf system operating at the second harmonic, f = 202 kHz. A peak rf voltage of 40 kV per ring will be provided by four ferrite loaded cavities. The total rf power requirements of this system is 1.25 MW per ring. The dynamic impedance seen by the beam will be kept below a Z/n = 25 Ω per cavity.

Adiabatic rebunching of the beam can, in principle, be accomplished without significant phase-space dilution or loss of beam. As long as the Z/n < 5 Ω criterion for very large values of n is maintained during the accelerating cycle, the bunched beam will also be stable for those modes. Stability at the lower frequencies can be achieved by feedback, if it should be required.

Because of the large stored energy in the beams (about 20 MJ) and the high specific density of the beams at 200 GeV (typically 10 A within a beam cross section of a few square millimeters) major damage could be incurred if

the beam would exit from the ring vacuum chamber in an uncontrolled fashion either due to orbit perturbations or due to beam growth as a result of beam instabilities. For this reason, a fast protective extraction system will be incorporated capable of extracting the beam in the time of one revolution, about 10 μsec. It will direct the beam to an external dump absorber and defocus the beam to reduce the energy density. The absorber will be beryllium, 2.5 m long, followed by iron to spread the beam energy sufficiently to avoid damage to the absorber. An internal dump absorber will be added for redundancy to give a second level of protection for vacuum tank and magnets. In case of failure of the primary system the beam will hit the internal absorber, which can be replaced easily, and damage will be localized there.

C. Lattice Structure

The separated function lattice structure is designed to have quasi-eight-fold symmetry. The layout of the magnets in one octant is shown in Fig. 7. The main portion of the bending is done in 56 regular FODO cells, 7 per octant. A small part of the bending is performed in the three modified cells adjacent to the insertion, 1½ on each side. These cells are the same as the regular bending cells in terms of their focusing structure. The bending magnets, however, are arranged so that the beams begin to converge towards each other heading for the proper collision point. Furthermore, the bending is designed such that the dispersion function is brought to zero in both inner and outer arc configurations. The collisions take place at the center of the insertion where there is ±20 m of free space provided for experimental apparatus. This free space is ended by quadrupoles and then there is another large free space of almost 30 m which will be available to some extent for experimental apparatus. These straight sections will also be used for equipment needed for various machine functions, such as, injection, ejection, rf systems, and special beam diagnostics.

The small crossing angle of 11.4 mrad implies that at a distance of 20 m from the collision point, where the first magnetic element is encountered by the beam, the beams are separated by 22.8 cm. To allow the rings to be magnetically independent, we must be able to interpose two separate quadrupoles in this small space. This can be accomplished by using long, low gradient quadrupoles with a minimum of both superconducting coil and iron shielding and by placing the corresponding quadrupoles of the two rings in a common dewar.

The beams in the two rings are counterrotating in essentially separate vacuum chambers of 8 cm aperture. However, the focusing structure causes wide fluctuations in beam size as the particles traverse their cycles around the rings. The variation in beam size follows directly from the betatron amplitude function and the dispersion functions depicted in Fig. 8. The arrangement of the two rings in a common horizontal plane eliminates all vertical dispersion and thus leads to the smallest vertical beam size at the crossing point.

The ISABELLE operational procedure maintains the standard 8-fold symmetry during stacking and acceleration. After an initial phase where collisions take place with the standard 8-fold symmetry, operation will shift to a reduced symmetry mode. Although under such conditions the momentum aperture is reduced, there is also a corresponding reduction in the aperture required since a substantial fraction of the aperture is needed at injection for the purposes of stacking and bunching for acceleration. The focusing arrangement in the insertions, consisting of two quadrupole pairs, allows changeover from the standard into "low" and "high" beta configurations solely by quadrupole tuning, i.e., requiring no quadrupole movements. To reach the design luminosity of 10^{33} $cm^{-2}sec^{-1}$, large aperture bending magnets as sketched in Fig. 9 are required to reduce the crossing angle from its standard value of 11.4 mrad to 4.8 mrad. If a very short interaction length (small target area) were needed,

an arrangement similar to that shown in Fig. 9, but with a different magnet

configuration, could produce a crossing angle of 50 mrad and an interaction length

of ±2 cm. A reduction of the free space to ±2.5 m would be a consequence.

D. The Magnet and Refrigeration System

The magnet system will be superconducting because of the enhanced

performance and reduced electric power consumption possible with this ap-

proach. The lattice structure assumes dipole magnets which are 4¼ m in

length and operate at 40 kG to achieve 200 GeV beam energy. The regular

quadrupole magnets are about 1½ m in length, and would operate with a

gradient of 5.4 kG/cm. There would be a total of 528 dipoles (of which 80

are special magnets in the matching sections) and 432 quadrupoles (of which

128 are special quadrupoles in the experimental insertions) in the two rings.

The smallest unit of the regular magnet lattice is represented by a

half-cell consisting of two dipoles and one quadrupole as shown in Fig. 10.

Each magnet of the inner and outer ring will be contained in its own dewar.

This configuration has the advantage that all vacuum joints are directly

accessible for leak tests at room temperature and that the position of each

magnet is separately adjustable. Dipoles and quadrupoles are in series elec-

trically. In order to minimize heat loads, the leads between all magnets of

each octant are kept cold. In this arrangement the magnet current can be

chosen to meet other conditions. In the dipole 3.3 kA at full field was

selected so as to keep voltages induced during a quench within tolerable

bounds. However, for the purpose of magnet protection during a quench, it is

necessary to provide protective current leads which are connected to shunting

diodes. Since these leads are not required to operate continuously, they can

be designed for lower steady-state current carrying capacity (about 1 kA) but

large heat capacity (Güsewell, 1970). Each quadrupole has a separately powered

auxiliary quadrupole "trim" coil winding to correct differences between dipole

and quadrupole iron saturation behavior at high fields and to provide a 10%

tune variation flexibility.

The magnets proper are supported inside evacuated tanks which provide

the thermal insulation for the helium cooling system (Fig. 11). Helium flows

through the magnets and through header pipes which also run inside the magnet

tanks taking advantage of the magnet thermal insulation. The magnet tanks

are supported on jacks and are adjustable horizontally as well as vertically.

The jacks rest on stands attached to the tunnel floor. The magnet coil and

core are mounted inside the vacuum tank by supports having low heat conducti-

vity. The stainless steel tube containing the core laminations is wrapped with

superinsulation. First an inner blanket is formed of about 10 sheets of aluminized

mylar. Surrounding the inner blanket is a copper heat shield attached to the helium

return pipe which operates a few degrees above the magnet temperature. Outside the

shield is another 5 cm of superinsulation, consisting of about 100 sheets of alumin-

ized mylar interspersed with polyester spacer sheets. The insulation around the

warm bore vacuum chamber must withstand baking to 300°C and will utilize aluminized

kapton without spacer material.

Dipoles and quadrupoles are very similar in design, both using a circular

cosine coil configuration. Figure 12 shows the cross section of the two mag-

nets. A cutaway dipole magnet in isometric projection is shown in Fig. 13.

The conductor arrangement in the magnets approximating ideal cosine current

distributions is depicted in Fig. 14. The dipole uses six current blocks per

quadrant, containing 19, 18, 16, 13, 9, and 5 turns of a wide braid arranged

in a single layer. The quadrupole uses a conductor arrangement with three

current blocks per octant, containing 17, 14, and 8 turns, respectively. The

conductors are spread over their block areas by inserting spacer braids of copper wire in order to minimize the peak field (the two-dimensional peak field in the coil aperture is 4% higher and the peak field at the ends 6% higher than the central field in the dipoles). Exact positioning of the blocks is determined in such a way as to suppress the lowest field harmonics. The ends of the coil blocks are displaced axially with respect to each other so as to correct the total field integral seen by a beam passing through the coil end (Mills, 1973).

The current blocks are built up with a single layer of wide flat braid (bare dimensions about 1.7 cm x 0.06 cm). The braid consists of 97 twisted composite wires, 0.3 mm in diameter, each containing 517 superconducting NbTi filaments of 10 μm diameter. The braid is fully locked and has a transposition length of about 11 cm and a packing density of 71%. The $4\frac{1}{4}$ m magnets require 90 kg of superconducting wire each, in 1400 m of braid. The braid is filled with Sn-3 wt% Ag solder to give mechanical rigidity and electrical stability. The wires in the braid have a 0.01 mm thick Cu-10 wt% Ni jacket to increase the coupling resistance between wires and decrease eddy current effects.

Dipoles and quadrupoles will have additional windings to correct for deviations from the required magnet field shape and to provide control over the "working line" in the betatron tune diagram (Parzen, 1975). There will be provided an equilibrium orbit coil system consisting of vertical and horizontal dipole windings in the quadrupoles to correct random errors caused primarily by misalignment of the quadrupoles, rotation of dipoles, and random errors in the effective length of the dipoles. A field correction system consisting of sextupole and decapole windings in the dipoles will ensure a flat

dipole field in spite of systematic errors resulting from iron saturation effects at high field level, as well as superconductor magnetization and eddy current effects due to changing fields at low field levels. Control over the working line is obtained by sextu-, octu-, deca-, duodecapole windings in the regular quadrupoles. Skew quadrupoles are provided in the insertion quadrupoles to decouple horizontal and vertical motion.

The iron shield, or core, of the magnet provides mechanical constraint preventing the coil members from moving due to the magnetic forces and, as an integral part of the construction, will also be at helium temperature. In addition, it largely determines the dimensional accuracy of the coil with respect to longitudinal straightness and angular twist. The iron laminations, stamped as 1.25 mm thick washers from low-carbon steel (vitrenamel), are contained within an accurately machined heavy wall stainless steel tube. The lamination length of the dipole is 4.15 m and that of the quadrupole 1.5 m. Overall the dipole magnet, including iron core, weighs about 6300 kg. The small clearance between laminations and the tube (maximum 0.2 mm) necessitates that the stack of laminations be inserted while the tube is maintained at elevated temperature. Prior to inserting the coil, the bore of the laminations is honed, thereby further reducing the possibility of significant magnet training. Coil insertion into the core is accomplished with the coil precooled in liquid nitrogen and the core at room temperature. This ensures an interference fit between core and coil of approximately 0.15 mm resulting in a coil compression at operating temperature. End plates welded to the stainless steel core support tube form a closed vessel for containment of the helium coolant, thus eliminating the need for a separate inner helium vessel.

The design operating temperature for the superconducting magnets is 4.5 K. The conventional way of cooling the magnets would be to use pool

boiling of liquid helium. However, the analysis of various systems for the production and distribution of refrigerant for the ISABELLE magnets pointed to forced circulation of supercritical helium as the most effective cooling method (Brown, 1976). Supercritical helium is a single phase gas with high density and extremely low viscosity. These properties make it a virtually ideal heat transfer medium (Kolm, 1965). Forced circulation of supercritical helium through the small cooling channels in the magnets shown in Fig. 13 requires a small pressure drop only, allowing a long string of magnets to be cooled in series. Heat transfer to supercritical helium, which is important for magnet stability during pulsing or radiation heating, is in the general range of nucleate pool boiling or better under conditions applicable to ISABELLE (Giarratano, 1971).

The estimated steady-state heat load is 17 kW, which will be removed by a single 25 kW refrigerator. Sufficient distances can be spanned without undue pressure drop or other penalties using the distribution system envisaged so that all the refrigeration can be supplied from a single point. An alternative design might use several smaller refrigerators, but a single unit was chosen primarily on the basis of reliability and cost considerations. The refrigerator design utilizes the Claude cycle without liquid nitrogen precooling. Cooldown of the entire system will require about two weeks. Input power required for the refrigeration compressors is 12 MW. Either centrifugal or screw compressors will be used.

A simplified schematic of the helium distribution system is shown in Fig. 15. The helium which cools the magnets leaves the refrigerator at a pressure of 15 atm and a temperature of 2.8 K. As many as 52 magnets (one octant of one ring, less the insertion quads) will be cooled in series. The steady-state design temperature for the warmest magnet is 4.3 K. This temperature will rise to no higher than 4.5 K during the acceleration cycle and

then returns to the refrigerator at 14.3 atm and 6.2 K. Some flow will be removed from the refrigerant stream as required to cool magnet power leads. This flow returns to compressor suction at 300 K. In order to attain the low (2.8 K) temperature refrigerant which is distributed to the magnets, it is required that a bath of liquid helium at subatmospheric pressure be produced in the subcooler part of the refrigerator. The high pressure refrigerant is there cooled to 2.8 K by means of a heat exchanger in the liquid bath. The pressure of the bath is maintained at the required low pressure by pumping the vapor from the boiling liquid with a turbocompressor which is driven by a turboexpander operating on the gas returning from the magnets. No liquid helium storage facilities are required for this system. Most of the piping required to distribute refrigerant is contained in the vacuum annulus of the magnets. Where there are no magnets (primarily at the insertion sections) vacuum-insulated piping will transport the refrigerant.

E. Parameter List

The above description of the proposed proton-proton storage accelerator facility is summarized and complemented by the parameter list in Table I.

F. Options

The possibility of producing, storing and accelerating antiprotons is an important potential of the facility. Colliding $\bar{p}p$ experiments with c.m. energies from 60 to 400 GeV at luminosities of up to 10^{29} cm^{-2}sec^{-1} are possible. The antiproton option involves a comparatively simple addition to the basic ISABELLE facility. One method involves the fast ejection from one ring of the bunched 200 GeV proton beam which would be focused onto a target in the

external dump line. Bunches of 30 GeV antiprotons, produced in the target

and transported via room temperature magnets, would be injected into the

other proton ring and captured by a separate low-power rf

system. Due to the large acceptance of the ISABELLE ring and the strongly

forward peaking of the $\bar{p}$ production, it would be possible to collect almost

all antiprotons produced within a 2.5% momentum bite. With the use of super-

conducting septum magnets which would reduce the p-$\bar{p}$ crossing angle to a few

milliradians, luminosities $\approx 10^{29}$ cm^{-2}sec^{-1} seem attainable.

It would be very attractive to add a facility for ep collisions at a later

stage. Electrons would be accelerated to 4 GeV in the AGS, then transferred

to an additional ring and accelerated to 15 GeV, thus providing high c.m.

energy for ep collisions ($\sqrt{s} = 109$ GeV). The electron ring, with room tem-

perature magnets, would fit in the ISABELLE tunnel. Two e-p interaction

regions would be provided. The e-p interaction regions would employ a small

vertical crossing angle. With 6 MW of rf power in the electron ring, a lumin-

osity of $\sim 0.5 \times 10^{32}$ cm^{-2}sec^{-1} seems feasible at 15 GeV electron energy. Lumin-

osities several times 10^{32} cm^{-2}sec^{-1} seem   possible at lower energies.

IV. PHYSICS POTENTIAL

ISABELLE will provide the capability for exploring proton-proton collisions with c.m. energies continuously variable from 60 GeV to 400 GeV and with luminosities of 10^{32} to 10^{33} cm^{-2}sec^{-1} over this entire energy range. Such a large extension of the energy range combined with the substantial increase in expected luminosity and the flexibility inherent in the acceleration process ensures the utility of ISABELLE in the detailed investigation of the strong, electromagnetic and weak interactions. The excitement generated by the prospect of such investigations is the natural result of the recent discoveries in particle physics.

Examples abound. The unfolding of a totally unpredicted new spectroscopy of hadrons, launched by the J/ψ discovery (Aubert, 1974; Augustin, 1974), supports the conjecture of the quark substructure of the well known hadrons. Such conjecture is supported elsewhere by the results of systematic studies of deeply inelastic electron, neutrino, and proton scattering. Whether this substructure will be dramatically revealed by the actual production of quarks or whether it will be revealed merely by the kinematic distribution of particles emerging from high energy proton-proton collisions is clearly a major question which can be examined at ISABELLE.

The weak interactions are currently the focus of enormous interest, brought about by the discovery and confirmation of the existence of neutral weak currents (Hasert, 1973; Benvenuti, 1974a), the linear increase with energy of the neutrino total cross sections (Benvenuti, 1974b; Sciulli, 1975; Barish, 1975), and the discovery of charmed particles. The experimental data coupled with the advent of gauge theories reinforces the belief that weak and electromagnetic forces can be described by a unified theory (Weinberg, 1967; Salam, 1968). These experimental results and theoretical approaches imply the existence of charged and

neutral intermediate vector mesons in the 40-100 GeV/c^2 mass range, well

within the capabilities of production and detection at ISABELLE.[3]

And, in the strong interactions, the unexpected hadron production at

large values of the transverse momentum and the proton-proton total cross

section measurements are of intense interest in the energy range accessible

at ISABELLE. The beautiful results from the CERN ISR and from FNAL which show

the total cross section again increasing (Fig.16) demand an explanation based

on fundamental principles.

A. Weak Interactions[4]

Currently the "Holy Grail" of experimental particle physics is the inter-

mediate vector boson. If the mass is of the order of $(\alpha/G)^{\frac{1}{2}}$ (α is the fine

structure constant, G is the Fermi constant) or roughly 40-100 GeV/c^2 as

expected in current theories of unified weak and electromagnetic interactions,

then only the ISR at CERN has sufficient energy ($\leq$ 62 GeV) to explore a

limited part of this mass range. However, no indication of intermediate

vector bosons has been found. The best hope of producing them is with very

high energy, high luminosity proton-proton colliding beams, as would be avail-

able at ISABELLE. The Q^2-s plot of Fig.17 shows the vast new terrain available at

---

[3]The current experimental lower limit on the mass of the W$^{\pm}$ is m_W >24 GeV/c^2,

with 95% confidence.

[4]The following discussion of physics possibilities at ISABELLE has drawn ex-

tensively on these sources:

a. ISABELLE, A Proposal for Construction of a Proton-Proton Storage Accelerator

    Facility, Brookhaven National Laboratory 50519, May 1976.

b. Proceedings of the 1975 ISABELLE Summer Study, Brookhaven National Laboratory

    20550, July 14-25, 1975.

c. Palmer, R. B., E. A. Paschos, N. P. Samios, Ling-Lie Wang, Phys. Rev. D14,

    118 (1976).

d. Paschos, E. A., R. F. Peierls, T. L. Trueman, Ling-Lie Wang, to be published.

    A follow up on (c) with latest lepton pair production data incorporated.

ISABELLE energies. A very large portion of the new kinematic region is accessible to experiment as can be seen from the cross-section estimates which follow. The expected W production rates and decay modes have been estimated in terms of our present day understanding of weak interactions.

1. Charged W-Production

The production of $W^{\pm}$ in the reaction

$$p + p \rightarrow W^{\pm} + \text{anything} \tag{4.1}$$

is related to the electromagnetic production of dileptons of the same mass and at the same c.m. energy by protons,

$$p + p \rightarrow \ell^{+}\ell^{-} + \text{anything}, \tag{4.2}$$

through the conserved vector current (CVC) hypothesis. The cross sections for the production of W's of different charges are thus related to each other and to the electromagnetic matrix elements. However the cross section relation will be an inequality since CVC does not predict the semi-weak axial current, nor does it relate the semi-weak current to the isoscalar electromagnetic current. Define

$$\sigma_W = \tfrac{1}{4}\left[\sigma(pp \rightarrow W^{+}) + \sigma(pp \rightarrow W^{-}) + \sigma(pn \rightarrow W^{+}) + \sigma(pn \rightarrow W^{-})\right] \tag{4.3}$$

then it can be shown that

$$\sigma_W \gtrsim K\ M_{\ell\ell}^{3}\ \left.\frac{d\sigma}{dM_{\ell\bar{\ell}}}\right|_{M_{\ell\bar{\ell}} = M_W} \quad ,$$

$$K = \frac{3}{4}\ \frac{G\ \cos^{2}\theta_c}{2^{\frac{1}{2}}\alpha^{2}} = 0.09\ \text{cm}^2 \quad , \tag{4.4}$$

where $d\sigma/dM_{\ell\bar{\ell}}$ is the cross-section for the electromagnetic production of a lepton pair of mass $M_{\ell\bar{\ell}}$, G, α are defined above, θ_c is the Cabbibo angle, M_W is the vector boson mass. If $d\sigma/dM_{\ell\bar{\ell}}$ were known in the mass region expected for the W-meson, the above equation would provide a lower bound for the production of $W^{\pm}$. The necessary high energies are not available, but the dimensionless cross section $M^3_{\ell\bar{\ell}} \, d\sigma/dM_{\ell\bar{\ell}}$ may scale, i.e., depend only upon the parameters s and M^2 through the dimensionless ratio s/M^2.

In principle we should be able to check the scaling hypothesis at lower energies and then use it to extrapolate to ISABELLE energies and W masses. Figure 18 shows the available lepton pair production data from FNAL. These data are subject to a number of uncertainties, such errors as are shown being purely statistical. First of all, especially for lower masses, the subtraction of background due to J/ψ resonances and other sources is somewhat uncertain. Second, the longitudinal momentum regions in which the various observations were made are quite different, thus a model, in this case that of Drell-Yan (a quark-parton model), was used to integrate each data set over the complete longitudinal momentum region. The data included are listed on Fig. 18. From these data at lower energies we can deduce a scaling law and apply it at higher energies. With the uncertainties noted, the data appear consistent with a smooth scaling hypothesis. The smooth curve is calculated from the parton model with an anti-quark distribution proportional to $(1-x)^7$ where x is the fraction of the proton momenta carried by the quark. Quarks of three colors are assumed.

In Fig. 19 the production cross-sections for W^+ and W^- are shown as a function of the parameter s/M^2, using the model discussed above. The W^+ cross-section is naturally larger than that of W^- because there are more u quarks than d quarks in the proton. In $\bar{p}p$ collisions the cross-sections for W^+ and W^-

are equal and Fig.19 also contains their production cross section. As a consequence of the fact that there are more antiquarks in the antiproton than in the proton the $\bar{p}p$ cross section is about an order of magnitude larger than those for the pp interaction. One expects the hadronic backgrounds in $\bar{p}p$ and pp to be about equal, thus the signal for W production is about a factor 10 better for the $\bar{p}p$ interaction than for the pp interaction at the same luminosity.

The experimental detection of the $W^{\pm}$ will depend upon its leptonic decay $(W^{\pm} \rightarrow \ell^{\pm}\nu)$ and consequently upon the branching ratio

$$B = \frac{\Gamma(W \rightarrow \mu\nu) + \Gamma(W \rightarrow e\nu)}{\Gamma(W \rightarrow \text{hadrons})} \quad . \tag{4.5}$$

In the 4 quark model with color, $B = 1/3$. Assuming the isoscalar component is small and heavy leptons are not produced, then

$$B = 1/R, \quad R = \frac{e^{+}e^{-} \rightarrow \text{hadrons}}{e^{+}e^{-} \rightarrow \mu^{+}\mu^{-}} \quad . \tag{4.6}$$

Currently for $s \approx 50$ GeV^2, $R = 5.5$ as observed at SPEAR (Schwitters, 1976). Even if R continues to increase logarithmically, as suggested by some gauge theories (Appelquist, 1973), $B \approx 0.1$ for $M_W = 100$ GeV/c^2. With this branching ratio detection should be possible. Figure 20 shows the $p_{\perp}$ distribution for three different M_W values, based upon the parton model discussed above.

2. Neutral W Production

The expectation for the production of neutral intermediate vector bosons is similar to those for the charged bosons, but the cross section depends also on the form of the weak neutral current. In models of the Weinberg-Salam kind

$$\sigma_W 0 \geq 3/8 \frac{GM^3}{\sqrt{2} \alpha^2} (1 - 2 \sin^2\theta_W)^2 \frac{d\sigma}{dM_{\ell\bar{\ell}}} \tag{4.7}$$

at $M_{\ell\bar{\ell}} = M_W$, θ_W is the Weinberg angle. Again this assumes that the isoscalar terms of the electromagnetic and the weak neutral current are neglected.

In this case a pair of charged leptons is produced, either e^+e^- or $\mu^+\mu^-$, and a resonant peak may be easier to detect than in the $W^{\pm}$ decay, although the production rate may be lower by an order of magnitude. Even at energies below the threshold for the production of W^o's, one might observe effects in the interference of the weak and electromagnetic amplitudes.

3. Decay Modes

After the production of W's one would like to study their decay characteristics. Their decays provide an ideal method for producing new hadronic states containing heavy quarks. In fact, the ratio 1/B counts the number of different quark channels to which the W can decay.

Detection of the hadronic decay modes is facilitated by the presence of jets resulting from the sequential decays

$$
\begin{array}{c}
W^o \rightarrow q \qquad\qquad\div\ \bar{q} \\
\quad\ \big\lfloor\!\!\rightarrow \text{hadrons} \quad \big\lfloor\!\!\rightarrow \text{hadrons}
\end{array}
\qquad\qquad (4.8)
$$

The observation of jets and a comparison to leptonic decays will provide a measurement of B.

B. Strong Interactions

Particle physics is currently focused on weak interactions, charm, and the possibility of the fusion or unification of the weak and electromagnetic interactions. Nevertheless, understanding of the sources and the properties of the strong forces is a compelling need both logically and practically. The new wide range of c.m. energies available at ISABELLE (60-400 GeV) will provide a rich source for detailed and varied studies of the strong interaction. It may also give the crucial experimental information which would lead to the inclusion of the strong force with the description of the unified weak and electromagnetic forces.

1. Hadron Production at High Transverse Momentum, $p_\perp$

The uncertainty principle clearly shows that in order to extend our knowledge of the internal structure of the proton to smaller distances, it will be necessary to examine produced particles having larger transverse momenta. Experiments at FNAL (Cronin, 1973) and at the CERN ISR (Büsser, 1973, 1974) show an unexpectedly larger yield of produced hadrons with $p_\perp > 1$ GeV/c than had been anticipated from lower ($p_\perp < 1$ GeV/c) energy work. It seems quite likely that these data indicate the onset of new phenomena, not yet understood, which may hold the clue to unraveling the proton structure.

a) <u>Scaling predictions</u>. Present experimental information reaches $p_\perp = 9$ GeV/c. In principle, $p_\perp$ can be as large as 200 GeV/c with ISABELLE but it must be anticipated that cross sections will have fallen below measurable values at values of $p_\perp \sim 30$ GeV/c. It is important to have some estimate of how large the hadron yield will be as a function of $p_\perp$ in order to assess how far the range of knowledge can be extended with ISABELLE. At present, our best assumption is that the invariant cross section satisfies a scaling law,

$$E \frac{d\sigma}{d^3 p} = \left(\frac{1}{p_\perp}\right)^n f(x_\perp) \qquad (4.9)$$

where

$$x_\perp = \frac{2p_\perp}{\sqrt{s}} \qquad (4.10)$$

and $\sqrt{s}$ denotes the c.m. total energy. This is the form expected from several models for the particle of momentum p and energy E detected at 90° in the c.m.

Naturally the range of validity of this law is not known and one of the important experimental programs to be carried out at ISABELLE will test it by varying $\sqrt{s}$ and $p_\perp$ over the widest ranges possible.

Fits to ISR and FNAL data (Cronin, 1973; Büsser, 1973, 1974; Eggert, 1975) have been made using this form with n ranging between 7 and 11. The value of n required decreases as $x_\perp$ decreases. With ISABELLE at its maximum energy, $x_\perp$ will be very small, and thus n is also expected to have a smaller value. Theoretical models give values as small as n = 4. In order to give an estimate of the $p_\perp$ values attainable, we have assumed this scaling law for various values of n, used the measured cross section from the ISR experiment for several values of $x_\perp$ attainable at ISABELLE, and calculated the cross section for 200 x 200 GeV collisions at the corresponding value of $p_\perp$. The results are shown graphically in Fig.21a where $E(d\sigma/d^3p)$ is plotted as a function of n for various fixed $p_\perp$. From the ISR experience and the high ISABELLE luminosity, it is reasonable to expect to measure invariant cross sections of 10^{-38} $(cm^2 GeV^{-2}/sr)$, corresponding to a cross section of about 4×10^{-37} cm^2 for a detector with a one steradian and 10% momentum acceptance. It also seems quite possible to extend $p_\perp$ measurement out to 25 GeV/c or more.

The ISR experiment (CERN, Columbia, Rockefeller) (Büsser, 1973, 1974) fits their data with the form

$$E\frac{d\sigma}{d^3p} = \frac{1.54 \times 10^{-26}}{(p_\perp)^{8.24}} e^{-26.1\ p_\perp/\sqrt{s}} \quad (cm^2 GeV^{-2}/sr) \quad . \tag{4.11}$$

In Fig.21b this function is plotted along with the prediction of the electromagnetic contribution to the cross section based on Berman (BBK) (1971). The curve for smaller values of $x_\perp$ is not based on measurements or theory and it

will be very important to determine its actual shape. If the function given above remains valid as $x_\perp \to 0$, then, for example, the cross section at $p_\perp$ = 20 GeV/c and <u>infinite</u> energy is larger by a factor of 3.7 than at the 400 GeV c.m. ISABELLE energy.

At the same time as it extends the $x_\perp$ region to much smaller values than presently attainable for high $p_\perp$ processes, ISABELLE can utilize its high luminosity over the entire energy range from $\sqrt{s}$ = 60 to 400 GeV, overlapping the ISR range in $x_\perp$. This is a very important feature since it will permit a smooth continuation of the present data to the highest available energy. Not only is the overlap valuable for normalization purposes, but the continuous energy range at high luminosity is essential for seeing thresholds for new processes which affect the $p_\perp$ distribution, such as the production of new massive particles.

In addition to the single particle distribution at 90°, there are a great many other important high $p_\perp$ studies that can be done at ISABELLE. For example, the type of particles produced can be identified for $p_\perp \leq$ 20 GeV/c, multiplicities of particles produced in conjunction with a high $p_\perp$ particle can be measured; correlation in momentum and angle between high $p_\perp$ particles can be investigated, etc. These are all straightforward extensions of lower energy experiments already done at the ISR. Of particular interest will be the study of the dependence on the production angle θ of the high $p_\perp$ particle with respect to the beam direction. This should be a sensitive test for the production mechanism and the structure functions of the proton. It is, however, necessary to vary it over a rather wide range: not much change is expected for $45^\circ \leq \theta \leq 135^\circ$. The cross section at smaller angles is predicted to fall off faster with $p_\perp$ than at 90° and so the maximum measurable value of $p_\perp$ will be smaller. However, the shape of the curve as it falls is a very important measure of the proton structure.

b) <u>Jets</u>. An exciting prospect for ISABELLE is the study of jets; that
is, a spray of particles, each of whose momenta is nearly (to within 0.3
GeV/c) aligned. These are conjectured to be the residue of the elementary
part of the proton (the parton) which interacted strongly in the collision.
If they exist, the measurement of their distributions in momentum and angle
will give much more direct information about the crucial questions than the
single particle measurements discussed above. There is good evidence from
SPEAR (Schwitters, 1975) that jets of exactly the sort expected are produced
in e^+e^- annihilation, and measurements of various correlations at the ISR
(Darriulat, 1975) are consistent with the picture, although no clear jets
have been seen. Bjorken (1973) makes it clear why they have not been observed.
Small deviations in momentum of the various particles from the parton direc-
tion cause a certain amount of energy to be lost outside of any reasonable
cone; it is thus necessary to go to $p_\perp \gtrsim 5$ GeV/c for the parton to get a 20%
accurate determination of its momentum. Thus, jets should show up clearly
at ISABELLE. There is no experimental information comparable to the CCR
experiment at the ISR on which to base estimates for jet cross sections at
ISABELLE. Rather, some curves based on Bjorken's speculations are presented.
(Reference d, footnote 4.) The important assumptions are:
(a) the partons are distributed in the proton according to the electromagnetic
structure function, (b) the basic interaction is vector gluon exchange, just
as the photon but with coupling

$$\frac{g^2}{4\pi} \approx 10\alpha \approx \frac{1}{13.7} \ . \tag{4.12}$$

While a stronger coupling, of order 100α, may at first seem more reasonable,
it would predict far too large a cross section at the ISR; the above value is
consistent with the absence of $p_\perp^4$ terms in the CCR experiment. Figure 22 shows

the single jet $p_\perp$ distributions for three angles. The rapid fall for small

angles is clear. (The single particle distribution should be similar but

scaled down by a factor of 5 to 10.) Figure 23a shows the cross section for

two jets coming out back-to-back at 90°. This is important in estimating

the background for W-production. Figure 23b shows the same for one at 90°

and the other at 30°. Finally, (in Fig.23c) the cross section is shown for

one jet at 90° as a function of the angle of the other jet. These curves

are intended to illustrate measurements which will give information of a

most fundamental nature, even if some of the detailed assumptions used in

calculating them are not exact.

2. Energy Dependence of the Strong Interactions

The importance of the 60-400 GeV energy range available with ISABELLE for

exploring proton structure at small distances has been emphasized in the pre-

ceding sections. Of equal importance is the study of the strong interaction

itself. What is the nature of the force ultimately responsible for the

structure of matter?

A quantitative understanding of this force has yet to be formulated,

mainly because of its strength and complexity. There are good reasons to

believe that with experimental data at sufficiently high energies the essen-

tial properties of the basic hadronic interaction will begin to emerge from

the sea of detail.

Existing information suggests that the measurement of total and elastic

cross sections and the elucidation of the characteristics of single and mul-

tiparticle inclusive production at these high energies should give significant

new insights.

a) <u>Total cross sections</u>. Figure 24 shows the measured total pp cross section through ISR energies. The rise at the end of the curve is tantalizing. Does it herald a continuing indefinite rise, or is it merely some kind of threshold behavior? In Fig.24a several different possible theoretical fits (Hendrick, 1975; Mazur, 1975; Sidhu, 1975) are shown. In Fig. 24b the $\bar{p}p$ cross section is also shown, demonstrating that the ISABELLE range is crucial to understanding the difference between pp and $\bar{p}p$ cross sections (Sec. II.E).

The measurement of the total cross section is one of the most straightforward at conventional accelerators where the transmission method can yield accuracies of 1/2% or better. This simple method is, of course, not available to colliding beam experimenters. Three other methods can, however, provide 1% measurements:

i) In the first method a nearly 4π detector would be used. The total cross section σ_T is determined from

$$\sigma_T = R_T/L \qquad (4.13)$$

where R_T is the total interaction rate and L is the luminosity.

The interaction region must be surrounded by detectors as completely as is physically allowed. To minimize the loss of very small angle events, detectors must be close to the proton beam, for example, 2.75 cm, which corresponds to $t = -0.01$ (GeV/c)^2 at 200 GeV. Less than 1 mb of the total cross section would be undetected in the beam pipe and that can be corrected by extrapolating the observed events to 0°. This correction should contribute <1/2% to the error in the total cross section. The limitation of this method is likely to be the knowledge of the absolute luminosity, L, which currently can be determined to about 1%.

The variable energy feature of ISABELLE is particularly attractive for the σ_T measurement. The functional form of the total cross section can be determined from $s = 3 \times 10^3$ (GeV)^2, which overlaps with the ISR data, out to $s \geq 10^5$ (GeV)^2.

ii) A second method is to extrapolate the differential cross section to $0°$ and use the optical theorem, namely

$$\sigma_T = \frac{4\pi}{p} \text{ Im } f(0)$$

$$= \frac{4\pi}{p} \left[\frac{d\sigma}{d\Omega} (\theta = 0) \right]^{\frac{1}{2}} \qquad (4.14)$$

$$= \frac{4\pi}{p} \left[R_E (\theta = 0)/L \right]^{\frac{1}{2}} ,$$

Where R_E is the elastic rate. Assumptions about the spin dependence and the real part of the elastic scattering amplitude have to be made.

iii) The third method combines the measurements of both preceding methods. Combining the two expressions gives an expression for σ_T independent of luminosity, L, namely

$$\sigma_T = \frac{R_T}{R_E} \times \left(\frac{4\pi}{p} \right)^2 . \qquad (4.15)$$

b) <u>Elastic scattering in the Coulomb-nuclear interference region</u>. The ratio (ρ) of the real to the imaginary part of the forward scattering amplitude is a quantity of fundamental interest which should be measured through the Coulomb-nuclear interference in an early experiment at ISABELLE. If small angle proton-proton elastic scattering is spin independent, then the optical theorem, crossing symmetry, and the basic tenets of quantum field theory allow

ρ to be written as a dispersion integral of $\sigma_T(s)$ over s. The test of such dispersion relations at higher energies serves to confirm the validity of these assumptions over increasingly smaller distances. Figure 25a depicts the behavior of ρ as a function of $E_{lab} \simeq \sqrt{s}/2$ for various models of the high-energy behavior of the total cross section (Hendrick, 1975; Mazur, 1975; Sidhu, 1975). Figure 25b shows the present measurements for both pp and $\bar{p}p$; the curves are theoretical predictions using derivative analyticity relations (Sidhu, 1975).

The Coulomb-nuclear interference is maximal at $|t| \approx 0.002 \, (\text{GeV/c})^2$. Although difficult, measurements should try to include this value.

c) <u>Elastic scattering at larger $|t|$</u>. At values of $|t|$ larger than the Coulomb region, the elastic scattering cross section illustrates the clarification revealed by going to high energies, as shown in Fig. 26 (Morrison, 1973). Beyond the forward diffractive peak there is structure whose nature is unclear at lower energies, but resolves into a sharp minimum and secondary maximum at higher energies. The location of the minimum, and the height of the secondary maximum, together with the forward diffractive slope:

$$b(s) = - \frac{d}{d|t|} \log \frac{d\sigma(s,t)}{d|t|} \Bigg|_{t=0} , \qquad (4.16)$$

are three parameters whose energy dependence can provide strong clues as to the dynamical nature of elastic scattering. Figure 27 shows the slope, together with that for $\bar{p}p$, while Figs. 28a and 28b show the position of the first minimum and height of the second maximum. The curves are smooth interpolations of the data. Measurements at high energy are clearly needed. The maximum value of $|t|$ should be >10 $(\text{GeV/c})^2$ and will be limited by the small size of the cross section.

d) <u>Multiparticle production at small $p_\perp$:</u> <u>One particle inclusive reactions.</u>
One-particle inclusive reactions provide a measure of the average behavior
of multiparticle production. They account for roughly 80% of the proton-
proton total cross section. At ISABELLE one could study the inclusive reac-
tions

$$p + p \to c + X, \qquad c = \pi^\pm, \ K^\pm, \ p^\pm, \ \ldots \qquad (4.17)$$

as a function of energy and the longitudinal and transverse momenta of c.
Several aspects of these reactions are of particular significance.

i) Rapidity dependence. An important concept to verify or refute is the
existence of a central plateau in the rapidity plot. Define the rapidity y of
a produced particle by

$$\tanh y = p_{\parallel} /E \ , \qquad (4.18)$$

when $p_\parallel$ is the longitudinal momentum of the particle and E is its energy.
Multiperipheral and multi-Regge models predict a rapidity independence of
the inclusive cross section $d\sigma/dy$ over a range of rapidity values lying
between those of the incident particles. In sharp contrast, hydrodynamical
models predict a gaussian behavior in y (Cooper, 1975). ISR experiments
suggest that the fragments of the beam particles occupy about two units of
rapidity; so, the length of the expected central region is (Lillethun, 1973;
Giacomelli, 1975)

$$\Delta y = \log \left(\frac{s}{m^2} \right) - 4 \ . \qquad (4.19)$$

This gives

$$\Delta y = 4 \text{ at ISR ,}$$

$$\Delta y = 8 \text{ at ISABELLE .}$$

At ISABELLE energies a large fraction of the available rapidity will be in the central region, allowing a clear distinction between gaussian and plateau behavior.

ii) Multiplicities. Either by integrating over inclusive cross sections or by direct observation, one can study the multiplicity distributions of produced particles. Here again the hydrodynamic and multiperipheral models differ sharply as can be seen from Fig. 29. Extrapolating present data to an $s = 1.6 \times 10^5$ at ISABELLE, the hydrodynamic $s^{\frac{1}{4}}$ multiplicity growth (Carruthers, 1973) predicts an average of 35 charged secondaries per primary collision whereas the multiperipheral logarithmic extrapolations (Antinucci, 1973) give only 19. (See also Ferbel, 1976.)

iii) Energy dependence. At the ISR inclusive cross sections have been observed to scale (Gunion, 1972; Brodsky, 1973; Amaldi, 1973)

$$E\frac{d\sigma}{d^3 p} = f(y - y_o, \ p_\perp^2) \text{ independent of } s \qquad (4.20)$$

where y_o is the rapidity of either beam particle and one restricts $|y - y_o|$ $\leq \Delta y$. With the Mueller-Regge model this scaling is understood by assuming that the Pomeron is a simple Regge pole. There are both experimental (Amaldi, 1973; Amendolia, 1973; Carroll, 1974a, 1974b) and theoretical (Jones, 1972; Brower, 1972) indications that this assumption is incorrect; consequently, the energy dependence (or lack thereof) of inclusive cross sections at ISA-BELLE energies will be of basic importance.

iv) Behavior near x = 1. In the triple-Regge model (deTar, 1971) the behavior of the pp → pX cross section for $x = p_{||}/p_{||\ beam} \approx 1$ is dominated by the triple-Pomeron graph. The model is certainly oversimplified, but nevertheless the cross section in this region should give information on Pomeron interactions.

e) <u>Inclusive cross sections at small $p_{\perp}$</u>. One of the major challenges to the experimenters at ISABELLE involves the measurement of particle production at very small angles and very high momenta. Since by definition the trajectories followed by these particles are very close to those of primary beam particles, special techniques are required to detect them. However, the great interest in this region (the realm of the triple-Regge pole model) demands that all efforts be made to study it. The capability of varying the two beam energies independently should prove useful in this respect (Peierls, 1975).

f) <u>Correlations</u>. The very high energies available at ISABELLE are particularly useful in studying both correlations between particles in the central region and correlations between a proton near x = 1 and particles in the missing mass.

In the central region it is useful to distinguish long-range and short-range correlations. In the Mueller-Regge model short-range correlations are associated with secondary Regge poles (Mueller, 1970, 1971), while long-range ones are associated with Pomeron-Regge cuts (Ambramovskii, 1972), or more generally, with any nonfactorizable part of the Pomeron. In other models, short-range correlations come from clusters or similar effects (Ranft, 1974), while long-range correlations can arise from the production of particles off multiple chains or from absorption (Cheng, 1973; Auerbach, 1972). Additional

long-range correlations are introduced by energy-momentum conservation, especially near the boundary of phase space.

The Stony Brook-Pisa experiment (Amendolia, 1974) at the ISR has shown that there is a substantial short-range correlation in the central region. Since the size of the central region is limited, it is difficult to separate dynamical long-range correlation effects from those due to energy-momentum conservation. At ISABELLE the central region extends over about double the range of rapidity, and the study of dynamical long-range correlations would therefore be facilitated.

For a proton near $x = 1$ Pomeron exchange should dominate. An inclusive reaction involving a proton near $x = 1$ and another particle contributing to the missing mass (M) can thus be viewed as a one-particle inclusive reaction for Pomeron-proton scattering (Frazer, 1973). Such a reaction probes the nature of high-mass diffraction. In the triple-Regge model Pomeron-particle cross sections at large M^2 should be similar to particle-particle cross sections at large s (Frazer, 1973).

At ISABELLE energies one can reach $M^2 = 3200$ $(GeV/c^2)^2$ for $x = 0.98$, for which the Pomeron should certainly dominate. This value of M^2 is comparable to the values of s reached at ISR. If the triple-Regge model is at all correct, the rapidity plot for particles contributing to the missing mass should show a clear central plateau. In any event it would be most interesting to explore Pomeron-particle scattering at such large values of M^2.

C. Searches for New, Massive Particles

The J/ψ discovery in 1974 strongly suggested a new quantum number, charm. Recently there has been reported more direct evidence for charmed baryons (Cazzoli, 1975; Knapp, 1976) and charmed mesons (Goldhaber, 1976; Peruzzi, 1976)

opening a new hadron spectroscopy in the region of 2 GeV/c^2 mass.

The   important implication of these discoveries and speculations for

ISABELLE lies in the possibility of still larger mass J-like objects with

corresponding implications for hadron spectroscopy on larger mass scales.

The present theoretical picture calls for matter to be constructed from

ordinary quarks with mass $\sim$300 MeV/c^2, strange quarks with mass $\sim$500 MeV/c^2,

and charmed quarks of mass $\sim$1.5 GeV/c^2. There is no reason to suppose this

is the last such level; indeed 6 and 8 quark schemes have already been sug-

gested (Harari,1975; Suzuki, 1975), and the mass scale for higher levels

could be 10 GeV/c^2 or more.

In the search for higher mass particles,   the large c.m. energy

of ISABELLE can be important or even crucial because of the rapidly rising

excitation curve expected for large-mass objects. This effect can be esti-

mated by an appropriate scaling of and comparison to the energy dependence

for production of known massive hadrons, such as $K\bar{K}$ and $p\bar{p}$ (Gaisser, 1975).

Figure 30 shows an estimate of the quantity

$$R(m) = \frac{(d\sigma_m/dy)_{ISA}}{(d\sigma_m/dy)_{FNAL}}\bigg|_{y=0} \tag{4.21}$$

for production of a particle of mass m. Since the J excitation curve is some-

what steeper than the scaled hadron pair curves, this effect should be even

more pronounced for J-like objects. The general features of Fig. 30 are pre-

sumably also applicable to other possible new massive objects, such as quarks,

monopoles, heavy leptons, etc.

For production of pairs of particles with mass up to 10 GeV/c^2, the cross

sections in the central region will have reached a saturation value relative

to background kaons and pions. With $\sqrt{s}$ = 400 GeV, ISABELLE will, of course, also be able to explore the mass range up to $\gtrsim$100 GeV/c^2 for particle production in the threshold region. The case of W-boson production is discussed in detail elsewhere. We here mention a few speculative, very massive objects and their specific signatures that make a search for their production near threshold feasible:

1. Very massive J-like objects could be detected via the $\ell^+\ell^-$ decay mode.

2. Hadrons with masses comparable to $\sqrt{s}$ will be produced near rest in the ISABELLE lab system. If the average multiplicity for decay of such an object follows other hadronic interactions ($\langle n \rangle \propto \ell n M$) then the mean momentum of the decay products will be large (e.g., $\sim$5.5 GeV/c for M = 100 GeV/c^2). It has been pointed out that such an event would show up as an unusual "fireworks" of prongs which have very large momentum transverse to the incident beam line (Rubbia, 1975).

3. Fractionally charged quarks, if they are not permanently confined within hadrons, could be detected by the ionization characteristic of fractional charge by collecting samples in material surrounding the detector. Present upper limits are of the order of 10^{-34} cm^2 for M_q <25 GeV/c^2. It is anticipated that a limit of 10^{-36} cm^2 for M_q <200 GeV/c^2 could be achieved (Foley, 1975).

4. Integrally charged quarks could be detected either by specific decay modes, as in the Pati-Salam scheme (Pati, 1973), or, more definitively, by detecting nonconservation of baryon number in an interaction. Since protons cannot easily be distinguished from pions and kaons at these energies, the baryon nonconservation would have to be detected by observing pp $\rightarrow$ no hadrons (Nauenberg, 1975).

5. Magnetic monopoles with masses comparable to $\sqrt{s}$ could be detected in three ways (Giacomelli, 1975):

   a) Immediately after production, by the characteristic heavy, constant ionization, e.g., in plastic detectors;

   b) By capture in iron surrounding the intersection and subsequent detection either by induction or by extracting monopoles and looking for the characteristic ionization; or

   c) By looking for multigamma events due to monopole-monopole annihilation at production.

D. The Unknown

In spite of the fascinating physics now being studied and projections of the physics to come in the c.m. energy to be available at ISABELLE, it may well turn out that the most fundamental discoveries of all are still unthought of by theorists. Such has been the history at most accelerators. Some general possibilities were catalogued in the Proceedings of the 1975 ISABELLE Summer Study (Lederman, 1975).

1. New Symmetry Violations

a) $p + p \rightarrow$ nothing. This implies a search for violation of baryon number, charge, or both.

b) Familiar symmetry violations might change their character in the intense fields of a 400 GeV collision. For example, the K^o-$\bar{K}^o$ particle mixture could show interference effects of opposite sign.

c) Lorentz invariance breakdown at very small distances should be suspected.

2.   Search for New Objects

Here quarks, monopoles, etc. are defined as old familiar objects.

a) Particles of high mass that are stable, perhaps because they are the ground states of new families carrying new quantum numbers. A sudden increase in the production of antiparticles might be a particular example.

b) Particles of long lifetime or neutral massive leptons should not be overlooked as possible items for search.

c) Particles of very high mass and short lifetimes which decay hadronically. Naturally by definition the unique discovery goes unmentioned.

E.   Strong Interactions with $\bar{p}p$

One of the major limitations of storage rings is that one cannot vary the projectile and targets being used. This makes the unravelling of different components of the dynamics and the testing of alternative theories more difficult. In principle, the addition of the $\bar{p}p$ option provides the necessary kind of information. Several types of experiment will be discussed in this context.

a) We can first ask what can be done with $\bar{p}p$ that cannot be done with pp? Evidently, one can check charge conjugation invariances, for example, by comparing particle and antiparticle spectra. This would probably be most interesting at high $p_\perp$ where new distance scales are being explored. Although one could directly form any high lying mesonic resonances that may exist, the cross section is certainly much too small to be detectable. The major difference between pp and $\bar{p}p$ is that $\bar{p}p$ can produce systems which have no baryons in the final state. However, the cross section for this is small and falling with energy and, although annihilation experiments may provide some useful information in studying reaction mechanisms, it is difficult to point to anything of singular interest to be found in such a difficult experiment.

b) Probably the most useful information obtainable from the $\bar{p}p$ option will come from comparison with pp results. Clearly, the primary measurement of this type is σ_T. Do the pp and $\bar{p}p$ total cross sections continue to approach each other as predicted by the Pomeranchuk theorem? Closely related questions will be answered by comparison of the real parts of the forward amplitudes and the differential cross sections.

Figures 24a and 25b show predictions of some models for the behavior of these quantities as s increases.

If the cross sections do not come together, we would be blessed with a most unexpected result and the possibilities for searching for the source of the difference would be most exciting. If, as expected, they do come together, then obviously any studies of the comparison will involve the measurement of small differences and are likely to require very difficult experiments.

The comparison of various final state distributions will throw light on the reaction mechanisms. To be more specific, the process of diffraction production can be studied by comparison of

$$p + p \rightarrow N^* + p \qquad (4.22)$$

with

$$\bar{p} + p \rightarrow \bar{N}^* + p \ . \qquad (4.23)$$

For example, the rate at which these cross sections approach each other will enable some separation of the various Regge exchange contributions to the process. Similarly, the comparison of

$$p + p \rightarrow p + X \qquad (4.24)$$

with

$$\bar{p} + p \rightarrow \bar{p} + X \qquad (4.25)$$

in the triple-Regge region will enable the separation of various components there. Note that this involves a small effect because the difference will lie only in the non-scaling piece, if the Pomeron has positive charge conjugation as expected. This is illustrated in Fig. 31. In going from p to $\bar{p}$, the contribution change sign if R_1 and R_2 have opposite C; otherwise they are the same. Hence, the difference can come only for the parts with R having C = -1. The size of these "off-diagonal" couplings is presently not at all well known and so we cannot estimate the size of the difference; it is safe to say that it is small and will probably be most important for s/M^2 not too large.

c) Since we are dealing with small cross sections, the differences may prove to be most enlightening in the region where both pp and $\bar{p}p$ cross sections are small. We know the cross section for W production and lepton pair production are expected to be very different. In strong interactions high $p_\perp$ is a similar region. Whereas W or $\ell^+\ell^-$ production requires annihilation of a q and a $\bar{q}$, this is only one component of the cross section for high $p_\perp$. High $p_\perp$ can also be achieved by scattering, e.g.,

$$q + q \rightarrow q + q$$
$$\qquad (4.26)$$
$$q + M \rightarrow q + M .$$

In some models this component is considerably larger than the annihilation cross section. Figure 32 shows the results of a calculation using the BBK model (Weinberg, 1967; Salam, 1968) and the distribution functions used in the W production calculations in the summer study. The figure shows the ratio of

$$\frac{E\dfrac{d^3\sigma(\bar{p}p \to \pi)}{dp^3} - E\dfrac{d^3\sigma(pp \to \pi)}{dp^3}}{E\dfrac{d^3\sigma(pp \to \pi)}{dp^3}} \qquad (4.27)$$

as a function of $x_\perp = \dfrac{2p_\perp}{(s)^{\frac{1}{2}}}$ at 90°. (The charges of the π's are summed.) We

see it varies from about 3% in the easily measured region of small $x_\perp$ and in-

creases to only about 6% at $p_\perp = 50$ GeV/c. Different distribution functions

with less antiquark content at large $x_\perp$ will increase this ratio, especially

at the largest $x_\perp$, and so it is a good way of separating q and $\bar{q}$ distribu-

tions. However, the effect is very small.

We can also view the process using the constituent interchange model of

Blankenbecler, Brodsky, and Gunion (1972, 1973). (We don't present a curve

because the necessary parameters are not known yet.) In that model, several

subprocesses contribute to the $p_\perp^{-8}$ behavior seen at the ISR. These processes

have very different dependence on $(1 - x_\perp)$ in pp and $\bar{p}p$. Denoting the be-

havior as $(1 - x_\perp)^F$ the values for various processes are shown in Table II.

Determinations of these differences can help unravel the dominant subprocess,

but they again require hard experiments at least for moderately large $x_\perp$.

d) In summary, the testing of the Pomeranchuk theorem is the most impor-

tant reason in strong interactions for the $\bar{p}p$ option. Barring surprises,

other experiments will be dealing with small effects. In principle, impor-

tant information can be obtained to help unravel structure from dynamics, but

it will be difficult and there is a real chance that there will be no de-

tectable differences between pp and $\bar{p}p$.

V. BEAM ANALYSIS AND PERFORMANCE IN ISABELLE

A. Overview

The design of proton storage rings rests upon principles which must guarantee a few prime objectives. In the first place, we demand high luminosity and high energy including a large range of operating energies. Second, we ask for sufficient space for experimental detection equipment in the collision regions and for a certain measure of flexibility in shaping the beam overlap region where the collisions take place. Finally, we expect that background levels in the interaction regions will be adequately low so that particular event signals can be observed.

Does the physical system we have discussed allow these general objectives to be realized? To provide an answer to this question and, in fact, to estimate in quantitative terms the performance potential of the ISABELLE complex, we require an understanding of the behavior of proton beams as they proceed through the various channels from the ion source, through the linac and the AGS, to the top energy of ISABELLE. Our procedure is to take the physical system as we have described it and to estimate its performance levels. These performance levels are meaningful only if the colliding beams are stable and do not change their character over many hours. Thus, we must deal with both the instantaneous performance characteristics and the length of time over which such conditions must prevail.

On the one hand we have the prediction for ISABELLE of high performance and long lifetime and on the other hand we have the requirements of high density beams and beam stability. It is our main objective in this section to assess the consistency of the ISABELLE design parameters with the design objectives insofar as they relate to the attainment of the necessary dense,

stable beams; and, in particular we will seek out those critical areas which could play a role in limiting the expected performance levels.

In Section V.B we discuss the collision overlap region and estimate the ISABELLE luminosity. Section V.C deals with the single beam coherent instabilities. In Section V.D we review various analyses pertaining to the electromagnetic interaction between the two beams. The concern here is for an incoherent growth of the transverse beam dimensions due to the strongly nonlinear beam-beam force. Although the beam growth is incoherent, the force is conservative, and so the process is related to phase space filamentation due to the nonlinear fields. In Section V.E the effects of the "nonLiouvillian" forces are treated. Both scattering of protons off the residual gas and between each other (intrabeam scattering) are dealt with. We discuss in this section also effects indirectly arising from the beam gas interaction. In particular, the produced electrons which are trapped in the coasting proton beam can cause coupled electron-proton oscillations. We also consider here the pressure bump instability which is related to molecular desorption from the vacuum chamber surface due to bombarding positive ions.

The performance of a pp colliding beam device is restricted by the aperture available to accumulate the beam. This is a rather complicated subject, and we discuss it in two parts -- the momentum aperture in Section V.F and the spatial aperture in Section V.G. A detailed consideration of the implications of our choice of beam stacking is given in Section V.H. Finally, in Section V.I we review and discuss the overall performance that the ISABELLE complex should be capable of achieving.

B. Collision Region and Luminosity

The interaction rate for any given scattering process can be written as a product of two factors, the cross section, σ, which characterizes the particular type of scattering event, and the luminosity, L, which is independent of the specific interaction and depends only on the nature of the beams and the collision geometry.

The luminosity (Möller, 1945) in storage rings is related to how many particles there are in each beam, how localized the region of beam collisions is, and how frequently each particle returns to the domain of collision. In particular, for coasting beams, the collision region is simply related to the volume of overlap of the two beams. If V represents the volume, ρ_1 and ρ_2 the particle densities for the two beams, and $\underset{\sim}{v_1}$ and $\underset{\sim}{v_2}$ the velocities of the two beams, then the luminosity can be expressed in general as

$$L = \left[(\underset{\sim}{v_1} - \underset{\sim}{v_2})^2 - \frac{1}{c^2} (\underset{\sim}{v_1} \times \underset{\sim}{v_2})^2 \right]^{\frac{1}{2}} \int \rho_1 \rho_2 \, dV \quad , \qquad (5.1)$$

with c the velocity of light and e the unit of electric charge. In the case of two relativistic coasting beams crossing at a small angle, α, and neglecting terms of order α^2, the luminosity becomes

$$L = 2c \int_{-\infty}^{\infty} \int_{-\infty}^{\infty} \int_{-\infty}^{\infty} \rho_1(x, y, s) \, \rho_2(x, y, s) \, dx \, dy \, ds \quad , \qquad (5.2)$$

with x, y, and s the orthogonal coordinates of a cartesian system: y is normal to the collision plane, s is on a line in the collision plane running midway between the two beams, and x is normal to the s coordinate and in the collision plane. The details of the ISABELLE collision geometry have been previously described.

In ISABELLE the momentum dispersion of each beam is brought to zero in the insertions. The betatron distributions can be taken to be Gaussian. In this case, the integrations over x and y can be performed analytically and we have for the specific luminosity, that is, the luminosity per unit length along s (Montague, 1975),

$$\frac{dL}{ds} = \frac{I_1 I_2}{e^2 c \, \pi} \left\{ \left(\sigma_{h1}^2 + \sigma_{h2}^2 \right) \left(\sigma_{v1}^2 + \sigma_{v2}^2 \right) \right\}^{-\frac{1}{2}} \exp \left[\frac{- s^2 \alpha^2}{2(\sigma_{h1}^2 + \sigma_{h2}^2)} \right] \quad , \qquad (5.3)$$

where $I_{1,2}$ are total currents for the coasting beams, $\sigma_{1,2}$ are rms beam sizes and h, v refer to horizontal and vertical (orthogonal to s), respectively. The rms beam size is related to the normalized phase space emittance, E, containing 86.5% of the particles by (Courant, 1958)

$$\sigma^2(s) = \frac{E\beta(s)}{4\pi\beta\gamma} \quad . \qquad (5.4)$$

The beam size depends on s through the variation of the beta function in the magnet free region:

$$\beta(s) = \beta^* + (s^2/\beta^*) \quad , \qquad (5.5)$$

with $\beta_{h,v}^*$ the values of the amplitude functions at the crossing point.

Defining an effective beam size at the crossing point (s = 0) by

$$\sigma^* = \left[(\sigma_1^2 + \sigma_2^2)/2 \right]^{\frac{1}{2}} \quad , \qquad (5.6)$$

and writing the rms interaction length as

$$\sigma_\ell^* = \sqrt{2} \; \sigma_h^*/\alpha \quad , \qquad (5.7)$$

then, if the condition

$$\sigma_\ell^* \ll \tfrac{1}{2}\, \beta_{h,v}^* \qquad\qquad (5.8)$$

is satisfied, the specific luminosity becomes

$$\frac{dL}{ds} = \frac{I_1 I_2}{e^2 c\, \pi} \; \frac{1}{2\sigma_h^* \sigma_v^*} \, \exp\left[- s^2/2\sigma_\ell^{*2}\right] \quad . \qquad\qquad (5.9)$$

From this expression we see that the total length of beam overlap containing 95% of the collisions is simply given by

$$\ell_{int} = 4\sigma_\ell^* = 4\sqrt{2}\; \sigma_h^*/\alpha \quad . \qquad\qquad (5.10)$$

The total luminosity can be obtained by integrating Eq. (5.9) over s, leading to

$$L = \frac{I_1 I_2}{\sqrt{\pi}\; e^2 c\; \sigma_v^* \alpha} \quad . \qquad\qquad (5.11)$$

Thus, for coasting proton beams crossing in a horizontal plane, the factors determining the luminosity are current, beam height, and crossing angle (or, interaction length). In a rough sense, arriving at a satisfactory set of these parameters, together with the energy, can be considered as the main effort of the design procedure for the ISABELLE storage ring system.

C. The Single Beam Coherent Instabilities

A charged particle beam enclosed within a generally complicated vacuum chamber tends to induce electromagnetic fields which in turn act on the beam (Sessler, 1973; Teng, 1975). This yields a somewhat intractable equation for the resulting time evolution of such a system. For the purpose of studying stability in particle beams, we can ignore the self-consistency requirement, thus leading to the Boltzmann equation as the description of the behavior of the beam. For long-range forces where the direct interaction between the particles in the beam is neglected, there results the collisionless Boltzmann equation, also referred to as the Vlasov equation:

$$\frac{d\psi}{dt} = 0 \quad , \tag{5.12}$$

where ψ represents the distribution function in the particle phase space and (d/dt) means the total time derivative. This equation is simply a statement of local conservation of phase space area. For a system of conservative forces, it is an expression of Liouville's theorem, following from the assertion that the total number of particles remains constant.

When a beam of particles suffers a "small" coherent deformation, an induced field results which acts back on the beam. The question, then, is whether or not the interaction will lead to growing oscillations. The interest is, therefore, in the onset of instability and its immediate evolution. To obtain this information, the Vlasov equation can usually be linearized which results in a major simplification and in general provides threshold conditions and growth rates by standard techniques.

1. Beam Density Oscillations (Longitudinal Instabilities)

Beam density oscillations are analyzed in the energy-azimuth phase plane. The Vlasov equation for a beam of particles in terms of the energy deviation from the synchronous energy, $x = \Delta E/E$, and θ the angular distance in the coordinate frame moving with the beam, is (Sacherer, 1972)

$$\frac{\partial \psi}{\partial t} + \dot\theta \frac{\partial \psi}{\partial \theta} + \dot x \frac{\partial \psi}{\partial x} = 0 \quad , \tag{5.13}$$

where $\psi \equiv \psi(x, \theta, t)$. The equations of motion are given by (Nielsen, 1959)

$$\dot\theta = \frac{2 \pi f_o \eta}{\beta^2} x \quad ,$$

$$\tag{5.14}$$

$$\dot x = \frac{e c \beta}{E_o} \xi_\theta - \frac{\Omega^2}{2 \pi f_o \eta} \theta \quad ,$$

with f_o the particle revolution frequency, η the energy slipping factor,

$$\eta = \frac{1}{\gamma_{tr}^2} - \frac{1}{\gamma^2} \quad , \tag{5.15}$$

γ_{tr} the transition energy in units of the proton rest mass energy ($E_o = 938$ MeV), and β, γ the usual relativistic parameters. ξ_θ is the perturbing longitudinal electric field, and Ω is the synchrotron frequency,

$$\Omega = 2\pi f_o \nu_s = 2\pi f_o \left(\frac{h\eta eV}{2\pi \beta^2 \gamma E_o}\right)^{\frac{1}{2}} \quad , \tag{5.16}$$

h the harmonic number of the rf system, V the peak voltage per turn of the rf system, and we take the case of no acceleration.

There are three different beam configurations which are potentially vulnerable to longitudinal instability. These are the low current bunched beams on the injection orbit (Messerschmid, 1976a; 1976b), the bunched high current stack during acceleration, and the stored coasting beam (Neil, 1965). However, since low current beams of high longitudinal density tend to be the most susceptible, the critical stability criterion is related to the case of the injected bunches. This results from the fact that stability is related to the quantity $I/(\Delta p)^2$, with Δp the beam momentum spread and I the average current (Keil, 1969). Since the density $I/\Delta p$ can only decrease during all three ISA-BELLE phases — stacking, acceleration, and storage — and since Δp keeps increasing as the stack is built up, it follows that the beam becomes progressively more stable as the current is accumulated. It is therefore sufficient to treat here in detail the implications which result from requiring that the injected bunches remain stable against longitudinal instability from the time of injection until they are deposited in the growing stack.

Unstable oscillation modes due to the interaction between the bunches comprising a given beam have been analyzed in general (Sacherer, 1973). These tend to be connected with beam induced fields of relatively low frequency and long wakes. Thus, two means of control are available if necessary: 1) the sources of the longitudinal impedances leading to such beam induced fields are large objects, of the order of a meter or longer, and as such they are relatively easily identified and neutralized; 2) the low frequency essentially means that feedback techniques (Boussard, 1971; Schnell, 1975a) are feasible although at present they are not contemplated for ISABELLE.

Of immediate concern to ISABELLE is the "fast" longitudinal instability induced by high frequency, short wake fields and manifested in the injected bunches as they are being stacked. The high frequency and short wake

characteristics essentially mean that we are dealing with single bunch instabilities and the interaction of any given bunch with the others can be neglected (Messerschmid, 1976a; 1976b; Hereward, 1975a). Since these single bunch instabilities which have been observed experimentally both at the PS (Boussard, 1975) and the ISR (Hansen, 1975; Hofmann, 1975) are fast compared to the synchrotron motion, we can neglect the latter and the linearized Vlasov equation for the perturbed density distribution, ψ_1, becomes

$$\frac{\partial \psi_1}{\partial t} + \dot{\theta} \frac{\partial \psi_1}{\partial \theta} + \dot{x}_p \frac{\partial \psi_0}{\partial x} = 0 \quad , \tag{5.17}$$

where $\dot{x}_p$ is just the term arising from the perturbing force and $\psi_0 (x,\theta)$ is the equilibrium unperturbed bunch distribution function.

The induced electric field can, in general, be approximated in terms of a translation invariant "impedance" kernel, $Z(\theta)$, and the perturbed linear charge density

$$\lambda_1 (\theta) = \frac{I_0}{c} \int \psi_1(x,\theta) \; dx \quad , \tag{5.18}$$

where we have dropped the time dependence, which is assumed to have the steady state form at frequency, ω, i.e., $\sim e^{-i\omega t}$, and I_0 is the dc current of the beam. The relationship is given by (Sacherer, 1972)

$$\xi_\theta (\theta) = - f_0 \int Z(\theta - \theta') \lambda_1 (\theta') \; d\theta' \quad . \tag{5.19}$$

The linearized Vlasov equation leads to a dispersion relation which is an implicit equation for the frequency ω. If $\text{Im}(\omega)$ is the imaginary part of the solution and if $\text{Im}(\omega) > 0$, instability exists. The threshold is given by the

solution $\text{Im}(\omega) = 0$. The dispersion relation can be expressed by (Messer‑schmid, 1976b)

$$1 = \frac{ieI_o}{2\pi\eta E_o\gamma} \left(\frac{Z_{eff}}{n_o}\right) \int \frac{dG(x')/dx'}{y - x'}\, dx' \quad . \qquad (5.20)$$

G represents the normalized energy distribution in the bunch,

$$y = \frac{\omega}{n_o 2\pi f_o \eta} \quad , \qquad (5.21)$$

n_o is the mode number for the "unstable" density oscillation, that is, the number of oscillations along the machine circumference, $C = 2\pi R$, and Z_{eff} is an effective impedance which for Gaussian bunches is given by

$$Z_{eff} = \sum_n Z_n \, e^{-(n-n_o)^2\theta_{rms}^2} \quad . \qquad (5.22)$$

Z_n is the usual longitudinal coupling impedance and θ_{rms} the rms bunch size in radians, $\theta_{rms} = \text{(rms bunch length)}/\text{(machine radius)}$.

A similar analysis for a coasting beam leads to a dispersion relation of the same form, but with Z_{eff} given by (Neil, 1965)

$$Z_{eff} = Z_n \, \delta_{nn_o} \quad . \qquad (5.23)$$

The result is the usual coasting beam dispersion relation.

Solving the dispersion relation (Ruggiero, 1968; Hübner, 1970; Keil, 1969), we find the threshold criterion for the microwave (i.e., fast) instability for single bunches to be

$$\left| \frac{Z_{eff}}{n_o} \right| < F \frac{E}{e} \frac{\eta}{I_o} \left(\frac{\Delta E}{E} \right)^2 , \tag{5.24}$$

where the form factor F is close to unity for realistic energy distributions

if ΔE is taken as the full spread at half maximum at the bunch center,

$\Delta E \equiv (\Delta E)_h$.

The growth rate α_g for small unstable oscillations can also be estimated

by standard techniques (Hereward, 1975b):

$$\alpha_g = \frac{f_o e I_o}{(\Delta E)_h} Z_{th} \left[1 + \left(\frac{Z_{eff}}{Z_{th}} - 1 \right)^2 \right]^{\frac{1}{4}} \sin \psi , \tag{5.25}$$

with

$$\psi = \frac{1}{2} \arctan \left(\frac{Z_{eff}}{Z_{th}} - 1 \right) , \tag{5.26}$$

and

$$Z_{th} = n_o F \frac{E}{e} \frac{\eta}{I_o} \left(\frac{\Delta E}{E} \right)^2 . \tag{5.27}$$

In terms of the synchrotron oscillation frequency

$$\alpha_s = \Omega/2\pi = \nu_s f_o , \tag{5.28}$$

the growth rate near threshold can be written in the simple form

$$\frac{\alpha_g}{\alpha_s} = \pi n_o \theta_{rms} \left(\frac{Z_{eff}}{Z_{th}} - 1 \right) . \tag{5.29}$$

In other words, the growth rate is proportional to the mode number, n_o. That is, high frequencies and high growth rates tend to be synonomous. This is why the labels "microwave" and "fast" instability can be used interchangeably. Of course, the growth rate tends to zero as the effective impedance approaches the threshold value.

The phenomenon of a threshold is a manifestation of the process of Landau damping (Jackson, 1960; Hereward, 1965). The beam becomes unstable if the forces are such that a small coherent density fluctuation is enhanced. However, any frequency spread will induce a tendency in the oscillation toward decoherence. This process which opposes a developing oscillation is generally referred to as Landau damping and leads to a threshold value for the perturbing force. It is interesting that in this case the decoherence effect is proportional to the square of the spread in energy.

When the bunches enter ISABELLE from the AGS, they have a sufficiently high momentum density so that the bunches are vulnerable to this high frequency longitudinal instability. As already mentioned, these have been observed and studied at the ISR during the stacking process. For impedances having a broad frequency spectrum, the stability criterion takes a rather simple form. As a limit on the high frequency (i.e., microwave) longitudinal impedance and using our previous analysis, this can be expressed roughly as

$$\left|\frac{Z_n}{n}\right| \lesssim \frac{(E/e) \, \eta \, B}{2I_o} \left(\frac{\Delta E}{E}\right)^2_{total} \quad , \tag{5.30}$$

where B is the bunching factor (bunch length/bunch separation). For ISABELLE, the number of injected particles is 5.2×10^{12} in 11 bunches, so that $I_o = 0.34$ A. At injection, we have E = 29.5 GeV and $\eta = 1.13 \times 10^{-3}$. For a stable rf phase angle $\phi_s \sim 40°$, the voltage required to enclose the injected bunches is V $\approx$ 0.75 kV.

Therefore the energy spread, given by

$$\left(\frac{\Delta E}{E}\right)_{total} = F(\phi_s) \left(\frac{8eV}{\pi}\frac{1}{\eta}\frac{1}{hE}\right)^{\frac{1}{2}} \, , \tag{5.31}$$

with $F(40^{\circ}) = 0.45$ (Cole, 1964) and $h = 44$, is $(\Delta E/E)_{total} = 5.1 \times 10^{-4}$. The bunching factor, a function only of ϕ_s, is $B = 0.43$ (Cole, 1964). Thus the impedance limit for the injected bunches in ISABELLE is

$$\left|\frac{Z_n}{n}\right| \lesssim 5.5 \,\Omega \, . \tag{5.32}$$

This small impedance limit is a reflection of the fact that the frequency slipping factor is very small for large rings, especially when the injection energy is near the transition energy. Thus, compared to the ISR, where we have $\eta_{ISR} \approx 14 \, \eta_{ISA}$, the stability conditions are much more stringent for ISABELLE.

2. Transverse Oscillations: Dipole Mode

As a result of electromagnetic image fields produced in the surrounding medium, intense particle beams can develop transverse coherent oscillations as well as longitudinal density oscillations. In particular, if the electric image fields arise from resistive chamber walls, the result could be an exponentially growing transverse oscillation of the beam (Laslett, 1965).

However, an infinitesimal transverse coherence arising from beam noise can only be sustained if there is sufficiently small betatron frequency spread in the beam. If the frequency spread is large enough, finite coherence cannot materialize. This suppression of the instability is another manifestation of the phenomenon of Landau damping. For a given spread in beam betatron frequency, there exists a threshold beam current above which transverse coherence can develop.

Consider a distribution function in one of the transverse phase planes $[y, \dot{y} = dy/dt]$. For a beam of circulating particles, we may write this distribution function ψ as a function of θ, the ring azimuth and ν the betatron wave number; that is,

$$\psi \equiv \psi(y, \dot{y}, \theta, \nu, t) \quad . \tag{5.33}$$

The betatron frequency f_β is related to ν by

$$f_\beta = \nu f_o \quad . \tag{5.34}$$

It may be instructive to see how the Vlasov equation in this situation can be derived.   Consider a system whose time evolution is given by

$$\begin{aligned}
\dot{y} &= \partial H/\partial \dot{y} \\
\ddot{y} &= -\partial H/\partial y \\
\dot{\theta} &= 2\pi f_o \\
\dot{\nu} &= 0 \quad ,
\end{aligned} \tag{5.35}$$

where the transverse Hamiltonian is given by

$$H = \tfrac{1}{2}\dot{y}^2 + \tfrac{1}{2}(2\pi f_o \nu)^2 y^2 - y\, F\,(\theta, t) \quad , \tag{5.36}$$

with

$$F = \frac{e^2 c^2}{E_o \gamma} \xi_\perp\,(\theta, t) \quad . \tag{5.37}$$

The perturbing function $\xi_\perp$ is the transverse electric field averaged over the beam cross section. We limit ourselves to the relatively simple case of an unperturbed uniform beam, which is probably the case of primary interest in

ISABELLE. The more complicated bunched beam case has been studied in detail elsewhere (Courant, 1966; Sacherer, 1974). We also restrict our analysis to the case where the tune, ν, is not a function of betatron amplitude but only of an "external" variable, that is, the momentum, p, or average ring radius, R. Finally, we limit ourselves to the dipole mode of oscillation by including only the force term independent of y.

Since the number of particles in an infinitesimal volume, dV, remains unchanged as the system evolves in time,

$$\delta(\psi dV) = 0, \text{ after a time } \delta t \quad . \tag{5.38}$$

Then since for a conservative system the volume dV remains invariant,

$$\delta\psi = 0, \text{ after } \delta t \quad . \tag{5.39}$$

This is equivalent to the Vlasov equation,

$$\frac{d\psi}{dt} = 0 = \frac{\partial\psi}{\partial t} + \dot{y}\frac{\partial\psi}{\partial y} + \ddot{y}\frac{\partial\psi}{\partial\dot{y}} + \dot{\theta}\frac{\partial\psi}{\partial\theta} + \dot{\nu}\frac{\partial\psi}{\partial\nu} \quad . \tag{5.40}$$

Let us introduce the dipole moment per unit azimuth per unit tune, $D(\nu, \theta, t)$ and the number density per unit azimuth per unit tune, $\lambda(\nu, \theta, t)$, through the relations

$$D(\nu, \theta, t) = \int y\psi \, dy \, d\dot{y} \quad , \tag{5.41}$$

and

$$\lambda(\nu, \theta, t) = \int \psi \, dy \, d\dot{y} \quad . \tag{5.42}$$

Substituting into the Vlasov equation leads to the following equation for D:

$$\ddot{D} + (2\pi f_o \nu)^2 D = \lambda F \quad , \tag{5.43}$$

where the differentiation symbol d/dt is the total or hydrodynamic derivative,

$$\frac{d}{dt} \equiv \frac{\partial}{\partial t} + 2\pi f_o \frac{\partial}{\partial \theta} \quad . \tag{5.44}$$

Now consider a perturbed oscillation of frequency ω. Since there is no unperturbed dipole term, the perturbed dipole moment can be written,

$$D(\nu, \theta, t) = D(\nu, \theta) e^{-i\omega t} \quad . \tag{5.45}$$

For the charge density, only the unperturbed part is retained, since F is proportional to the perturbation:

$$\lambda = \lambda_o(\nu) \quad . \tag{5.46}$$

Writing the force in terms of a translation invariant kernel, K, (Sacherer, 1972)

$$F(\theta) = \int K(\theta - \theta') D(\theta') d\theta' \quad , \tag{5.47}$$

in which the time dependence is suppressed for simplicity. $K(\theta)$ is related to the transverse impedance kernel, $Z_\perp(\theta)$, and

$$D(\theta) = \int D(\nu, \theta) d\nu \quad . \tag{5.48}$$

Then a Fourier analysis leads directly to

$$D_n(\nu) = \frac{\lambda_o(\nu) K_n D_n}{(\omega_o \nu)^2 - (\omega_o n - \omega)^2} \quad , \tag{5.49}$$

with

$$\omega_o = 2\pi f_o \quad . \tag{5.50}$$

The quantities K_n and $D_n(\nu)$ are the Fourier components of the kernel $K(\theta)$ and $D(\nu,\theta)$, respectively, while

$$D_n = \int D_n(\nu) \, d\nu \quad . \tag{5.51}$$

Integrating over ν, the dispersion relation for the mode n is

$$1 = K_n \int \frac{\lambda_o(\nu) \, d\nu}{\left\{ (\omega_o \nu)^2 - (\omega_o n - \omega)^2 \right\}} \quad . \tag{5.52}$$

This can be written in terms of a normalized tune distribution function $N(\nu)$,

$$\int N(\nu) \, d\nu = 1 \quad , \tag{5.53}$$

and the Fourier transform of the transverse impedance kernel. Referring to this latter quantity by Z_T, a function of n, related to K_n by

$$K_n = \frac{i f_o e^2 c^2 \beta}{2\gamma E_o} Z_T \quad , \tag{5.54}$$

then the dispersion relation can be put in the form

$$1 = - \frac{iec I_o Z_T}{4\pi\gamma E_o \omega_o} \int \frac{N(\nu) \, d\nu}{\left\{ \left[(\omega/\omega_o) - n \right]^2 - \nu^2 \right\}} \quad . \tag{5.55}$$

This leads to the stability threshold (Hübner, 1970; Schnell, 1976),

$$I_o |Z_T| < F \frac{E_o}{e} \frac{4\nu\beta\gamma}{R} \Delta\nu \quad , \tag{5.56}$$

where F is a form factor depending on the tune distribution, never varying much

from unity, and $\Delta\nu$ is the tune spread, the full width at half maximum.

For transverse oscillations, coherence damping comes from the spread in tune. Since in ISABELLE the tune spread from momentum spread can be adjusted through the chromaticity (i.e., by sextupoles), there is a degree of direct control over the potential instability.

Upon solving the dispersion relation, only modes with $n > \nu$ are found to be unstable. The frequency of the unstable oscillation for a given mode, n, is therefore, near

$$f = (n - \nu) \, f_o \quad . \tag{5.57}$$

Actually, decoherence of an incipient transverse oscillation can result not only from a tune spread, but from a spread in revolution frequency, Δf_o. Taking this into account properly, the threshold criterion is

$$I_o \left| Z_T \right| < F \, \frac{E_o}{e} \, \frac{4\nu\beta\gamma}{R} \, \left| \Delta\nu + (n - \nu) \, \frac{\Delta f_o}{f_o} \right| \quad . \tag{5.58}$$

This has an interesting implication. For high mode numbers, if the chromaticity

$$\xi = p \, \frac{\partial \nu}{\partial p} \tag{5.59}$$

and the frequency slip factor,

$$\eta = - \, \frac{p \partial f_o}{f_o \partial p} \tag{5.60}$$

have different signs, then certain high order modes will be particularly susceptible to instability. Thus, in the ISABELLE design, the working line (in tune) is so chosen that both vertical and horizontal chromaticities are positive.

Noting that ISABELLE operates above transition, η is also positive. Thus $\Delta\nu$ and Δf_o have the same signs and their contributions to Eq. (5.58) always add.

For the case of a smooth, resistive vacuum tube wall of radius b and a circular beam (radius a),

$$Z_T = iRZ_o \left[\frac{1}{\beta^2\gamma^2} \left(\frac{1}{a^2} - \frac{1}{b^2} \right) - (1 + i) \frac{\delta}{b^3} \right] , \qquad (5.61)$$

where $Z_o = \mu_o c$ is the free space impedance, μ_o is the free space permeability, and δ is the skin depth at the unstable oscillation frequency, f, given by

$$\delta = \left(\frac{\rho}{\pi\mu_o f} \right)^{\frac{1}{2}} , \qquad (5.62)$$

with ρ the wall resistivity. It is tacitly assumed that δ is smaller than the wall thickness.

It is clear from the form of the impedance that at low energy (low γ), the beam dependent part, i.e., $Im(Z_T)$, could be important, while at high energy the tube radius is the important parameter. To see the relative importance of these two parameters, beam density and tube radius, consider the constraint that each imposes separately on the length of the working line; that is, what is the minimum $\Delta\nu$? Taking the form factor, $F = 1$, we have

$$\Delta\nu > \frac{eI_o R|Z_T|}{4\nu\beta\gamma E_o} , \qquad (5.63)$$

where

$$|Z_T| = \frac{\sqrt{2}\, RZ_o\delta}{b^3}, \text{ for the case of dominating wall resistivity,}$$

and

$$|Z_T| = \frac{RZ_o}{\beta^2\gamma^2a^2} , \text{ when the beam density term dominates.}$$

We use the ISABELLE parameters, I_o = 10 A, R = 471.1 m, ν = 25.6, γ = 31.4 (injection energy of 29.5 GeV), b = 4 cm, and a = 3.3 mm (a corresponds to the half beam size or twice the rms size). The lowest unstable mode, n = 26, gives a frequency, f $\approx$ 40.6 kHz and corresponds to a skin depth for stainless steel of δ = 2.4 mm. This is larger than the vacuum tube wall thickness and the image field at this frequency will, in fact, penetrate. In any case, the required tune spread is not too sensitive to the skin depth. We could, for example, replace this by the chamber thickness, say t = 1.5 mm. Thus, we find that the minimum values of $\Delta\nu$ are given by $\Delta\nu$ > 0.025 due to the beam density term and $\Delta\nu$ > 0.01 due to the resistive wall. The required spread due to the high beam density is larger in the bunched stack and could go as high as 0.03 – 0.035 just prior to acceleration. In the ISABELLE design such a beam tune spread can be accommodated between the 5th and 3rd order resonances with the working line chosen to occupy the region between ν = 25.6 and 25.67.

If the working line is not straight, the tune distribution function becomes modified with a resulting decrease in the current threshold. This phenomenon has been observed at the ISR (Zotter, 1972) and is referred to as the "brick wall effect" (Month, 1973a). In the ISR the curvature arises predominantly from image space charge fields. In ISABELLE, on the other hand, because of the large radius circular vacuum chamber this effect is not expected to be as serious; although because part of the stacked beam must be off the central axis, the effect on the working line is not negligible (Zotter, 1975a). Therefore, for this reason as well as the working line distortion resulting from magnetic field errors, three high order multipole terms (octupole, decapole, and duodecapole) are being designed into the ISABELLE magnets for the purpose of shaping the working line.

It should be pointed out that direct feedback damping of "small" oscillations could in principle be used, thus reducing the need for Landau damping. This technique has been tried at the ISR with some limited success (Thorndahl, 1973).

D. The Beam-Beam Interaction

When two beams collide, they exert an electromagnetic force upon each other. The force is in fact similar to the direct space charge force on a particle in an intense beam. Both forces are highly nonlinear, the extent of the nonlinearity depending on the transverse beam distribution. However, there are two major differences. First, the beams are moving in opposite directions. This means that the characteristic cancellation of electric and magnetic contributions does not occur in the beam-beam case. In particular, the single beam direct space charge force is proportional to $(1-\beta^2)$, while the beam-beam force is proportional to $(1+\beta^2)$. For high energy collisions $\beta \rightarrow 1$ and the direct single beam force goes to 0 like $1/\gamma^2$, while the beam-beam force approaches the constant value 2. This makes the beam-beam force important even at high energies, contrary to the direct single beam space charge, which diminishes in importance at high energy. A second major distinction between the two types of forces is that the single beam force is essentially uniform around the ring circumference; on the other hand, the beams collide only at a few discrete azimuthal locations. The significance of this is that the beam-beam force is rich in azimuthal harmonics, contrary to the direct single beam force which is dominated by the 0th harmonic. This characteristic makes the beam-beam nonlinearity a factor of importance. The reason is simply that the nonzero azimuthal harmonics are responsible for the excitation of nonlinear resonances which in turn are responsible for the deleterious effects of the beam-beam interaction.

Once the transverse beam distribution is given, the beam-beam force can be completely characterized by one strength parameter (Amman, 1973; Keil, 1972; Month, 1975a). For two beams colliding at an angle, α, and for a Gaussian beam distribution, this strength parameter can be written,

$$\xi = \left(\frac{2}{\pi}\right)^{\frac{1}{2}} \left(\frac{I}{ec}\right) \frac{r_p \beta_v^*}{\pi \gamma \alpha \sigma_v^*} \quad , \tag{5.64}$$

where r_p is the classical proton radius. We have written only the vertical beam-beam strength parameter, assuming the beam crossing to be in the horizontal plane. Under this condition, the $1/\alpha$ term in the horizontal force vanishes. Thus, only terms of higher order in $1/\alpha$ enter, i.e., only the long range beam-beam interaction contributes to the horizontal beam-beam force. It can be shown in fact that retaining only the $1/\alpha$ term is valid when (Keil, 1973)

$$\frac{\alpha \beta_h^*}{\sigma_h^*} > 1 \quad ; \tag{5.65}$$

that is, α greater than a few mrad. We can readily assume that any practical design will satisfy this criterion, meaning that it is adequate to ignore terms of order $(1/\alpha^2)$ and further that the beam-beam force is essentially a one-dimensional interaction. That is, only the vertical force is relevant for horizontal crossing, and so only vertical resonances are excited.

The beam-beam force during ideal collisions (i.e., beam centers super-imposed) is an even function of transverse displacement and thus its lowest multipole is the gradient (defocusing) term. The strength parameter has con-ventionally been normalized so that it is equivalent to the linear tune shift

in each collision region: i.e., $\xi = (\Delta\nu)_{bb}$, per interaction (Buon, 1974; SPEAR, 1973). This quantity is related to the first term in an expansion of the perturbing vertical electric field, E_v, in the vertical displacement, y, and can be expressed as

$$\Delta\nu_{bb} = \frac{1}{4\pi} \int \beta_v(s) k_v(s) \, ds \quad , \tag{5.66}$$

where

$$k_v(s) = \left(\frac{e}{E_o}\right) \frac{(1 + \beta^2)}{\beta^2 \gamma} \left[\frac{\partial E_v}{\partial y}\right]_{y = 0} \quad . \tag{5.67}$$

It has become customary to speak of the tune shift per interaction, $(\Delta\nu)_{bb}$, as representing the total beam-beam interaction and assigning an upper limit to this value. This so-called beam-beam limit is supposed to represent the maximum tolerable beam-beam strength, above which one or more of the following are unacceptable: beam loss rate, the induced background to experiments, or the beam lifetime.

Although it is apparent that the nonlinear resonance excitation charac-teristic of the interaction of two beams plays a dominant role, the precise mechanism through which the nonlinear beam-beam force exerts its influence on the beam lifetime and loss rate is a matter of some dispute. The central point of the dispute is whether the nonlinear beam-beam resonances act in a manner consistent with a conventional, isolated resonance treatment or whether these effects are a result of the combined influence of many resonances acting simultaneously (Month, 1975b).

The conceptual basis for the multiresonance approach is the simulation of stochastic behavior by the interaction of overlapping resonances. Stochastic behavior is known to occur in strongly nonlinear systems or at sufficiently

large betatron amplitudes. For a given beam, the question to be answered is,

at what beam-beam strength does typical stochastic behavior begin to develop?

Although, in principle, this is a well defined mathematical question and

could possibly be answered by sophisticated methods which exist (Henon, 1969;

Eminhizer, 1976), a quantitative analysis still eludes us.

However, there are two approaches which have been tried in an attempt to

shed some light on this question. First, there is the speculative theory of

Chirikov (Zaslavskii, 1972). He conjectures that if the nonlinear resonances

extend their influence over larger and larger regions of tune space, eventu-

ally they will overlap, and at this point, the motion will become stochastic.

The Chirikov criterion of overlap has been applied to the case of an ellipti-

cal beam of Gaussian density (Keil, 1972). Rough agreement was obtained with

the observed beam-beam limit in electron-positron machines (Keil, 1971b), where

a limiting tune shift on the order of ~ 0.05 is found. However, there are cer-

tain unsatisfactory aspects of this calculation. First, the resonance widths

are calculated using a multipole expansion. This by itself cannot be a mean-

ingful quantity for "weak" particles (i.e., those feeling the force) moving near

the fringes of the "strong" beam (i.e., the particles causing the force) where

the force is rapidly decreasing. Second, this calculation of the stochasticity

limit ignores the rather strong resonance detuning terms which, for single

resonances, are stabilizing factors. In light of this, it would seem that a

more comprehensive justification of this approach is needed. A second means

of looking at stochastic phenomena in the electromagnetic interaction of two

beams has been through the use of numerical simulation (Laslett, 1974). The

results of such computations are inconclusive. On the one hand, it appears

clear that for sufficiently large beam-beam strengths the system is unstable.

On the other hand, the dependence of the instability on various parameters such as

tune, time, and initial conditions is vague and uncertain. The situation is further compounded by the numerical accuracy problems inherently associated with strongly nonlinear equations. In fact, the only conclusions that can be derived from this approach at present are rough limiting strengths (Month, 1975b).

However, the existence of a limiting beam-beam strength is not in question. The question is whether the limitation which develops first is connected with the "stochasticity limit," or whether perhaps other effects enter as the primary limitation on colliding beam performance. A counter suggestion to the multiresonance approach is that single resonance effects could be significant, although the mechanism by which they are manifested is more complicated than for standard nonlinear resonance effects (Jejcic, 1971; Hereward, 1972; Augustin, 1970; Ruggiero, 1973; Keil, 1972; Month, 1975a,b).

It has been shown at the ISR that beam growth and beam loss result from the excitation of nonlinear beam-beam resonances (Bryant, 1974; Henrichsen, 1974), and one should expect such effects in any future p-p storage ring complex. However, there are two related conceptual difficulties in understanding just how single resonances could be the source of such beam growth. First, beam-beam resonances have only a short range in betatron amplitude, with the width dropping off rapidly at the edge of the "strong" beam; and second, they are associated with large detuning factors. That is, any particle on resonance would be detuned from that resonance as its amplitude changed because of the large variation of tune with amplitude. This was, in fact, the basis of the historical statement that resonances of order 5 or higher were ineffective because of the "large" octupole detuning characteristic of ordinary machines (Schoch, 1957).

The clue as to how single resonances might in fact cause such beam growth was the recognition that there must be a mediating resonance feeding process. It has been pointed out that scattering processes can induce momentum diffusion and through the chromaticity, tune fluctuation and drift. In this way particles are fed into the resonant tune range for particular single resonances. Momentum diffusion arising from intrabeam scattering is the strongest of such scattering processes in the ISR and this seems to be the dominant resonance feeding mechanism (Hereward, 1972; Keil, 1973a; Month, 1975a,b). However, bringing particles into resonance is not enough. In a coasting proton beam, where there is no tune modulation such as is caused by the synchrotron motion in a bunched beam, one might expect that in the presence of sufficient nonlinear detuning the resonances would be quite harmless, producing only a slight effective betatron amplitude increase (Schoch, 1957). This is in fact not the case. With tune modulation, nonlinear resonances, even in the presence of large detuning, can cause significant amplitude growth and beam loss to an aperture boundary (Chao, 1974). Thus, it has been suggested that in addition to feeding a resonance, tune diffusion into, within, and out of a resonance can allow trapped particles to stream toward the physical aperture boundary (Hereward, 1972; Month, 1975a,b; LeDuff, 1972).

One approach to combining the effects of tune fluctuation and nonlinear resonances is to include the resonance in the form of streaming terms in a diffusion equation for the tune drift. The basic idea is that the resonance will enhance the diffusion or beam growth rate. LeDuff found an approximate expression for a threshold and diffusion growth rate depending on the beam-beam strength as well as on the distance of the mean tune from resonance (LeDuff, 1972). Hereward, on the other hand, found that the diffusion rate was significant in determining whether amplitude growth was enhanced (Hereward, 1972). It was conjectured that the physical mechanism for the growth is simply

that the tune fluctuations can cause particles to jump randomly from one invariant curve to another. This method of dealing with the problem emphasizes the diffusion process and in order to obtain solutions to the Fokker-Planck equation, drastic approximations to the resonance form are necessary. For example, Hereward neglects the dependence of the betatron resonance width on amplitude, while LeDuff uses an approximate linear dependence. This approach is thereby deficient to the extent that the enhancement depends on the particular details of the resonance characteristics, specifically the amplitude dependence of the resonance width and the nonlinear detuning.

Month (1975b) has applied the idea of combining tune diffusion with resonance excitation in a different way. Rather than superimpose the resonance as a streaming term in the diffusion equation, he treats the diffusion as a mechanism for tune variation and then determines the influence of this tune variation on the behavior of a beam of particles (the weak beam) near a beam-beam resonance induced by the strong beam. The weakness here is that the diffusion process is simplified to the extent that the fluctuation becomes equated to a smooth drift. The particle loss mechanism proposed is via the migration in betatron amplitude of particles trapped in phase space islands created by the nonlinear beam-beam resonances. The motion of these islands is governed by the tune drifting in a random walk. The islands pass through the beam of particles (in phase space) and the rate of their motion determines whether or not particles will be trapped by a drifting island. Thus, even though the islands are small due to the large detuning characteristic of the beam-beam resonances, there can be a slow beam loss determined essentially by the rate of diffusion feeding superimposed on the continuous trapping and transport of particles from small to large amplitudes.

The effects of the beam-beam interaction have surfaced at the ISR at far lower values of $(\Delta v)_{bb}$ than might have been anticipated. The tune shift at the ISR is typically $(\Delta v)_{ISR} \approx 3 \times 10^{-4}$ for a beam of current ~ 10 A. Even at this low level there is clear evidence of the excitation of high order odd nonlinear resonances. Strong resonant behavior for resonances as high as the 7th have been studied and even higher order resonances observed (Bryant, 1974; Henrichsen, 1974). However, due to the symmetry of the beam-beam force, only even-ordered resonances can be excited when the beams are ideally colliding, i.e., with their centers matched. Thus, the strong excitation of odd-ordered resonances is clear evidence that the beam-beam tune shift is not the only parameter involved. Indeed, it was discovered that the extra excitation parameter was the beam separation at the collision point, and to keep the loss rate down to the level of the beam-gas loss rate (i.e., $\dot{I}/I \sim 10^{-6}$ min^{-1}), control of beam position must be in the region of 0.1 mm or about 5% of the rms beam size (Bryant, 1974). In ISABELLE these two parameters, beam-beam tune shift and relative beam-beam position, must be carefully controlled. Given a beam position control tolerance in ISABELLE of ~ 0.03 mm, it is likely that a background acceptable for most experiments can be achieved. To attain this end, the ISABELLE design has been conceived so that standard conditions are characterized by beam-beam tune shifts only about four times higher than at the ISR, although if higher background is tolerable, there is the potential capability of going to higher tune shifts and therefore higher luminosities than the nominal values quoted (ISABELLE, 1976).

E. Effects of Scattering Processes

1. Nuclear Scattering from the Residual Gas (Single Events)

Beam protons will have interactions with the nuclei of the residual gas. The loss rate due to single nuclear scattering events (assumed large enough to cause particles to be lost to the beam aperture boundary) can be written

$$(\dot{I}/I)_{bg} = - cn\sigma \quad . \tag{5.68}$$

Here n is the density of molecules per unit volume, c the velocity of light, and σ the total nuclear scattering cross section for protons interacting with the nuclei of the gas molecules within the vacuum chamber, that is, the nucleon cross section times the mean number of nucleons per molecule. In terms of P, the average gas pressure, the density is

$$n = kP \quad , \tag{5.69}$$

where k is a constant having the value $k = 3.3 \times 10^{16}$ molecules/cm^3 Torr. Thus, the beam-gas loss rate is given by

$$(\dot{I}/I)_{bg} = - ck\sigma P \quad . \tag{5.70}$$

Taking $\sigma_{nucleon} = \sigma_{pp} = 40$ mb, we have for pure hydrogen, $\sigma = 80$ mb. For an average pressure of 10^{-11} Torr, the loss rate $\approx 3.0 \times 10^{-6}$/hour. For pure N_2 or CO, on the other hand, the loss rate increases to 40×10^{-6}/hour.

The nuclear scattering from the interaction of the two beams also contributes to the loss rate and it is interesting to compare this with the beam-gas loss rate. For n_{INT} interaction regions, the beam-beam loss rate is given by

$$(\dot{I}/I)_{bb} = - \frac{ef_{rev}n_{INT}\sigma_{pp}L}{I} \tag{5.71}$$

where σ_{pp} = 40 mb is the total p-p cross section, L is the luminosity, I is the average beam current, and f_{rev} is the proton revolution frequency. For eight intersections, with I = 10 A, and L = 10^{33} cm^{-2}sec^{-1}, then $(\dot{I}/I)_{bb}$ = 1.9 x 10^{-3}/hour. If, however, seven intersections have a luminosity 10^{32}, while only one has a luminosity 10^{33}, then $(\dot{I}/I)_{bb}$ = 4 x 10^{-4}/hour.

Thus, the loss rate of protons from each beam due to beam-beam nuclear scattering events is much larger, for the parameters considered, than the loss due to beam-gas scattering.   In obtaining these loss rates, we have assumed that the total   cross section is roughly 40 mb and energy independent. This is not strictly true, especially in the unknown energy region of hundreds of GeV, but it is adequate for the estimations required here.

2. Beam-Gas Multiple Scattering

Multiple Coulomb scattering of protons from the atomic electrons of the residual gas causes the proton beam emittance to grow. This diffusion process induces a linear growth with time. We give a short derivation of the beam-gas multiple scattering growth rate.

The rms multiple scattering projected angle, $\langle\theta\rangle$, can be expressed by (Bethe, 1953)

$$\langle\theta\rangle = \frac{15}{p\beta}\left(\frac{\ell}{\ell_{rad}}\right)^{\frac{1}{2}} , \tag{5.72}$$

where p is the proton beam momentum in MeV/c, ℓ is the length of the scatterer, or in our case the length of the orbit of time Δt,

$$\ell = c \ \beta \ \Delta t \quad , \tag{5.73}$$

and ℓ_{rad} is the radiation length of the scatterer. For hydrogen gas

$$\ell_{rad} = \frac{5 \times 10^6}{P} \text{ meters} \quad , \tag{5.74}$$

with the pressure P in Torr. Since the change in beam vertical emittance is related to the scattering angle by

$$\Delta \varepsilon_v = \frac{4\pi R}{\nu} \langle \theta \rangle^2 \quad , \tag{5.75}$$

we obtain the growth rate for the fractional change in rms beam height,

$$\frac{1}{\sigma_v} \frac{d\sigma_v}{dt} = \frac{0.03 \ \pi R P}{\nu \ E_v \ \beta^2 \ \gamma} \quad , \tag{5.76}$$

where E_v is the normalized vertical beam emittance. For gases other than hydrogen, the multiple scattering pressure is proportional to $Z_{gas}(Z_{gas} + 1)/Z_H(Z_H +1)$, with Z the number of atomic electrons. Taking typical ISABELLE parameters, with pressure $P = 10^{-11}$ Torr (assuming pure hydrogen), then we find a multiple scattering growth rate, 0.3×10^{-4}/hour at 30 GeV and less at higher energies. The time in which the beam height grows by 1% is therefore $\sim$320 hours. For 5% heavier gases such as CO and 95% hydrogen the multiple scattering pressure increases by 1.7, and the time for a 1% growth in beam height is $\sim$200 hours. Thus, beam-gas multiple scattering does not have a significant effect on ISABELLE performance.

3. Experimental Background from Beam-Gas Interactions

The experimental detecting equipment at the intersection point of the beams will experience particle background which arises as a result of beam gas

interactions. These interactions in the long straight sections produce many particles, some of which strike the beam vacuum tube producing yet further unwanted particles. In these straight sections there are no bending magnetic fields which, in the curved part of the machine, tend to sweep produced particles out of the machine. Calculating the exact background from beam-gas interactions is difficult and only possible using computer techniques. A simple calculation of the total particle production in a straight section shows how important it is to produce a very good vacuum indeed and thus reduce the potential problem.

From the beam-gas nuclear loss rate given earlier and assuming a uniform interaction rate over the entire ISABELLE circumference, we have for the interaction rate over a length ℓ,

$$\dot{N} = \frac{I}{ec} \ell \left| \dot{I}/I \right|_{bg} \, .$$

(5.77)

Assuming pure hydrogen, $\sigma = 80$ mb, $I = 10$ A, and $P = 10^{-11}$ Torr, we have, with ℓ in meters and $\dot{N}$ in sec^{-1},

$$\dot{N} = 174 \, \ell \, .$$

(5.78)

The total particle background includes the average multiplicity of produced particles. Ferbel (1976) gives the most recent data on charged particle multiplicities in hadron-hadron collisions,

$$m = A + B \ln s + c(\ln s)/s^{\frac{1}{4}}$$

(5.79)

where s is the square of the c.m. energy and for pp collisions

$$A = 5.35 \pm 1.5$$

$$B = 1.36 \pm 0.05$$

(5.80)

$$C = -4.26 \pm 0.92 \, .$$

We then have for 200 GeV particles striking gas nuclei

$$m(\text{charged particles}) \approx 8$$

and including neutrals

$$m(\text{total}) \approx \frac{3}{2} m(\text{charged}) \approx 12 \quad .$$

For a length $\ell = 60$ m and remembering that we have two beams

$$2\dot{N}m \cong 2.5 \times 10^5 \text{ particles/sec} \tag{5.81}$$

produced in beam-gas interactions which must be considered a general background, not associated with beam-beam interactions. At the ISR the vacuum in the straight sections is nearer 10^{-12} Torr and thus the beam-gas background is not a problem. This would also be true for ISABELLE.

For completeness we also indicate the particle production rate in the desired beam-beam collisions. Again we assume $\sigma_{pp} \approx 40$ mb, $L \approx 10^{33}$ cm^{-2}sec^{-1}, so the interaction rate (at one intersection point) is 40×10^6 sec^{-1}. The extrapolated charged particle multiplicity from Ferbel is ≈ 20, or a total of charged and neutral particles of ≈ 30. Thus the particle production rate is $\approx 1.2 \times 10^9$ sec^{-1}.

4. Pressure Bump Current Threshold

The observation at the ISR of rapid beam decay associated with localized pressure rises (i.e., pressure bumps) was the first indication of a current dependent vacuum instability. It has in fact been established that the mechanism for this instability is the ionization of the residual gas by the beam and the subsequent bombardment of the chamber surface by energetic positive ions. These bombardments liberate surface molecules by desorption, increasing the pressure, which further increases the ionization (which is proportional to

beam current times pressure), and so on, resulting in the avalanche process characteristic of the instability.

The instability has been analyzed by including a beam desorption term in the dynamic vacuum equation (Fischer, 1972; 1973). The variation of gas density,n, in a tubular vacuum chamber as a function of time, t, and position, x, along the tube is governed by the second order partial differential equation

$$A \frac{\partial n}{\partial t} = a + bn + C \frac{\partial^2 n}{\partial x^2} \qquad (5.82)$$

where

$$a = \pi d G \quad,$$

with d the diameter of the circular tube and G the outgassing of the surface, i.e., molecules per unit surface area per unit time; b is the coefficient for gas desorption per unit length of tube per unit time; $A = \pi d^2/4$ is the tube cross section area; and C is the specific conductance of the tube. The quantity b can be expressed by

$$b = \eta \, \sigma \, (I/e) - \frac{1}{4} \pi d \, \bar{v} \, s \quad, \qquad (5.83)$$

where η is the net desorption factor, the effective number of molecules desorbed per ion incident on the surface, σ is the ionization cross section, I is the proton current, $\bar{v}$ is the average velocity of the residual gas molecules, and s is the sticking coefficient. In both the ISR and ISABELLE vacuum designs the sticking coefficient is so small that the second term can be disregarded. We consider the case of a tube of length L with pumps on either end, each of pumping speed S. The boundary conditions for such an idealized system, equalizing the gas flow at the two

pumps, are given by

$$C \frac{\partial n}{\partial x} = Sn/2 \text{ at } x = -L/2 \quad ,$$

and

(5.84)

$$C \frac{\partial n}{\partial x} = -Sn/2 \text{ at } x = +L/2 \quad .$$

If $\eta > 0$, which is usually the case even for chamber surfaces baked to high temperatures, the solution of the density equation with these boundary conditions leads to an instability threshold for the beam current. Above this threshold a finite equilibrium pressure cannot exist, signifying the onset of a pressure blowup. The critical current is found to be given by the expression

$$(\eta I)_{crit} = \frac{4eC}{\sigma L^2} \chi^2 \quad ,$$

(5.85)

where χ is the lowest root of the transcendental equation

$$\chi \tan \chi = \frac{SL}{4C} \quad .$$

For high pumping speeds, we approach the "conductance limited" case, that is, the solution χ approaches $\frac{1}{2}\pi$ and the critical current becomes independent of the pumping speed. In the limit of high S, we therefore have

$$(\eta I)_{crit} = \frac{\pi^2 e \, C}{\sigma L^2} \quad .$$

(5.86)

The ion desorption factor, η, is a function of both the surface cleanliness and the energies of the incident ions. To achieve acceptably low values, surfaces must be thoroughly outgassed, perhaps by glow discharge or by baking

to 300°C for stainless steel. The gas conductance of a long pipe depends

strongly on the chamber geometry but rather weakly on the temperature, T, as

well as the atomic mass, M, of the residual molecules. For a cylinder of

diameter, d, the specific conductance can be expressed by

$$C = \left(\frac{\pi}{18}\right)^{\frac{1}{2}} \left(\frac{RT}{M}\right)^{\frac{1}{2}} d^3 \quad , \tag{5.87}$$

with R the gas constant, $R = 8.314 \times 10^7$ erg mol^{-1} K^{-1}. If d is expressed in cm,

then C can be written

$$C = 0.038 \left(\frac{T}{M}\right)^{\frac{1}{2}} d^3 \text{ (m-liter/sec)} \quad . \tag{5.88}$$

For example, taking typical ISABELLE parameters, d = 8 cm, M = 28 (CO),

a length between pumps, L = 5 m, a pumping speed, S = 500 liter/sec, and the

temperature of the gas in the chamber, T = 293 K (i.e., room temperature), we

find C = 63.1 m-liter/sec, and thus (SL/4C) = 9.9. This is sufficiently high

so that we are near the "conductance limited" condition. Using an ionization

cross section, $\sigma = 1.2 \times 10^{-18}$ cm^2, the value for 25 GeV protons on heavy mole-

cules such as CO, then there results $(\eta I)_{crit} \approx 33$ A. If, for example,

$\eta \approx 3$ (a value actually achieved at the ISR), we find a critical current limit

for ISABELLE, $I_{crit} \approx 11$ A.

5. Instability due to Coupled Oscillations of Electrons
Trapped in the Coasting Proton Beam

When an intense proton beam interacts with the rest gas, the molecules

become ionized. The liberated electrons can be trapped in the attractive

force field of the coasting proton beam. Thus the proton beam moving at

velocity (βc) contains within it free electrons which are essentially azimu-

thally stationary. With the use of clearing electrodes, an equilibrium

neutralization can be established. The neutralization factor, η_e, is defined as the ratio of the total number of electrons N_e, to the total number of protons, N_p

$$\eta_e = N_e/N_p \quad . \tag{5.89}$$

Each beam is influenced by the space charge field of the other and thus there arises the possibility of growing coherent oscillations (Hereward, 1971). The presence of frequency spread in both electron and proton beams implies Landau damping and a resulting current threshold for the instability (Keil, 1971a). For a given proton beam current, this becomes a limitation on the equilibrium neutralization, η_e.

In the case of high energy storage rings, the coupled oscillations are characterized by (1) very high frequency, (2) electrons and protons oscillating coherently at the same frequency, (3) very large electron frequency spreads due to the rapidly changing beam shape along the ring azimuth, and (4) very small proton tune spread relative to the electron spread.

The electron oscillation wave number for coupled vertical oscillations, ν_e, can be written as a function of the azimuthal distance, s, and is given by

$$\nu_e^2 = \frac{4N_p r_e \nu \beta_v(s)}{\pi b \; (a + b)} \tag{5.90}$$

where r_e is the classical electron radius, and a and b are the mean horizontal and vertical half sizes of the proton beam as determined by both betatron and momentum characteristics. Since ν_e varies as a function of s, it is not unreasonable to take as an estimate that the total spread in ν_e, Δ_e, is roughly equal to ν_e: i.e., $\Delta_e/\nu_e \approx 1$. To obtain a feeling for the magnitude of ν_e, one can take a typical value, given by

$$\nu_e^2 \text{ (typical)} = \frac{2N_p r_e \nu \gamma}{E} \quad , \tag{5.91}$$

which, with $N_p = 6.2 \times 10^{14}$ (10 A in ISABELLE), the tune, $\nu = 25.6$, the normalized betatron emittance, $E = 20 \pi \times 10^{-6}$ rad-m, $\gamma = 213$ (Energy = 200 GeV), gives $\nu_e \approx 1.7 \times 10^4$. In the case of a large electron frequency spread, the electron wave number actually corresponds to the coherent frequency for the most unstable mode (i.e., most rapid growth rate). This frequency is therefore approximately given by,

$$f_{ep} \approx \nu_e f_o = \frac{\nu_e c}{2\pi R} \quad , \tag{5.92}$$

or, with $R = 471.1$ m, $f_{ep} = 1.8$ GHz is obtained, a high frequency indeed. We note that this frequency varies with proton energy as $\gamma^{\frac{1}{2}}$.

Under the circumstances we have described, oscillations will not develop if the neutralization factor is small enough. Using the results of Keil and Zotter (1971a), we can obtain a simple approximate expression for the maximum allowable or threshold neutralization:

$$\eta_e < \left(\frac{4}{3\pi}\right)^2 \frac{\Delta}{(\Delta\nu)_p} \quad , \tag{5.93}$$

where Δ is the total tune spread in the proton beam and $(\Delta\nu)_p$ is the vertical proton tune shift for 100% neutralization,

$$(\Delta\nu)_p = \frac{N_p r_p}{\pi^2 \gamma R} \int \frac{\beta_v(s)ds}{b(a+b)} \quad . \tag{5.94}$$

This shift is especially large in the case of storage ring designs, such as ISABELLE, with long straight sections having no dispersion. For example, in the ISABELLE design, about 45% of the circumference is without dispersion. Because of the comparatively high beam density here, the tune shift is dominated by the contribution from this region. Keeping this in mind, we can approximate the tune shift by

$$(\Delta\nu)_p \text{ (approximate)} = \frac{N_p r_p f_I}{E} , \qquad (5.95)$$

where f_I is the fraction of the circumference where there is zero dispersion. For ISABELLE parameters, taking $f_I = 0.45$, this expression yields $(\Delta\nu)_p = 7.1$. If the actual neutralization is $\eta_e = 10^{-3}$, this corresponds to a real tune shift for the protons of $(\Delta\nu)_p(\eta_e = 10^{-3}) = 7 \times 10^{-3}$, which by itself is acceptably small.

However, to avoid any vertical beam size growth, i.e., to avoid an unstable condition for e-p oscillations, we must have the neutralization smaller than this value. Taking a total spread of 0.015 (say, from chromaticity) and a shift of 7.1, we obtain a threshold neutralization, $\eta_e < 3.8 \times 10^{-4}$.

Such a low level of neutralization appears attainable with a sufficient number of clearing electrodes (Angerth, 1971; Herrera, 1976). Although not explicitly stated, it is implied in our analysis that such a low level of neutralization is really required only in the nondispersion regions of the lattice, where the beam is dense. In the cells and particularly in the regions where the beam has high dispersion and is much less dense, the clearing criterion can be relaxed.

6. Multiple Coulomb Scattering of Protons in an Intense Beam (Intra-Beam Scattering)

Particles in a beam can Coulomb scatter off one another leading to the possibility of beam growth. The term "intra-beam scattering" is used to designate multiple Coulomb scattering. The effect of this interaction is a coupling of the mean betatron oscillation energies and the longitudinal energy spread. Above the transition energy the total oscillation energy can increase and there results a diffusion-like change in the horizontal and vertical beam emittances and energy spread.

A nonrelativistic analysis in the beam c.m. system leads to expressions for the rate of change of the three beam parameters, vertical and horizontal betatron emittance and momentum spread. The scattering involved does not imply that all three of the oscillation energies must necessarily increase. In fact, for the ISABELLE machine parameters, the oscillation energy corresponding to the vertical emittance is found to decrease initially.

The rate of change of relative beam rms height, σ_v, betatron rms width, σ_h, and total momentum spread, $(\Delta p/p)_T$, have been derived by Piwinski (1974) and are expressed respectively by

$$\frac{1}{\tau_v} = \frac{1}{\sigma_v}\frac{d\sigma_v}{dt} = A\, f(a, b, c) \quad , \tag{5.96}$$

$$\frac{1}{\tau_h} = \frac{1}{\sigma_h}\frac{d\sigma_h}{dt} = A\left\{ f\left(\frac{a}{b}, \frac{1}{b}, \frac{c}{b}\right) + (1 - t)\, f\left(\frac{b}{a}, \frac{1}{a}, \frac{c}{a}\right)\right\} \tag{5.97}$$

$$\frac{1}{\tau_p} = \frac{1}{(\Delta p/p)_T}\frac{d(\Delta p/p)_T}{dt} = 2Atf\left(\frac{b}{a}, \frac{1}{a}, \frac{c}{a}\right) \quad , \tag{5.98}$$

where

$$A = \frac{\pi r_p^2 I}{e(\Delta p/p)_T E_h E_v \beta^2 \gamma^2} \quad ,$$

$$a = \frac{1}{(\Delta p/p)_T} \left\{ \frac{\gamma E_v \left[E_h \beta_h + \bar{x}_p^2 \beta\gamma(\Delta p/p)_T^2 \right]}{\beta E_h \beta_h \beta_v} \right\}^{\frac{1}{2}} \quad ,$$

$$b = \left[\frac{E_v \beta_h}{E_h \beta_v} \right]^{\frac{1}{2}} \quad ,$$

(5.99)

$$c = \left[\frac{\beta\gamma E_v}{4\pi r_p \beta_v} \right]^{\frac{1}{2}} \left(\frac{ec}{I} \right)^{1/6} \left\{ E_v \beta_v \left[E_h \beta_h + \bar{x}_p^2 \beta\gamma(\Delta p/p)_T^2 \right] \right\}^{1/12} \quad ,$$

and

$$t = \frac{E_h \beta_h}{\left[E_h \beta_h + \bar{x}_p^2 \beta\gamma(\Delta p/p)_T^2 \right]} \quad .$$

The quantities β_h, β_v, and $\bar{x}_p$ are the average values of the betatron parameters for the ring, while E_h and E_v are normalized emittances. The function f is the 3-dimensional integral,

$$f(a,b,c) = 2 \int_o^\infty \int_o^\pi \int_o^{2\pi} \sin\theta d\theta d\phi dr \, \exp\left\{ -r \left[\cos^2\theta + (a^2 \cos^2\phi + b^2 \sin^2\phi) \sin^2\theta \right] \right\}$$

$$\ln(c^2 r) \, (1 - 3 \cos^2\theta) \quad .$$

(5.100)

This integral can be evaluated numerically and plots in a range of parameters relevant to ISABELLE are shown in Fig. 33. To use these curves, we require the relations,

$$f(a, b, c) = f(b, a, c) ,$$

and   (5.101)

$$f(a, b, c) + \frac{1}{a^2} f\left[\frac{1}{a}, \frac{b}{a}, \frac{c}{a}\right] + \frac{1}{b^2} f\left[\frac{1}{b}, \frac{a}{b}, \frac{c}{b}\right] = 0 .$$

Note that for certain parameter values the f function becomes negative. This is the mathematical statement corresponding to the point made above that the particle distribution can actually damp in one of the dimensions.

The impact of the changing momentum distribution is not limited to the growth in overall magnitude of the momentum width. Since the momentum is related to the betatron tune via the chromaticity of the ring, momentum change implies tune change. Thus particles may move in the tune space and cross resonances. Combined with a beam-beam resonance model, this mechanism for tune fluctuation and resonance feeding provides a qualitative understanding of the observations at the ISR of the loss rate under colliding beam conditions. A similar influence of intra-beam scattering on beam loss rates can be expected in ISABELLE, as has been previously discussed.

To obtain estimates of the "growth" rates for ISABELLE, we use the parameter values $E_h = E_v = 20 \pi \times 10^{-6}$ rad-m, $\beta_h = \beta_v = R/\nu = 18.4$ m, $\bar{x}_p = R/\nu^2 = 0.72$ m, and $I = 10$ A. Since the energy range for ISABELLE is such that $\gamma > 30$, then we can take $\beta = 1$. Two cases of interest for ISABELLE are at low energy, where $\gamma = 31.4$ and $(\Delta p/p)_T = 0.7\%$, and at high energy, where $\gamma = 213.2$ and $(\Delta p/p)_T = 0.15\%$. The results for the growth rate computations are given in

Table III. Since for ISABELLE we can take b = 1, we need compute only the
quantity f(a, 1, c) = f(1, a, c). The other value of f required can be ob-
tained through the relation

$$f\left(\frac{1}{a}, \frac{1}{a}, \frac{c}{a}\right) = -2 a^2 f(1, a, c) \quad . \qquad (5.102)$$

From Table III it can be seen that we need the values of $f(1, 1.92, 10.3 \times 10^3)$
for the low energy case and $f(1, 19.8, 26.2 \times 10^3)$ for the high energy case.
These can be computed directly or estimated roughly from Fig. 33. As can be
seen from the table, the momentum growth rate at the top ISABELLE energy is
quite high. This implies that the value assumed for the momentum spread will
not be sustained over long times, but rather will tend to increase until the
growth time is of the order of the operating period.

It should be mentioned that the "growth" rates are in fact a sensitive
function of the emittances and momentum spread. Thus, appreciable increases
in beam density would cause the initial rates to be larger (Hübner, 1975).
The impact of intra-beam scattering must therefore be kept in mind if one
attempts to increase beam density for performance reasons. It is also note-
worthy that the beam height will be maintained during the "density redistribution"

period and, so, as long as there is no particle loss, the luminosity should not be affected to any substantial degree.

F. The Momentum Aperture

The momentum aperture or acceptance in high energy p-p storage rings plays an important role in determining the performance capability. The question we seek an answer to is: how much momentum spread is possible in a given ring? Because the momentum is correlated with horizontal position, the momentum aperture used corresponds to a specific amount of horizontal space occupied and as such is related to the spatial aperture. However, they are not identical and are generally associated with different design criteria. The design fact which essentially determines the momentum aperture in ISABELLE is the presence of the experimental insertions. In effect, the inclusion of long straight lengths for experimental apparatus coupled with the "low β_v^* - long free space" objective results in a relatively small momentum acceptance for the ISABELLE design (Month, 1972; Garren, 1975; Edwards, 1975; Chasman, 1975; Donald, 1975; Autin, 1975).

To minimize the impact on lattice stability of adding a small number of experimental insertions (eight in ISABELLE), the linear orbit functions are matched to the lattice cells with appropriately chosen dipole and quadrupole magnets. This avoids fluctuations around the ring of the betatron amplitude functions, β_h and β_v, and the dispersion function, x_p. In fact, the dispersion function is brought to zero in the collision regions. This is an important factor in the maximization of both the luminosity and the specific luminosity, i.e., the luminosity per unit length, in that the orbits for the different momenta are superimposed in the collision regions, thus maximizing beam density. The particular dipole and quadrupole arrangement used in the ISABELLE design to accomplish the matching has been described in a previous section. However,

the matching procedure is performed only for a particular momentum, corresponding to a central orbit. For particles deviating from this central momentum, a mismatch results. Thus, the beta function, $\beta(s)$, becomes a strong function of momentum, p. In particular, the tune, ν, (Courant, 1958)

$$\nu = \frac{1}{2\pi} \int_0^C \frac{1}{\beta(s)} \, ds \qquad (5.103)$$

is strongly affected. The linear variation of tune with momentum is characterized by the chromaticity,

$$\xi = p \, \partial\nu/\partial p \quad . \qquad (5.104)$$

In general, for large machines with long insertions, ξ, as well as being a function of p, is also large and negative. For example, in the standard ISABELLE configuration, $\xi \approx -40$. This means for a momentum spread, $\Delta p/p \approx 1\text{-}2\%$, the corresponding tune spread is, $\Delta\nu \approx 0.4$ to 0.8, clearly intolerable.

To enlarge the momentum aperture, sextupoles must be added to remove the chromaticity. With two sextupole families, one set of coils placed in the focusing quadrupoles and another in the defocusing quadrupoles, the chromaticity can be reduced to zero for both horizontal and vertical tune functions (ISABELLE, 1976; Garren, 1975). However, removing the "first order chromaticity" leaves us with a residual tune variation with momentum of higher order in $\Delta p/p$. Figure 34 shows the residual vertical tune variation with momentum for the standard ISABELLE configuration and when one or two (symmetrically located) low-β insertions are added. In addition, the 1st order momentum variation of β around the ring circumference still remains, and in Fig. 35 we plot β versus p at the ring azimuth location where the maximum $\Delta\beta/\beta$ occurs. The effect of introducing low-β insertions is evident in both figures. To a

large extent the strong variation of ν and β with p is a direct result of the

high β value in the strong focusing magnet a distance $\ell_{free} \approx 20$ m away from

the collision point. For $\beta^* < \ell_{free}$, $\beta_{max} \approx \ell_{free}^2/\beta^*$. Thus for the low β

case, $\beta^* \approx 1$ m, and $\beta_{max} \approx 400$ m.

Although somewhat arbitrary, it appears that for optimum storage ring

performance we can take the momentum aperture to be that corresponding to an

approximately ±5% variation in β. Thus, the ISABELLE design provides a momen-

tum aperture of about 2% in the standard configuration, with about 0.5% when

one or two low β insertions are tuned in. It is interesting to compare

these numbers with the momentum aperture at the ISR of $\gtrsim$ 4%, where there are

also eight straight sections, but of far more modest length and β variation.

The impact on the betatron motion of the strong nonlinearity introduced

by the sextupole correction is minimal in ISABELLE as a result of the high

symmetry in the sextupole configuration, the choice of the working line, and

the small betatron emittances of the ISABELLE beam design (Garren, 1975;

Edwards, 1975).

G. The Spatial Aperture

By spatial aperture, we mean the radius of the circular vacuum chamber

used, although in the superconducting ISABELLE design there is some signifi-

cance in the magnet aperture, which is the inner diameter of the supercon-

ducting coils. There are several factors which enter into the choice of

the vacuum chamber aperture and they all favor choosing a large diameter.

However, the single factor which forces a limitation on the aperture size

is the cost of the magnet system. Thus, we choose the smallest aperture

consistent with a reasonable performance expectation on the one hand and a

reasonable cost on the other.

There are five items, of varying importance, which have played a role in determining the diameters of the vacuum chamber (8 cm) and the superconducting magnet coil (12 cm ID). These are:

1. the space required for beam occupation, including that needed for stacking beam; (ISABELLE, 1976)

2. the implications for the stacking process resulting from the proximity of the superconducting coils; (Month, 1976)

3. the space charge image effect when the beam is off axis; (Zotter, 1975a)

4. the sensitivity of the transverse coherent instability threshold to the vacuum chamber radius; and

5. the pressure bump instability threshold which is directly proportional to the conductance of the vacuum pipe, which depends on the cube of the chamber radius.

We will consider each of these subjects in more detail.

1. Aperture for Beam Occupation

We can divide the beam occupation area within the vacuum chamber into two functionally defined regions. First the beam size itself. Second the aperture needed for stacking the beam. There are two components contributing to beam size in accelerators, one arising from the intrinsic nature of the beam itself, the other from the linear focusing properties of the accelerator design. For an accelerator constructed in a horizontal plane, the accelerator median plane, the local rms vertical size may be written

$$\sigma_v(s) = \left[E_v\beta_v(s)/4\pi\beta\gamma\right]^{\frac{1}{2}} , \qquad (5.105)$$

where s is the distance along the orbit, $\beta_v(s)$ is a function characteristic of the linear focusing properties of the accelerator and independent of the beam itself, while the emittance, E_v, is a property of the beam independent of the linear properties of the accelerator. The horizontal beam size, on the other hand, is a superposition of betatron size and width due to momentum dispersion.

Because the momentum distribution tends to be somewhat uniform, while the beta-tron distribution tends toward a Gaussian shape, the total width can be approximated by arithmetic addition. The beam half-width can therefore be written (ISABELLE, 1976)

$$a = \tfrac{1}{2} \, x_p(s) \, \Delta p/p + 2\sigma_h(s) \quad , \tag{5.106}$$

where the rms horizontal betatron width is given by

$$\sigma_h(s) = \left[E_h \beta_h(s)/4\pi\beta\gamma \right]^{\tfrac{1}{2}} \quad , \tag{5.107}$$

and $\beta_h(s)$ and $x_p(s)$ are local betatron functions on the equilibrium orbit.

The linear focusing functions are strongly momentum dependent because of the presence of the experimental insertions. However, within the momentum acceptance chosen for operation, this effect has only a relatively small impact on beam size. The emittance is therefore the significant parameter determining the beam size. For a given linear machine, the normalized emittance is an invariant characteristic of the beam, and is independent of energy, although the beam size is a function of energy $(\gamma^{-\tfrac{1}{2}})$. The constancy of the emittance is, however, only true for an ideal linear machine. In real machines the magnetic field is non-linear, there are scattering processes, and furthermore the particles in the beam interact through electromagnetic forces which couple their motion to structures in the external environment and through direct electromagnetic inter-action. The effect of this is a kind of "2nd law" which states that for a given current the real beam emittance can never be less than the initial, linear, ideal emittance, but can effectively increase by phase space filamentation, scattering processes and unstable coherent oscillations. In fact, one of the main objec-tives of any storage ring design must be to keep the growth time of the emit-tance sufficiently long compared to the required lifetime for the performance of useful physics.

In real storage ring systems there is another source of emittance growth which arises from the practical need for a sequence of different accelerators to achieve high energies. The reason is simply that the accumulation of current is strongly dependent on energy. Thus, the direct transverse space charge force of a particle beam greatly limits the stacking of intense beams at low energies (Laslett, 1963). At high energy, the need for a large machine circumference in order to bend the beam in a circle leads to a limitation on the stacking of beams due to high frequency longitudinal impedances, as we have previously discussed. The important point to keep in mind is that the lower energy limit is a direct limit on beam storage, while at high energy the limit is on the stacking process and not on the stored current itself. This point is significant in that it means that highest energies are achieved with highest current when the final step is acceleration. In general, to achieve these optimum conditions, we require a sequence of circular accelerators with the last being a storage accelerator. Since each accelerator has its own beam size structure functions (beta and dispersion functions), any transfer errors or mismatching of the structure functions between successive accelerators lead to an emittance growth. All emittance growth processes are essentially irreversible and the spatial aperture must be designed to accommodate them.

The critical period, the time during which the largest aperture is required, is during injection and stacking. In ISABELLE, using the momentum stacking method, the critical aperture at injection is near the horizontally focusing quadrupoles (points of maximum horizontal size) and is given by

$$A_p = 8\sigma_h + x_p \, (\Delta p/p)_T + \Delta \, , \qquad (5.108)$$

where $(\Delta p/p)_T = (\Delta p/p)_{\text{coasting stack}} + (\Delta p/p)_{\text{injected pulse}}$, and Δ is a reflection of the septum width. Taking the ISR as a model, we expect Δ to be of order of 1.5 cm. We must also include in Δ the sagitta and the aperture required for residual closed orbit errors in the ring. This should amount to ∿2 cm of additional required aperture.

2. Effects of Random Construction and Placement Errors in the Superconducting Coils

The presence of current carrying coils just outside the beam aperture in superconducting magnets has the effect of making the magnetic field within the aperture sensitive to coil positioning and support errors. The immediate consequence is the creation of field multipole components at the magnet center which are strong functions of the radial distance to the coils. Furthermore, for orbits off the magnet center the strength of the miltipoles is rapidly amplified as the coils are approached. Since the momentum method of beam stacking requires the injected beam orbit to be substantially off the chamber center, this amplification effect could be significant (Month, 1976).

The amplification factor for off-center orbits is the ratio of multipole components off and on center and is a function only of the ratio of the displacement of the off-center orbit, x_o, to the coil radius, R_c. Introducing

$$t = x_o/R_c \quad , \tag{5.109}$$

a pseudotheoretical analysis leads to a simple expression for the amplification factor $r_{m-1}(t)$ for the multipole of order m (m = 1 corresponds to the dipole case):

$$r_{m-1}(t) = 0.7/(1 - t)^{m+\frac{1}{2}} \quad . \tag{5.110}$$

This mathematical form has been shown to be in rough quantitative agreement with a computer model for random errors in coil block positioning using a cos θ coil distribution, as in the ISABELLE design (Month, 1976). To emphasize the strong variation of the multipoles across the spatial aperture, we plot this amplification factor for the first few multipoles in Fig. 36. The dependence on both the distance from the chamber center and the multipole order is striking.

The coil block positioning errors induce effects in the general class of random azimuthal perturbations. These are associated with the excitation of betatron resonances. These resonances restrict the regions of operating tune to be sufficiently far removed from their resonant values. The excitation of many resonances means that the tune "aperture" could be spotted with disallowed regions. Since, in general, the tune aperture and available beam aperture are in one-to-one correspondence, any particular storage ring design must insure that the required aperture for stacking and storing is free from harmful resonances.

An important aspect of the type of resonances we are considering here is the fact that their character depends on their location within the aperture. Such behavior is a direct consequence of the variation of multipole errors across the aperture. We must know not only whether or not a resonance is present within the aperture, but also where specifically in the given aperture it is located. Thus, there is added a new constraint in the design of the beam occupation of the spatial aperture for superconducting storage rings.

Although in any storage ring design a careful analysis of all errors which induce resonant effects must be performed, the impact of the nearby coils within the magnet aperture appears to be the most critical for ISABELLE. To give a general overview of the consequences of these coil block errors, we will estimate the effects of one-dimensional resonances.

The resonance width for a linear resonance (m = 1) is defined such that when the unperturbed tune reaches its edges, the betatron function reaches infinite magnitude. The nonlinear resonance width for a resonance of order m (m > 2) is defined as the tune shift from the resonance at which the unstable fixed points enter the beam betatron boundary. Their rms values, $\delta \nu_m$, are estimated to be, for m = 2,

$$\delta \nu_2 = r_1(t) \left(\frac{2}{N_b n_{mag}} \right)^{\frac{1}{2}} \frac{2\beta \langle \delta \rangle}{R_c^2} \tag{5.111}$$

and for m > 2

$$\delta \nu_m = r_{m-1}(t) \left(\frac{a_\beta}{2R_c} \right)^{m-2} \left(\frac{2}{N_b n_{mag}} \right)^{\frac{1}{2}} \frac{m\beta \langle \delta \rangle}{2R_c^2} \quad , \tag{5.112}$$

where n_{mag} is the number of magnets containing errors, N_b is the number of statistically independent coil units around each magnet aperture in error, β is the mean value of the amplitude function at the azimuthal positions of the errors, $\langle \delta \rangle$ is the rms error in the location of each independent coil unit, R_c is the radius of the coil block, taken to be the coil inner radius, and a_β is the mean betatron half-size.

The three basic "linear" machine parameters are also affected by the presence of the coil blocks within the aperture and also manifest the amplification effect. Thus, for the rms closed orbit error, A_{co}, the rms tune shift, $\Delta \nu$, and the maximum β variation around the ring, $(\Delta \beta / \beta)_{max}$, taking d as the distance of the tune from resonance, we have

$$A_{co} = r_o(t) \left(\frac{1}{N_b n_{mag}} \right)^{\frac{1}{2}} \frac{\beta \langle \delta \rangle}{|d| R_c} \qquad (5.113)$$

$$\Delta\nu = \frac{1}{2}\delta\nu_2 \quad , \qquad (5.114)$$

and

$$(\Delta\beta/\beta)_{max} = \Delta\nu/|d| \quad . \qquad (5.115)$$

Using ISABELLE parameters, $n_{mag} \approx 125$, $N_b = 24$, $\beta \simeq 30$ m, $R_c = 6$ cm, $a_\beta = 4.3$ mm, and taking $\langle\delta\rangle = 5 \times 10^{-3}$ cm and, where appropriate, $d = 0.1$, we show in Table IV some estimates of effects on the beam parameters. From these results we can conclude that the beam should occupy a relatively small fraction of the coil aperture. In ISABELLE the choice to use $\sim 35\%$ of this aperture for the stack and injection seems quite appropriate.

3. Space Charge Effect due to Image Fields

Although a centered beam in a circular chamber induces no tune shift due to image fields, by symmetry, a tune shift does result for a wide stack in a circular chamber, and is especially enhanced for off-center orbits (Zotter, 1975a). The consequence is a variation of tune across the stacked beam as well as across the full spatial aperture. The working line in the (ν_h, ν_v) plane becomes curved. The strongest effect is felt by the injected pulses near the end of the stacking process when the stack is most intense. However, these errors are systematic, possessing the 8-fold azimuthal symmetry characteristic of the ISABELLE design. As such they can be controlled to a large extent by the systematic field error correction system (ISABELLE, 1976).

4. Spatial Aperture from Transverse Resistive Wall Instability

The resistive wall instability current threshold depends upon the cube

of the chamber diameter, d, and is related to the tolerable tune spread, $\Delta\nu$.

For a given value of $\Delta\nu \approx 0.02$, corresponding to a 10 A stack, and taking a

stainless steel chamber, we find (Eq. (5.63)) a minimum chamber diameter, d $\gtrsim$ 6 cm.

The choice of an 8 cm vacuum tube thus seems entirely consistent with resistive

wall effects.

5. Spatial Aperture for Pressure Bump Current Threshold

For an 8 cm diameter chamber, we have determined a current threshold which

can be written $(\eta I)_{critical}$ = 33 A, or, with $\eta \approx 3$, I < 11 A.   Since ISABELLE

conditions are such that the critical current is essentially proportional to

the conductance and the conductance is proportional to the cube of the diameter,

then all other factors remaining the same, a reduction of the vacuum chamber

diameter to, say, d = 6 cm, leads to I $\lesssim$ 4.7 A.   Thus, it is clear that the de-

sign value of 10 A for ISABELLE and the assumption of $\eta \approx 3$, essentially fixes

the diameter of the tube to be in the range of 8 cm from the pressure bump re-

quirement alone.

H. The Accumulation of Current in ISABELLE

High luminosity is the ultimate objective in accumulating current in col-

liding beam rings. To achieve this goal, two factors must be taken into con-

sideration. First, we must sustain a high betatron density throughout the dif-

ferent phases of the process from linac to fast accelerating synchrotron and

finally to storage accelerator. High transverse density translates directly

into high luminosity. The second point concerns the longitudinal characteris-

tics of the beam, i.e., the particle momentum distribution. In

general, the spread in momentum does not enter directly into the luminosity, but rather through the fact that the momentum spread is correlated with the beam size. However, collision points around the accelerator are discrete and few in number and the dispersion function at these points can be made locally zero. Thus the beam size, and hence the luminosity, can be made essentially independent of momentum spread. It follows then that to attain high currents, the optimal stacking mode is in momentum.

Because current is to be stacked in momentum space, there will be a continual change in the momentum distribution and current characteristics during the various phases of the accumulation process. The beam design must insure longitudinal stability during each stage. As previously discussed, the strongest limitation is more precisely stated as an upper limit on high frequency longitudinal impedances, which allow the beam to couple to itself via small structures in the surrounding environment. Such high frequency excitations are not amenable to feedback damping.

Although the impedance limitation is basic, there are also other considerations. One is the fact that the spread in momentum is an important factor in the momentum analysis of collision events, and it should not be excessively high. Another factor is that high current beams must be handled, i.e., transferred and accelerated by rf systems. A limit on the peak voltage for these systems is equivalent to imposing a maximum value on the beam momentum spread. In these latter considerations, the specific limitation can be expressed as a lower bound on the longitudinal density, that is, the current per unit momentum bite.

Although several alternative beam accumulation schemes have been considered, the most efficient and technically feasible procedure for beam accumulation is the momentum stacking method, a technique which has been studied extensively

and perfected at the ISR. This system has been adopted for ISABELLE. There are several important factors related to stacking which differ in ISABELLE from the ISR. The new factors which the ISABELLE design must contend with are: 1) the superconducting environment; 2) the relatively limited momentum aperture due to the long straight sections and the strong focusing in them; 3) the somewhat large proportion of the aperture of the superconducting coils of the magnets which must be used for stacking; and 4) the greater susceptibility of the injected bunches to high frequency longitudinal instability in rings of large circumference compared to the ISR.

Because the beams are in superconducting magnets, there is the possibility of magnet quenches resulting from radiation heating of the superconducting coils, the source of this heating being particle loss. For example, at the ISR, beam loss from injected pulses generally amounts to about 50%. In ISABELLE, the beam is stacked when the magnets are operating at low field and thus the temperature rise required to reach the quench limit is relatively large (Month, 1974b). This low field injection may be crucial for ISABELLE because of the high potential particle losses. As a further precaution, the use of scrapers and absorbers to prevent unstable particles from reaching the coils is being planned.

The relationship of a high current ISABELLE design to the momentum and spatial aperture requirements has been extensively considered in previous sections. The main point with regard to the stability of the injected bunches is the conflicting desires for, on the one hand, high betatron density and, on the other hand, high longitudinal density. To achieve high transverse density it would appear to be preferable to inject single turn into the AGS. This is an efficient process as compared to multiturn injection and would

involve fewer particles, $\sim 2 \times 10^{12}$ in the AGS. This would alleviate the complicated space charge conditions at the low AGS injection energy of 200 MeV. The problem is that for the same longitudinal density, the impedance limit is essentially proportional to the number of protons injected into ISABELLE per AGS pulse, and so the impedance limit would decrease to $|Z/n| < 1.9 \, \Omega$. Thus, the ISABELLE choice is a compromise between attaining high longitudinal density, important for stacking current, and high transverse density, ultimately meaning a collision diamond with higher particle density.

I. Performance of the Colliding Beam Complex

In the analysis we have presented, it has become clear that underlying the performance of a colliding beam device are the basic beam invariants that are transferred from point to point in the system. It is fundamental that these, the horizontal and vertical emittance and the equivalent coasting beam momentum spread, cannot be reduced but, in fact, will tend to increase depending on the magnetic and space charge environments at the various stages as well as on errors in the transfer junctions. With this in mind, together with the constraint of facilities' cost, we have arrived at an ISABELLE colliding beam complex.

The ISABELLE system is composed of Linac (acceleration to 200 MeV), AGS (stacking of 6×10^{12} protons and acceleration to 29.5 GeV), and ISABELLE (stacking of I = 10 A, and acceleration to 200 GeV). It is capable of producing p-p collisions in the full range from 30 GeV x 30 GeV to 200 GeV x 200 GeV with a luminosity at the highest energy of $10^{33} \, cm^{-2} sec^{-1}$. It also has the capacity to operate at unequal energies over the entire energy range of 30 to 200 GeV. Finally, it offers ±20 m of free space for experimental apparatus around the collision point and with some trade-off of free space has a great deal of

flexibility in the choice of collision region "diamond" shape. Using

expressions given previously for luminosity, interaction length, and beam-

beam tune shift, we can compile a list detailing expected ISABELLE per-

formance. In particular, five possible operating configurations -- Standard,

Low-β, High-β, High Luminosity, and Small Diamond -- are described in Table V.

VI. SUMMARY

Over five years of design effort has resulted in a construction proposal for a 200 x 200 GeV proton-proton storage accelerator, ISABELLE. As exhibited in this paper, detailed investigation of all known degrading effects has produced a design in which considerable confidence exists that the very high expectations, regarding experimental flexibility, energy, and luminosity ($\sim 10^{33}$ cm^{-2}sec^{-1}), can be achieved comfortably. Research on superconducting magnets, the keystone to the design, has progressed through successful full-scale dipoles and quadrupoles which satisfy amply the strict field quality and mechanical and electrical stability required.

Consideration has also been given to future options. Antiproton-proton collisions could be achieved at full energy and with substantial luminosity ($\sim 10^{29}$ cm^{-2}sec^{-1}) in a straightforward manner with minimal additions of equipment. By adding a third ring in the same tunnel, electrons at 15 GeV could be stored so as to produce electron-proton collisions at 109 GeV in the c.m.

The physics possibilities with ISABELLE are outstanding. With considerable theoretical assurance, there exists a threshold for the intermediate vector bosons, the mediator of the weak force, which may be the single most exciting prospect for this machine. Only one prior case exists in high energy particle physics history where an accelerator, the Bevatron, was built to test such an important theoretical threshold, the production of antiprotons.

Clearly the enormous kinematic range to be available will produce dramatic new insights into the strong nuclear interaction, and could produce the experimental information needed for a complete understanding of the mathematical unification of the weak and electromagnetic interactions.

ACKNOWLEDGMENTS

Table I. Main ISABELLE Parameters

ENERGY

    Maximum energy   200 x 200 GeV

    Equivalent accelerator   85 TeV

LATTICE

    Circumference (3-2/3 x C_{AGS})   2960m

    Insertion length   8 x 116 m

    Regular cell length   56 x 25.40 m

    Modified cell length   24 x 25.40 m

    Horizontal separation of orbits   0.80 m

    Tune ($\nu_h = \nu_v$)   25.63

    Transition energy (γ_{tr})   21.6

    Amplitude function regular cell, β_{max} 42.7 m

                                     β_{min} 7.7

    Maximum dispersion, X_p 1.64 m

STANDARD EXPERIMENTAL INSERTIONS

    β_v^* (low-beta insertion)   4 (1) m

    β_h^* 20 m

    Maximum β^* (low-beta insertion)   100 (400) m

    Total free space around crossing point   40 m

    Crossing angle   11.4 mrad

    Interaction length   < 1 m

MAGNET SYSTEM

    Bending field at 200 GeV   39.4 kG

              at 29.4 GeV   5.8 kG

Number of dipoles/ring	264
Regular dipole length, effective	4.10 m
Dipole current @ 40 kG	3.3 kA
Stored energy @ 40 kG/dipole	465 kJ
Vacuum chamber aperture (warm bore)	8 cm
Main coil i.d.	12 cm
Operating temperature	< 4.5 K
Number of quadrupoles/ring	216
Regular quadrupole gradient	5.4 kG/cm
Quadrupole length, effective	1.45 m

CRYOGENIC SYSTEM

Total heat load at 4.5 K	17 kW
Total refrigeration capacity	25 kW
Power requirement of compressors	12 MW
Total liquid helium (equivalent)	30,000 liter
Cooldown weight	4.3×10^{6} kg

INJECTION

AGS energy	29.4 GeV
Number protons/AGS pulse (11 bunches)	5.2×10^{12}
AGS normalized emittance $E_h = E_v$	$20 \pi 10^{-6}$ m.rad
Longitudinal phase space per bunch	1 eV.sec
ISABELLE current/ring	10 A
Number protons/ring	6.2×10^{14}
Number of AGS pulses stacked/ring	$\simeq 120$
Stacked beam size	2.2 cm x 1.0 cm
Momentum spread	0.7%

rf frequency, stacking system (h = 44)   4.45 MHz

rf voltage   12 kV

Impedance tolerance Z/n $\approx 5\ \Omega$

Tune spread ≤ 0.02

ACCELERATION

Duration   3 min

rf frequency (h = 2)   202 kHz

Maximum energy gain/turn   12.5 kV

Peak rf voltage   40 kV

Total rf power/ring   1.25 MW

Momentum spread at 200 GeV   < 0.45%

Maximum momentum spread, bunched   1.6%

LUMINOSITY

Standard insertion, 200 GeV $2 \times 10^{32}\ cm^{-2}sec^{-1}$

Low-β insertion, 200 GeV $4 \times 10^{32}\ cm^{-2}sec^{-1}$

High luminosity insertion, 200 GeV $10^{33}\ cm^{-2}sec^{-1}$

Table II

Values of F in the function $(1 - x_\perp)^F$ for various processes as given by BBG (1972, 1973) constituent interchange model.

	pp →	$\pi^\pm$	K^+	K^-	p	$\bar{p}$
via	qM → qM	9	9	13	13	15
	$q\bar{q} \to M\bar{M}$	11	11	11	17	17
	qq → Bq	9	9	9	7	11
	$\bar{q}M \to \bar{q}M$	13	13	15	19	17

	$\bar{p}p$ →	$\pi^\pm$	K^+	K^-	p	$\bar{p}$
via	qM → qM	9	9	9	13	15
	$q\bar{q} \to M\bar{M}$	7	7	7	13	13
	$qq \to B\bar{q}$	13	13	13	11	15
	$\bar{q}M \to \bar{q}M$	9	9	9	15	13

Table III. Beam Growth Rates due to Intra-Beam Scattering

Parameter	Low Energy Case	High Energy Case
γ	31.4	213.2
$(\Delta p/p)_T$	0.7%	0.15%
A (hour^{-1})	6.14×10^{-5}	6.22×10^{-6}
a	1.92	19.8
b	1.0	1.0
c	10.3×10^3	26.2×10^3
t	0.59	0.82
$f(1, a, c)$	−52.9	−11.8
$f(\frac{1}{a}, \frac{1}{a}, \frac{c}{a})$	390	9252
$(1/\tau_v)$ (%/hour)	−0.3	−0.007
$(1/\tau_h)$ (%/hour)	+0.7	+1.0
$(1/\tau_p)$ (%/hour)	+2.8	+9.4

Table IV. Effects of Random Coil Block Errors

Orbit Parameter	Central Error	Error $t = 0.6$	Error $t = 0.4$	Error $t = 0.3$
Closed orbit (A_{co}, mm)	4.6	12.7	6.9	5.5
Tune shift ($\Delta\nu$)	0.01	0.07	0.025	0.017
Linear stopband width ($\delta\nu_2$)	0.02	0.14	0.05	0.034
$(\Delta\beta/\beta)_{max}$	0.10	0.70	0.25	0.17
Sextupole resonance width ($\delta\nu_3$)	5.8×10^{-4}	1.0×10^{-2}	2.4×10^{-3}	1.4×10^{-3}
Octupole resonance width ($\delta\nu_4$)	2.8×10^{-5}	1.2×10^{-3}	2.0×10^{-4}	9.8×10^{-5}
Decapole resonance width ($\delta\nu_5$)	1.2×10^{-6}	1.3×10^{-4}	1.4×10^{-5}	6.0×10^{-6}

Table V.   ISABELLE Performance

	Standard		Low-β		High-β		Small Diamond	High Luminosity
Energy (GeV)	200.0	29.4	200.0	29.4	200.0	29.4	200.0	200.0
Current (A)	10	10	10	10	4	4	10	10
Luminosity ($cm^{-2}sec^{-1}$)	2.1×10^{32}	0.8×10^{32}	4.2×10^{32}	1.2×10^{32}	8.1×10^{30}	3.1×10^{30}	1.0×10^{32}	1.0×10^{33}
Tune shift	1.4×10^{-3}	3.6×10^{-3}	6.9×10^{-4}	2.5×10^{-3}	2.3×10^{-3}	6.0×10^{-3}	1.5×10^{-4}	1.6×10^{-3}
Crossing angle (mrad)	11.4	11.4	11.4	11.4	11.4	11.4	50.0	4.8
Free space (m)	±20	±20	±20	±20	±20	±20	±2.5	±12.7
ℓ_{int} (m)	±0.17	±0.45	±0.17	±0.45	±0.30	±0.78	±0.02	±0.40
β_v^* (m)	4.0	4.0	1.0	2.0	69.2	69.2	1.0	1.0
β_{max} (m)	≈100	≈100	≈400	≈200	≈100	≈100	≈400	≈400
β_h^* (m)	20	20	20	20	61.7	61.7	5.0	20
σ_v^* (mm, rms)	0.30	0.80	0.15	0.56	1.27	3.32	0.15	0.15

REFERENCES

Abramovskii, V. M., O. V. Kancheli, E.V.N. Gribov, 1972, <u>Proc. 16th Intern. Conf.</u> <u>on High Energy Physics</u>, Batavia, IL, p. 389.

Amaldi, U., R. Biancastelli, C. Bosio, G. Matthiae, J. V. Allaby, W. Bartel, G. Cocconi, A. N. Diddens, R. W. Dobinson, V. Elings, J. Litt, L. S. Rochester, and A. M. Wetherell, 1971, Phys. Lett. <u>36B</u>, 504.

Amaldi, U., R. Biancastelli, C. Bosio, G. Matthiae, J. V. Allaby, W. Bartel, M. M. Block, G. Cocconi, A. N. Diddens, R. W. Dobinson, J. Litt, and M. Wetherell, 1973a, Phys. Lett. <u>43B</u>, 231.

Amaldi, U., R. Biancastelli, C. Bosio, G. Matthiae, J. V. Allaby, W. Bartel, G. Cocconi, A. N. Diddens, R. W. Dobinson, and A. M. Wetherell, 1973b, Phys. Lett. <u>44B</u>, 112.

Amendolia, S. R., G. Bellettini, P. L. Braccini, C. Bradaschia, R. Castaldi, V. Cavasinni, C. Cerri, T. Del Prete, L. Foa, P. Giromini, P. Laurelli, A. Menzione, L. Ristori, G. Sanguinetti, M. Valdata, G. Finocchiaro, P. Grannis, D. Green, R. Mustard, and R. Thun, 1973a, Phys. Lett. <u>44B</u>, 119; 1973b, Nuovo Cimento <u>17A</u>, 735.

Amendolia, S. R., G. Belletini, P. L. Braccini, C. Bradaschia, R. Castaldi, V. Cavasinni, C. Cerri, T. Del Prete, L. Foa, P. Giromini, P. Laurelli, A. Menzione, L. Ristori, G. Sanguinetti, M. Valdata, G. Finocchiaro, P. Grannis, D. Green, R. Mustard, and R. Thun, 1974, Phys. Lett. <u>48B</u>, 359.

Amman, F., 1973, IEEE Trans. Nucl. Sci. <u>NS-20</u>, p. 858.

Angerth, B., E. Fischer, and O. Gröbner, 1971, <u>Proc. 8th Intern. Conf. on</u> <u>High Energy Accelerators</u>, CERN, Geneva, p. 298.

Antinucci, N., A. Bertin, P. Capilappi, M. D'Agustino-Bruno, A. M. Rissi, and G. Vannini, 1973, Nuovo Cim. Lett. 6, 121.

Antipov, Yu. M., R. Busnello, G. Damgaard, M. N. Kienzle-Focacci, W. Kienzle, R. Klanner, L. G. Landsberg, A. A. Lebedev, C. Lechanoine, P. Lecomte, M. Martin, V. Roinishvili, R. D. Sard, F. A. Yotch, and A. Weitsch, 1972, Proc. 4th Intern. Conf. on High Energy Collisions, Oxford, U. K., 5-7 April.

Appelquist, T. and H. Georgi, 1973, Phys. Rev. D8, 4000.

Aubert, J. J., U. Becker, J. P. Biggs, J. Burger, M. Chen, G. Everhart, P. Goldhagen, J. Leong, T. McCorriston, T. G. Rhoades, M. Rohde, S.C.C. Ting, Sau Lan Wu, and Y. Y. Lee, 1974, Phys. Rev. Lett. 33, 1404.

Auerbach, S., R. Aviv, R. Sugar, and R. Blankenbeckler, 1972, Phys. Rev. D6, 2216.

Augustin, J. E., 1970, Linear Accelerator Laboratory, Orsay Report RT/8-70 JEA/LN(1970). (English translation: SLAC TRANS-117).

Augustin, J. E., A. M. Boyarski, M. Breidenbach, F. Bulos, J. T. Dakin, G. J. Feldman, G. E. Fischer, D. Bryberger, G. Hanson, B. Jean-Marie, R. R. Larsen, V. Lüth, H. L. Lynch, D. Lyon, C. C. Morehouse, J. M. Paterson, M. L. Perl, B. Richter, P. Rapidis, R. F. Schwitters, W. M. Tanenbaum, F. Vannucci, G. S. Abrams, D. Briggs, W. Chinowsky, C. E. Friedberg, G. Goldhaber, R. J. Hollebeek, J. A. Kadyk, B. Lulu, F. Pierre, G. H. Trilling, J. S. Whitaker, J. Wiss, and J. E. Zipse, 1974, Phys. Rev. Lett. 33, 1406.

Autin, B. and A. A. Garren, 1975, CERN Report CERN/ISR-GS-MA/75-32.

Barbiellini, G., M. Boyzo, P. Darriulat, G. Diambrini Palazzi, G. DeZorzi, A. Fainberg, M. I. Ferrero, M. Holder, A. McFarland, G. Maderni, S. Orito, J. Pilcher, C. Rubbia, A. Santroni, G. Sette, A. Staude, P. Strolin, and K. Tittel, 1972, Phys. Lett. 39B, 663.

Barish, B. C., J. F. Bartlett, D. Buchholz, T. Humphrey, F. S. Merritt, F. J. Sciulli, L. Stutte, D. Shields, H. Suter, E. Fisk, and G. Krafczyk, 1975, Phys. Rev. Lett. 35, 1316.

Bartel, W. and A. N. Diddens, 1973, CERN Report NP 73-3.

Bartenev, V., A. Kuznetsov, B. Morozov, V. Nikitin, Y. Pilipenko, V. Popov, L. Zolin, R. Carrigan, E. Malamud, R. Yamada, R. L. Cool, K. Goulianos, S. L. Olsen, I-Hung Chiang, A. C. Melissinos, and D. Gross, 1972, Phys. Rev. Lett. 29, 1755.

Bartenev, V., A. Kuznetsov, B. Morozov, V. Nikitin, Y. Pilipenko, V. Popov, L. Zolin, R. A. Carrigan, Jr., E. Malamud, R. Yamada, R. L. Cool, K. Goulianos, I-Hung Chiang, A. C. Melissinos, D. Gross, and S. L. Olsen, 1973a, Phys. Rev. Lett. 31, 1088.

Bartenev, V., R. A. Carrigan, Jr., I-Hung Chiang, R. L. Cool, K. Goulianos, D. Gross, A. Kuznetsov, E. Malamud, A. C. Melissinos, B. Morozov, V. Nikitin, S. L. Olsen, Y. Pilipenko, V. Popov, R. Yamada, and L. Zolin, 1973b, Phys. Rev. Lett. 31, 1367.

Belletini, G., G. Cocconi, A. N. Diddens, E. Lillethun, J. Pahl, J. P. Scanlon, J. Walters, A. M. Wetherell, and P. Zanella, 1965, Phys. Lett. 14, 164.

Benvenuti, A., D. C. Cheng, D. Cline, W. T. Ford, R. Imlay, T. Y. Ling, A. K. Mann, F. Messing, R. L. Piccioni, J. Pilcher, D. D. Reeder, C. Rubbia, R. Stefanski, and L. Sulak, 1974a, Phys. Rev. Lett. 32, 800.

Benvenuti, A., D. Cline, W. T. Ford, R. Imlay, T. Y. Ling, A. K. Mann, F. Messing, R. L. Piccioni, J. Pilcher, D. D. Reeder, C. Rubbia, R. Stefanski, and L. Sulak, 1974b, Phys. Rev. Lett. 32, 125.

Berman, S. M., J. D. Bjorken, and J. B. Kogut, 1971, Phys. Rev. D4, 3388.

Bethe, H. A. and J. Ashkin, 1953, Experimental Nuclear Physics (E. Segre, Editor), John Wiley & Sons, Inc., New York.

Beznogikh, G. G., A. Bujak, L. F. Kirillova, B. A. Morozov, V. A. Nikitin, P. V. Nomokonov, A. Sandacz, M. G. Shafranova, V. A. Sviridov, Truong Bien, V. I. Zayachki, N. K. Zhidkov, and L. S. Zolin, 1972, Phys. Lett. 39B, 411.

Beznogikh, G. G., A. Bujak, V. A. Nikitin, M. G. Shafranova, V. A. Sviridov, Truong Bien, L. V. Vikhlyantseva, V. I. Zayachki, and L. S. Zolin, 1973, Phys. Lett. 43B, 85.

Birnbaum, D., R. M. Edelstein, N. C. Hien, T. J. McMahon, J. F. Mucci, J. S. Russ, E. W. Anderson, E. J. Bleser, H. R. Blieden, G. B. Collins, D. Garelick, J. Menes, and F. Turkot, 1969, Phys. Rev. Lett. 23, 663.

Bjorken, J. D., 1973, Phys. Rev. D8, 4098.

Blankenbecler, R., S. J. Brodsky, and J. F. Gunion, 1972, Phys. Lett. 42B, 461.

Blewett, J. P., 1971, Proc. 8th Intern. Conf. on High Energy Accelerators, CERN, Geneva, p. 501.

Böckmann, K., B. Nellen, E. Paul, B. Wagini, I. Borecka, J. Diaz, U. Heeren, U. Liebermeister, E. Lohrmann, E. Raubold, P. Söding, S. Wolff, J. Kidd, L. Mandelli, L. Mosca, V. Pelosi, S. Ratti, and L. Tallone, 1966, Nuovo Cim. 42A, 954.

Boussard, D. and J. Gareyte, 1971, Proc. 8th Intern. Conf. on High Energy Accelerators, CERN, Geneva, p. 317.

Boussard, D., 1975, CERN Report Lab II/RF/Int. 75-2.

Brodsky, S. J. and G. R. Farrar, 1973, Phys. Rev. Lett. 31, 1153.

Bromberg, C., D. Chaney, D. Cohen, T. Ferbel, P. Slattery, D. Underwood, J. W. Chapman, J. W. Cooper, N. Green, B. P. Roe, A. A. Seidl, and J. C. VanderVelde, 1973, Phys. Rev. Lett. 31, 1563.

Brower, R. C. and J. H. Weis, 1972, Phys. Lett. 41B, 631.

Brown, D. P., 1976, BNL Report #50514.

Bryant, P. J. and J. P. Gourber, 1974, Proc. 9th Intern. Conf. on High Energy Accelerators, Stanford, CA, p. 87.

Buon, J., 1974, Proc. 9th Intern. Conf. on High Energy Accelerators, Stanford, CA, p. 83.

Burhop, E.H.S., 1963, Proc. 1963 Summer Study on Storage Rings, Accelerators, and Experimentation at Super High Energies, Brookhaven National Laboratory, p. 236.

Büsser, F.W., L. Camilleri, L. DiLella, G. Gladding, A. Placci, B. G. Pope, A. M. Smith, J. K. Yoh, E. Zavattini, B. J. Blumenfeld, L. M. Lederman, R. L. Cool, L. Litt, and S. L. Segler, 1973, Phys. Lett. 46B, 471.

Büsser, F. W., L. Camilleri, L. DiLella, G. Gladding, A. Placci, B. G. Pope, A. M. Smith, J. K. Yoh, E. Zavattini, B. J. Blumenfeld, L. M. Lederman, R. L. Cool, L. Kitt, and S. L. Segler, 1974, Phys. Lett. 53B, 212.

Calder, R., E. Fischer, O. Gröbner, and E. Jones, 1974, Proc. 9th Intern. Conf. on High Energy Accelerators, Stanford, CA, p. 70.

Carroll, S. S., I. H. Chiang, T. F. Kycia, K. K. Li, P. O. Mazur, P. Mockett, D. C. Rahm, R. Rubinstein, W. F. Baker, D. P. Eartly, G. Giacomelli, P.F.M. Koehler, K. P. Pretzl, A. A. Wehmann, R. L. Cool, and O. Fackler, 1974a, Phys. Rev. Lett. 33, 932; 1974b, Phys. Rev. Lett. 33, 928.

Carruthers, B. and M. Duong-van, 1973, Phys. Lett. 44B, 507.

Cazzoli, E. G., A. M. Cnops, P. L. Connolly, R. I. Louttit, M. J. Murtagh, R. B. Palmer, N. P. Samios, T. T. Tso, and H. H. Williams, 1975, Phys. Rev. Lett. 34, 1125.

Chao, A. W. and M. Month, 1974, Nucl. Instrum. Meth. 121, 129.

Chao, A. W., J. C. Herrera, and M. Month, 1975, Proc. 1975 ISABELLE Summer Study, Brookhaven National Laboratory, p. 418.

Charlton, G., Y. Cho, M. Derrick, R. Engelmann, T. Fields, L. Hyman, K. Jaeger, U. Mehtani, B. Musgrave, Y. Oren, D. Rhines, P. Schreiner, H. Yuta, L. Voyvodic, R. Walker, J. Whitmore, H. B. Crawley, Z. Ming Ma, and R. G. Glasser, 1972, Phys. Rev. Lett. 29, 515.

Chasman, R. W., E. D. Courant, and M. Month, 1975, IEEE Trans. Nucl. Sci. NS-22, 1429.

Cheng, H. and T. T. Wu, 1973, Phys. Lett. 45B, 367.

Chernev, Kh. M., I. M. Geshkov, N. L. Ikov, P. K. Markov, and V. I. Zaiachki, 1971, Phys. Lett. 36B, 266.

Coffey, H. T., J. K. Hulm, W. T. Reynolds, D. K. Fox, and R. E. Span, 1965, J. Appl. Phys. 36, 128.

Cole, F. T. and P. L. Morton, 1964, LBL Report UCID-10130 AS/Theoretical/02.

Cooper, F., 1975, Particles and Fields 1974, AIP Conf. Series, New York, p. 499.

Courant, E. D. and H. S. Snyder, 1958, Ann. Phys. 3, 1.

Courant, E. D. and A. M. Sessler, 1966, Rev. Sci, Instr. 37, 1579.

Cronin, J. W., H. J. Fisch, M. J. Shochet, J. P. Boymond, P. A. Piroue, and R. L. Summer, 1973, Phys. Rev. Lett. 31, 1426.

Dahl, P. F., 1976, BNL Report #50498.

Dao, F. T., D. Gordon, J. Lach, E. Malamud, T. Meyer, R. Poster, and W. Slater, 1972, Phys. Rev. Lett. 29, 1627.

Darriulat, P., 1975, Review Talk, Proc. European Physical Soc. (in press).

Denisov, S. P., S. V. Donskov, Yu. P. Gorin, A. I. Petrukhin, Yu. D. Prokoshkin, D. A. Stoyanova, J. V. Allaby, and G. Giacomelli, 1971, Phys. Lett. 36B, 415.

deTar, C. S., C. E. Jones, F. E. Low, J. H. Weis, J. E. Young, and Chung-I Tau, 1971, Phys. Rev. Lett. 26, 675.

Dew-Hughes, D., 1971, Rept. Prog. Phys. 34, 821.

Donald, M.H.R., M. R. Harold, J. Maidment, and H. G. Rees, 1975, IEEE Trans. Nucl. Sci. NS-22, 1433.

Duchateau, J. L., 1974, Particle Accelerators 6, 7.

Duchateau, J. J. and B. Turek, 1975, J. Appl. Phys. 46, 4989.

Edwards, D., S. Ohnuma, and L. T. Teng, 1975, IEEE Trans. Nucl. Sci. NS-22, 1426.

Eggert, K. et al., 1975, Proc. European Physical Soc. (in press).

Eminhizer, C. R., R.H.G. Helleman, and E. W. Montroll, 1976, J. Math. Phys. 17, 121.

Ferbel, T., 1976, University of Rochester Report COO-3065-152.

Fischer, E., 1972, J. Vac. Sci. Technol. 9, 1203.

Fischer, E. and K. Zankel, 1973, CERN Report CERN-ISR-VA/73-52.

Foley, K. J., S. J. Lindenbaum, W. A. Love, S. Ozaki, J. J. Russell, and L.C.L. Yuan, 1963, Phys. Rev. Lett. 11, 503.

Foley, K. J., R. S. Gilmore, R. S. Jones, S. J. Lindenbaum, W. A. Love, S. Ozaki, E. H. Willen, R. Yamada, and L.C.L. Yuan, 1965a, Phys. Rev. Lett. 14, 74.

Foley, K. J., R. S. Gilmore, S. J. Lindenbaum, W. A. Love, S. Ozaki, E. H. Willen, R. Yamada, and L.C.L. Yuan, 1965b, Phys. Rev. Lett. 15, 45.

Foley, K. J., R. S. Jones, S. J. Lindenbaum, W. A. Love, S. Ozaki, E. D. Platner, C. Q. Quarles, and E. H. Willen, 1967, Phys. Rev. Lett. 19, 857.

Foley, K. J. and B. T. Meadows, 1975, Proc. 1975 ISABELLE Summer Study, Brookhaven National Laboratory, p. 292.

Fowler, P. and D. Perkins, 1964, Proc. Royal Soc. A278, 401.

Frazer, W. R. and D. R. Snider, 1973, Phys. Lett. 45B, 136.

Gaisser, T. K., F. Halzen, and K. Kajantie, 1975, Phys. Rev. D12, 1969.

Galbraith, W., E. W. Jenkins, T. F. Kycia, B. A. Leontic, R. H. Phillips, A. L. Read, and R. Rubinstein, 1965, Phys. Rev. 138B, 913.

Gareyte, J. and J. P. Gourber, 1975, Proc. 1975 ISABELLE Summer Study, Brookhaven National Laboratory, p. 395.

Garren, A., 1975, Proc. 1975 ISABELLE Summer Study, Brookhaven National Laboratory, p. 372.

Giacomelli, G. and A. Thorndike, 1975, Proc. 1975 ISABELLE Summer Study, Brookhaven National Laboratory, p. 301.

Giarratano, P. J. V. D. Arp, and R. V. Smith, 1971, Cryogenics 11, 385.

Goldhaber, G., F. M. Pierre, G. S. Abrams, M. S. Alam, A. M. Boyarski, M. Breidenbach, W. C. Carithers, W. Chinowsky, S. C. Cooper, R. G. DeVoe, J. M. Dorfan, G. J. Feldman, C. E. Friedberg, D. Fryberger, G. Hanson, J. Jaros, A. D. Johnson, J. A. Kadyk, R. R. Larsen, D. Lüke, V. Lüth, H. L. Lynch, R. J. Madaras, C. C. Morehouse, H. K. Nguyen, J. M. Paterson, M. L. Perl, I. Peruzzi, M. Piccolo, T. P. Pun, P. Rapidis, B. Richter, B. Sadoulet, R. H. Schindler, R. F. Schwitters, J. Siegrist, W. Tanenbaum, G. H. Trilling, F. Vannucci, J. S. Whitaker, and J. E. Wiss, 1976, Phys. Rev. Lett. 37, 255.

Gourber, J. P., E. Keil, S. Pichler, 1975, IEEE Trans. NS-22, 1419.

Gunion, J. F., S. J. Brodsky, and R. Blankenbecler, 1972a, Phys. Lett. 39B, 649.

Gunion, J. F., S. J. Brodsky, and R. Blankenbecler, 1972b, Phys. Rev. D6, 2652.

Gunion, J. F., S. J. Brodsky, and R. Blankenbecler, 1973, Phys. Rev. D8, 287.

Güsewell, D and E. V. Haebel, 1970, Proc. 3rd Intern. Cryogenic Eng. Conf., Berlin, p. 187.

Halama, H. J. and J. C. Herrera, 1975, Proc. IEEE Trans. NS-22, 1492.

Hansen, S. and A. Hofmann, 1975, private communication (CERN ISR Performance Report 25 June).

Harari, H., 1975, Phys. Lett. 55B, 265.

Hasert, F. J., H. Faissner, W. Krenz, J. VonKrogh, D. Lanske, J. Morfin, K. Schultze, H. Weerts, G. H. Bertrand-Coremans, J. Lemonne, J. Sacton, W. VanDoninck, P. Vilain, C. Baltay, D. C. Cundy, D. Haidt, M. Jaffre, P. Musset, A. Pullia, S. Natali, J.B.M. Pattison, D. H. Perkins, A. Rousset, W. Venus, H. W. Wachsmuth, V. Brisson, B. Degrange, M. Haguenauer, L. Kluberg, U. Ngyuen-Khac, P. Petiau, E. Bellotti, S. Bonetti, D. Cavalli, C. Conta, E. Fiorini, M. Rollier, B. Aubert, L. M. Chounet, P. Heusse, A. Lagarrigue, A. M. Lutz, J. P. Vialle, F. W. Bullock, M. J. Esten, T. Jones, J. McKenzie, A. G. Michette, G. Myatt, J. Pinfold, and W. G. Scott, 1973a, Phys. Lett. <u>46B</u>, 121.

Hasert, F. J., S. Kabe, W. Krenz, J. VonKrogh, D. Lanske, J. Morfin, K. Schultze, H. Weerts, G. H. Bertrand-Coremans, J. Sacton, W. VanDoninck, P. Vilain, U. Camerini, D. C. Cundy, R. Baldi, I. Danilchenko, W. F. Fry, D. Haidt, S. Natali, P. Musset, B. Osculati, R. Palmer, J.B.M. Pattison, D. H. Perkins, A. Pullia, R. Rousset, W. Venus, H. Wachsmuth, V. Brisson, B. Degrange, M. Haguenauer, L. Kluberg, U. Nguyen-Khac, P. Petiau, E. Belotti, S. Bonetti, D. Cavalli, C. Conta, E. Fiorini, M. Rollier, B. Aubert, D. Blum, L. M. Chounet, P. Heusse, A. Lagarrigue, A. M. Lutz, A. Orkin-Lecourtois, J. P. Vialle, F. W. Bullock, M. J. Esten, T. W. Jones, J. McKenzie, A. G. Michette, G. Myatt, and W. G. Scott, 1973b, Phys. Lett. <u>46B</u>, 138.

Hendrick, R. E., P. Langacker, B. E. Lautrup, S. J. Orfanidis, and V. Rittenberg, 1975a, Phys. Rev. <u>D11</u>, 536.

Hendrick, R. and E. B. Lautrup, 1975b, Phys. Rev. <u>D11</u>, 529.

Henon, M., 1969, <u>Quarterly of Applied Mathematics</u>, Vol. XXVII, p. 291.

Henrichsen, K. N. and M. J. deJonge, 1974, <u>Proc. 9th Intern. Conf. on High Energy Accelerators</u>, Stanford, CA, p. 390.

Herrera, J., 1976, BNL Report #50533.

Hereward, H. G., 1965, CERN Report 65-20.

Hereward, H. G., 1971, CERN Report 71-15.

Hereward, H. G., 1972, CERN Report CERN/ISR-DI/72-26.

Hereward, H. G., 1975a, private communication (ISR Performance Report 8 January).

Hereward, H. G., 1975b, Proc. 1975 ISABELLE Summer Study, Brookhaven National Laboratory, p. 555.

Hofmann, A., 1975, private communication (CERN ISR Performance Report 10 December).

Hübner, K. and V. G. Vaccaro, 1970, CERN Report CERN-ISR-TH/70-44.

Hübner, K., 1975, Proc. 1975 ISABELLE Summer Study, Brookhaven National Laboratory, p. 729.

ISABELLE, 1976, A Proposal for Construction of a Proton-Proton Storage Accelerator Facility, BNL Report #50519.

Jackson, J. D., 1960, J. Nucl. Energy, Part C, Plasma Phys. 1, 171.

Jejcic, A. and J. LeDuff, 1971, Proc. 8th Intern. Conf. on High Energy Accelerators, CERN, Geneva, p. 354.

Johnsen, K., 1973, Nucl. Instr. Meth. 108, 205; Proc. Nat. Acad. Sci. USA 70, 619.

Jones, L. W., 1963, Proc. Intern. Conf. on High Energy Accelerators, Dubna, p. 300.

Jones, C. E., F. E. Low, S-H. Y. Tye, G. Veneziano, and J. E. Young, 1972, Phys. Rev. D6, 1033.

Keil, E. and W. Schnell, 1969, CERN Report CERN-ISR-TH-RF/69-48.

Keil, E. and B. Zotter, 1971a, CERN Report CERN-ISR-TH/71-58.

Keil, E., 1971b, Proc. 8th Intern. Conf. on High Energy Accelerators, CERN, Geneva, p. 372.

Keil, E., 1972, CERN Reports CERN/ISR-TH/72-7 and 72-25.

Keil, E., 1973a, "Beam Behavior in the ISR," Lectures given at the Intern. School of Appl. Phys., Erice, Italy, June, private communication.

Keil, E., C. Pellegrini, and A. M. Sessler, 1973b, CERN Report CERN/ISR-TH/73-44.

Keil, E., C. Pellegrini, and A. M. Sessler, 1974a, Nucl. Instr. & Meth. 118, 165.

Keil, E.,1974b, Proc. 9th Intern. Conf. on High Energy Accelerators, Stanford, CA, p. 660.

Kerst, D. W., F. T. Cole, H. R. Crane, L. W. Jones, L. J. Laslett, T. Ohkawa, A. M. Sessler, K. R. Symon, K. M. Terwilliger, and Nils Vogt Nilsen, 1956a, Phys. Rev. 102, 590.

Kerst, D. W., 1956b, Proc. CERN Symposium on High Energy Accelerators and Pion Physics, Geneva, p. 36.

Kim, Y. B., C. F. Hempstead, and A. R. Strnad, 1963, Phys. Rev. 129, 528.

Knapp, B., W. Lee, P. Leung, S. D. Smith, A. Wijangco, J. Knauer, D. Yount, J. Bronstein, R. Coleman, G. Gladding, M. Goodman, M. Gormley, R. Messner, T. O'Halloran, J. Sarracino, A. Wattenberg, M. Binkley, I. Gaines, and J. Peoples, 1976, Phys. Rev. Lett. 37, 882.

Kolm, H. H., 1965, Proc. Intern. Symposium on Magnet Technology, Stanford, CA, p. 611.

Koshiba, M., 1963, Nuovo Cim. Supple. 1, 1901.

Kunzler, J. E., E. Buehler, F. S. L. Hsu, and J. H. Wernick, 1961, Phys. Rev. Lett. 6, 89.

Laslett, L. J., 1963, Proc. Summer Study on Storage Rings, Accelerators, and Experimentation at Super-High Energies, Brookhaven National Laboratory, p. 324.

Laslett, L. J., V. K. Neil, and A. M. Sessler, 1965, Rev. Sci. Instr. 36, 436.

Laslett, L. J. and L. Resegotti, 1967, Proc. 6th Intern. Conf. on High Energy Accelerators, Cambridge, MA, p. 150.

Laslett, L. J., 1974, LBL Reports PEP 93 and 94; Proc. 9th Intern. Conf. on High Energy Accelerators, Stanford, CA, p. 394, and references therein.

Lederman, L. M., 1975, Proc. 1975 ISABELLE Summer Study, Brookhaven National Laboratory, p. 84.

LeDuff, J., 1972, Linear Accelerator Laboratory, Orsay, Report RT/6-72.

Lillethun, E., 1973, Acta Physica Polonica B4, 769.

Mazur, P., 1975, Bull. Am. Phys. Soc. 20, 82.

McInturff, A. D., P. F. Dahl, and W. B. Sampson, 1972, J. Appl. Phys. 43, 3546.

McInturff, A. D., 1976, "ISABELLE Ring Magnets" in Proc. 1976 Applied Superconductivity Conference, Stanford, CA (in press).

Messerschmid, E. and M. Month, 1976a, Nucl. Instrum. Meth. 136, 1.

Messerschmid, E. and M. Month, 1976b, BNL Report #21891; to be published in Nucl. Instrum. Meth.

Mills, F. E. and G. H. Morgan, 1973, Particle Accelerators 5, 227.

Möller, C., 1945, Kgl. Danske Videnskab. Selskab 23, No. 1, 18.

Montague, B. W. and B. W. Zotter, 1974, Nucl. Instrum. Meth. 120, 9.

Montague, B. W., 1975, CERN Report CERN/ISR-GS/75-36.

Month, M., 1972, Particle Accelerators 3, 183.

Month, M. and K. Jellett, 1973a, Nucl. Instrum. Meth. 113, 453.

Month, M., 1973b, BNL Report CRISP 73-17.

Month, M., 1974a, Proc. 9th Intern. Conf. on High Energy Accelerators, Stanford, CA, p. 593.

Month, M. and Y. Y. Lee, 1974b, BNL Report CRISP 74-10.

Month, M., 1975a, BNL Reports CRISP 75-1 and 75-2.

Month, M., 1975b, IEEE Trans. Nucl. Sci. NS-22, 1376.

Month, M. and G. Parzen, 1976, Nucl. Instrum. Meth. 137, 319.

Month, M., 1977, "A Low Energy Current Accumulator for High Energy Proton Rings" in Proc. 1977 Particle Accelerator Conf., Chicago, IL (to be published); and BNL Reports ISA 75-8 and 75-11 (1975).

Morrison, D.R.O., 1973, CERN Report CERN/D.Ph.II/Phys. 73-46, p. 22.

Mueller, A. H., 1970, Phys. Rev. D2, 2963.

Mueller, A. H., 1971, Phys. Rev. D4, 150.

Nauenberg, U., 1975, Proc. 1975 ISABELLE Summer Study, Brookhaven National Laboratory, p. 86.

Neil, V. K. and A. M. Sessler, 1965, Rev. Sci. Instrum. 36, 429.

Nielsen, C. E. and A. M. Sessler, 1959, Rev. Sci. Instrum. 30, 80.

O'Neill, G. K., 1956a, Proc. CERN Symposium on High Energy Accelerators and Pion Physics, Geneva, p. 64.

O'Neill, G. K., 1956b, Phys. Rev. 102, 1418.

O'Neill, G. K., 1966, Sci. Amer. 215, 107.

Parzen, G., 1975, Proc. 1975 ISABELLE Summer Study, Brookhaven National Laboratory, p. 573.

Pati, J. and A. Salam, 1973, Phys. Rev. Lett. 31, 661.

Peierls, R. F., 1975, Proc. 1975 ISABELLE Summer Study, Brookhaven National Laboratory, p. 327.

Peruzzi, I., M. Piccolo, G. J. Feldman, H. K. Nguyen, J. E. Wiss, G. S. Abrams, M. S. Alam, A. M. Boyarski, M. Breidenbach, W. C. Carithers, W. Chinowsky, R. G. DeVoe, J. M. Dorfan, G. E. Fischer, C. E. Friedberg, D. Fryberger, G. Goldhaber, G. Hanson, J. A. Jaros, A. D. Johnson, J. A. Kadyk, R. R. Larsen, D. Lüke, V. Lüth, H. L. Lynch, R. J. Madaras, C. C. Morehouse, J. M. Paterson, M. L. Perl, F. M. Pierre, T. P. Pun, P. Rapidis, B. Richter, R. H. Schindler, R. F. Schwitters, J. Siegrist, W. Tanenbaum, G. H. Trilling, F. Vannucci, and J. S. Whitaker, 1976, Phys. Rev. Lett. 37 569.

Piwinski, A., 1974, Proc. 9th Intern. Conf. on High Energy Accelerators, Stanford, CA, p. 405.

Proceedings, 1963, Summer Study on Storage Rings, Accelerators and Experimentation at Super-High Energies, Brookhaven National Laboratory Report #7534.

Proceedings, 1975, ISABELLE Summer Study, Brookhaven National Laboratory Report #20550.

Ranft, J., 1974, Proc. 5th Intern. Symposium on Many Particle Hadrodynamics, Leipzig, p. 210.

Reardon, P. J., 1976, "Superconductivity in High Energy Physics," Proc. 1976 Appl. Superconductivity Conf., Stanford, CA (to be published).

Report of the 1975 Subpanel on New Facilities of the High Energy Physics Advisory Panel, ERDA-83 UC-34d.

Rubbia, C., 1975, Proc. 1975 ISABELLE Summer Study, Brookhaven National Laboratory, p. 100.

Ruggiero, A. G. and V. G. Vaccaro, 1968, CERN Report CERN-ISR-TH/68-33.

Ruggiero, A. G. and L. Smith, 1973, PEP Summer Study, LBL and SLAC.

Sacherer, F. J., 1972, CERN Report CERN/SI-BR/72-5.

Sacherer, F. J., 1973, IEEE Trans. Nucl. Sci. NS-20, 825.

Sacherer, F. J., 1974, Proc. 9th Intern. Conf. on High Energy Accelerators, Stanford, CA, p. 347.

Salam, H., 1968, in Elementary Particle Physics, edited by N. Svartholm (Stockholm) p. 367.

Schnell, W., 1975a, Proc. 1975 ISABELLE Summer Study, Brookhaven National Laboratory, p. 131.

Schnell, W., 1975b, IEEE Trans. Nucl. Sci. NS-22, 1358

Schnell, W. and B. Zotter, 1976, CERN Report CERN-ISR-GS-RF/76-26.

Schoch, A., 1957, CERN Report CERN 57-21.

Schoch, A., 1963, Proc. 1963 Summer Study on Storage Rings, Accelerators, and Experimentation at Super-High Energies, Brookhaven National Laboratory, p. 128.

Schwitters, R. and F. Gilman, 1976, <u>Proc. 1975 Intern. Symposium on Lepton and Photon Interactions at High Energies</u>, Stanford, CA.

Sciulli, F. J., 1975, <u>Particles and Fields APS/DPF</u>, edited by H. J. Lubatti and P. M. Mockett (University of Washington, Seattle), p. 76.

Sessler, A. M., 1973, "The Self-Destructive Behavior of Intense Particle Beams," Lectures given at the Intern. School of Appl. Phys., Erice, Italy, June (private communication).

Sidhu, D. and L. L. Wang, 1975, Brookhaven National Laboratory Informal Report #19022.

SPEAR Storage Ring Group, 1973, IEEE Trans. Nucl. Sci. <u>NS-20</u>, 838.

Stevens, A. J. and A. M. Thorndike, 1976, BNL Report #50540.

Strauss, B. P., R. H. Remsbottom, P. J. Reardon, C. W. Curtis, and W. K. McDonald, 1976, "Results on the Fermilab Wire Production Program," <u>Proc. Appl. Superconductivity Conf.</u>, Stanford, CA (to be published).

Suzuki, M., 1975, Phys. Rev. Lett. <u>35</u>, 1553.

Symon, K. R. and A. M. Sessler, 1956, <u>Proc. Intern. Conf. on High Energy Accelerators</u>, CERN, Geneva, p. 44.

Teng, L. C., 1975, IEEE Trans. Nucl. Sci. <u>NS-22</u>, 1826.

Thomas, D. B., 1974, <u>Proc. 9th Intern. Conf. on High Energy Accelerators</u>, Stanford, CA, p. 164.

Thorndahl, L. and A. Vaughan, 1973, IEEE Trans. Nucl. Sci. <u>NS-20</u>, 807.

Touscheck, B. F., 1963, <u>Proc. 1963 Summer Study on Storage Rings, Accelerators, and Experimentation at Super-High Energies</u>, Brookhaven National Laboratory, p. 171.

Weinberg, S., 1967, Phys. Rev. Lett. <u>19</u>, 1264.

Wideröe, R., 1943, BRD patent 876279 (priority September 8, 1943); see also Particle Accelerators <u>3</u>, 127 (1972).

Willis, W. J., 1976, private communication.

Wilson, M. N., C. R. Walters, T. D. Lewin, and P. F. Smith, 1970, J. Phys. D-Appl. Phys. 3, 1518.

Wilson, M. N., 1976, "Stabilization of Superconductors for Use in Magnets," Proc. 1976 Appl. Superconductivity Conf., Stanford, CA (to be published).

Zaslavskii, G. and B. V. Chirikov, 1972, Sov. Phys. USPEKHI, 14, 549.

Zee, A., 1973, Phys. Rev. D8, 4038.

Zotter, B., 1972, CERN Report CERN-ISR-TH/72-36.

Zotter, B. W., 1975a, IEEE Trans. Nucl. Sci. NS-22, 1451.

Zotter, B. W., 1975b, CERN Report CERN/ISR-LTD/76-3.

FIGURE CAPTIONS

Fig. 1   Dependence of critical current density on temperature and

magnetic field.

Fig. 2   ISABELLE location on Brookhaven site.

Fig. 3   Sketch of ISABELLE-AGS complex and experimental halls. El is

the beam ejection hall. The other seven areas are for experi-

mental use.

Fig. 4   Sketch of experimental halls with suggested dimensions.

Fig. 5   ISABELLE ring tunnel cross section.

Fig. 6   Aperture subdivision at 30 GeV.

Fig. 7   Layout of magnets in one-half octant.

Fig. 8   Betatron amplitude function and dispersion function in experimental

insertions and regular lattice.

Fig. 9   High-luminosity insertion showing common bending magnets.

Fig. 10   Half-cell magnet system.

Fig. 11   Dipole magnet in vacuum tank showing support system and superinsulation.

Fig. 12   Magnet cross sections.

Fig. 13   Cutaway view of dipole magnet.

Fig. 14   Conductor arrangement in dipole and quadrupole coils.

Fig. 15   Helium distribution system.

Fig. 16   The proton-proton total cross section as a function of laboratory

momentum. Upper limits on momentum are shown for various proton

accelerators.

Fig. 17   The new kinematic region in a Q^2-s plot which would be available

at ISABELLE.

Fig. 18   Estimates for invariant cross section ($M^3 d\sigma/dM$) for $W^{\pm}$ production

from dilepton production data scaled to provide a lower bound.

Δ Binkley, M., et al. Phys. Letters <u>37</u>, 571 (1976).

● Hom, D. C., et al. Phys. Letters <u>36</u>, 1236 (1976).

▣ Kluberg, L., et al. Production of massive muon pairs by 300 and

400 GeV protons, Chicago and Princeton preprint #CP76-1, 1976.

Fig. 19   Parton model calculation for the total production cross section

for $W^{\pm}$.

Fig. 20   Distribution of single leptons from $W^{\pm} \to \ell^{\pm}\nu$ decay observed near

90° as a function of $p_{\perp}$. Calculations are from the quark parton

model for $M_W = 45$, 60, 70, and 100 GeV/c^2. The dashed curve is

an estimate of the lepton background from hadronic processes.

Fig. 21   Scaling predictions for hadron production at large $p_{\perp}$.

a) Dependence on the scaling exponent.

b) Extrapolation, via a scaling law, of the CERN, Columbia,

Rockefeller experimental data from the ISR (Büsser, 1973; 1974).

Fig. 22   Invariant cross section for single jet production in the quark

parton model as a function of transverse momentum and angle.

Fig. 23   Double jet production in the quark parton model with one jet

produced at 90°.

a) Second jet at 90° ("back to back").

b) Second jet at 30°.

c) Dependence upon angle of the second jet for various $p_{\perp}$.

Fig. 24   Extrapolation of existing measurements of total cross sections.

a) Theoretical extrapolations of pp cross sections.

b) Phenomenological fit to pp and $\bar{p}$p cross sections.

Fig. 35   Variation of vertical β function across the momentum aperture

at lattice point of maximum variation. The linear chromaticities,

vertical and horizontal, have been corrected with sextupoles (two

families).

Fig. 36   Multipole variation across the magnet aperture. Comparison with

a numerical computation (Month, 1976) has been used to determine

the normalization. "t=1" corresponds to the orbit, x_0, at the

coil block radius, R_0. r_m is the ratio of the mth multipole at

the orbit, x_0, to its value at the magnet center.

CRITICAL CURRENT

$J_C(B) \approx \dfrac{B_0}{B+B_0} J_0$

$J_C(T) \approx \left(1 - \dfrac{T-T_b}{\tau_C}\right) J_{Cb}$

B_{C2}

FIELD

T_b

$B_{C2}(T) \propto 1 - (T/T_C)^2$

T_C

TEMPERATURE

FIGURE 1

Route 25

N

0   1/2   1

KILOMETERS

ISABELLE RING

William Floyd Pkwy

AGS Ring

Long Island Expwy

FIGURE 2

E5

E6

E4

E7

E3

E8

E2

E1

AGS

N

0   300m
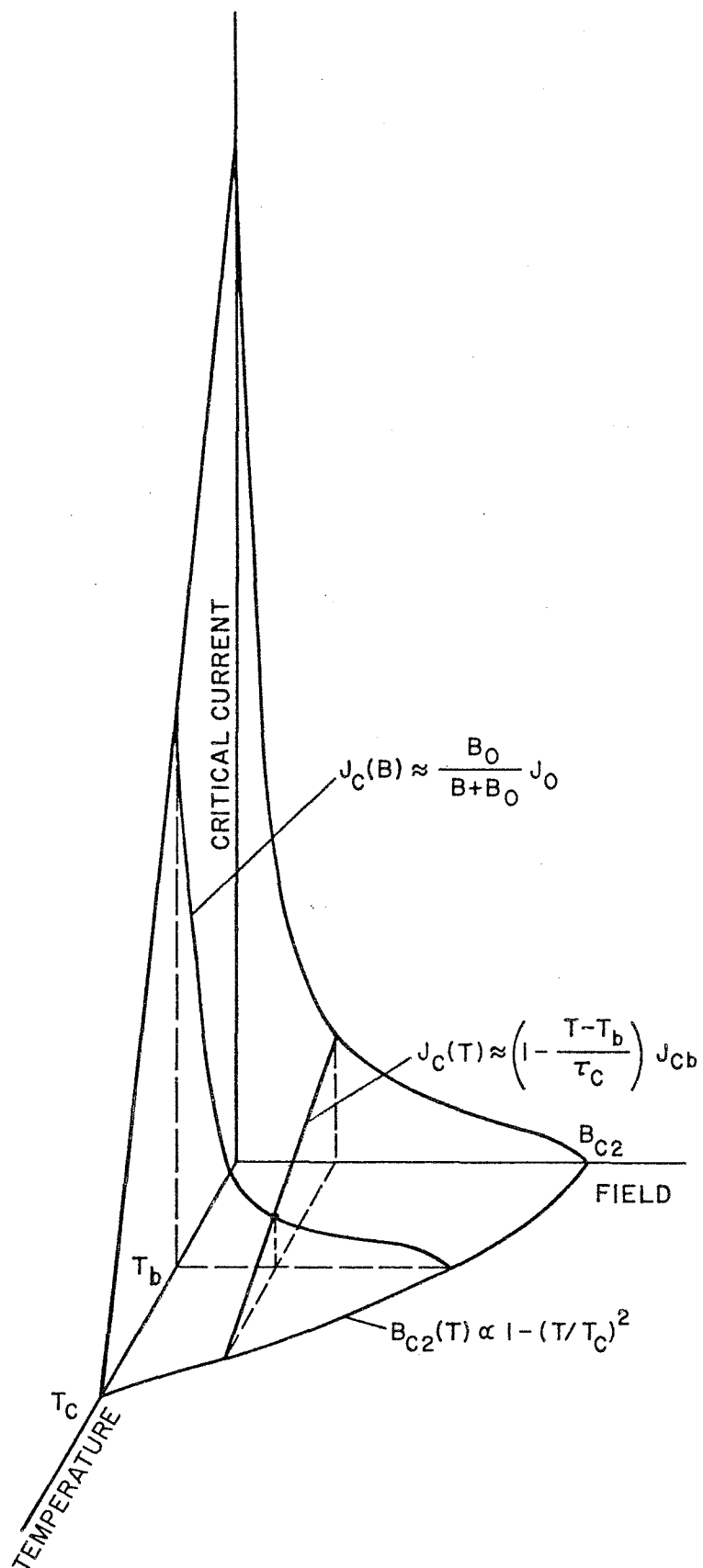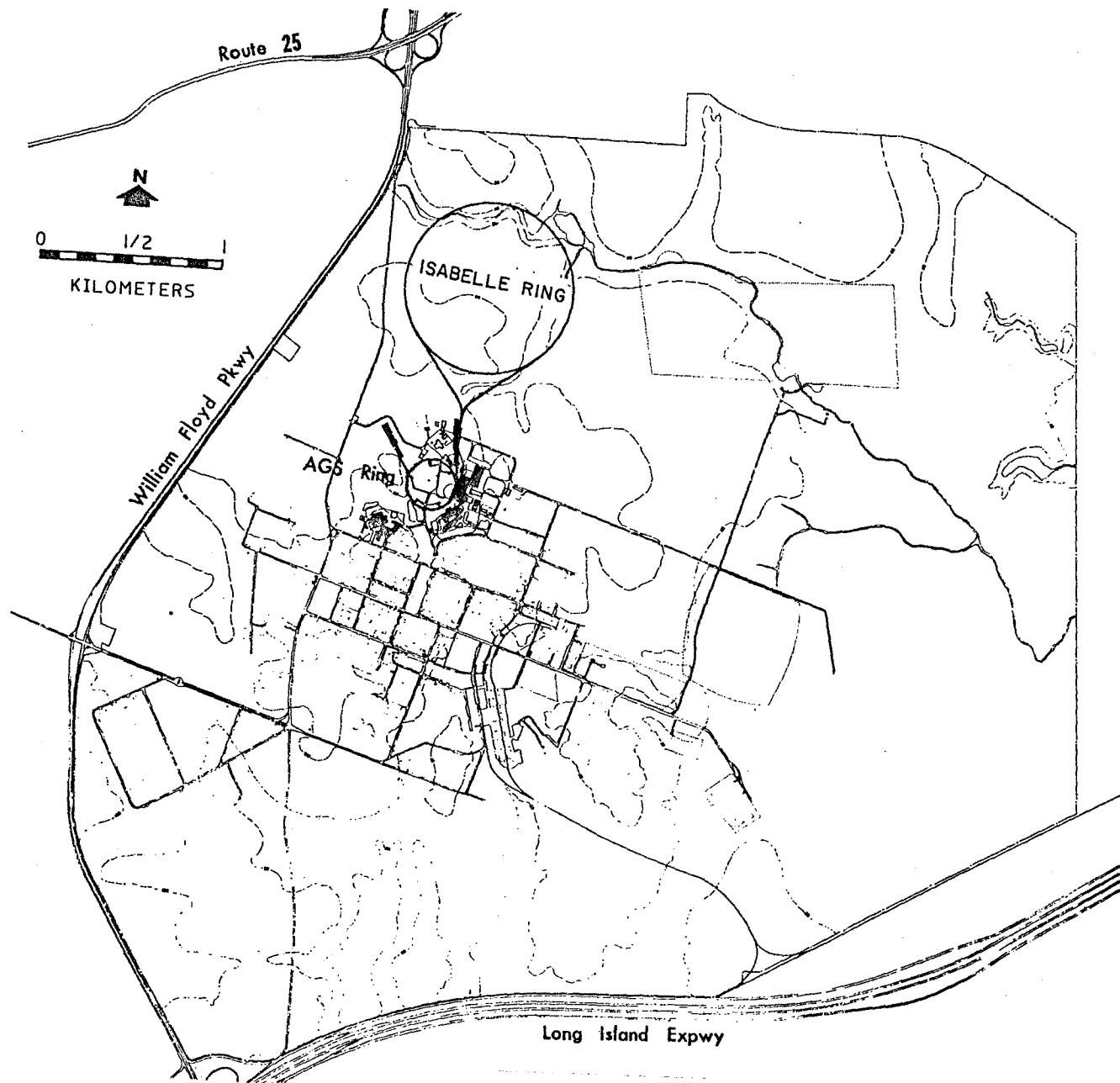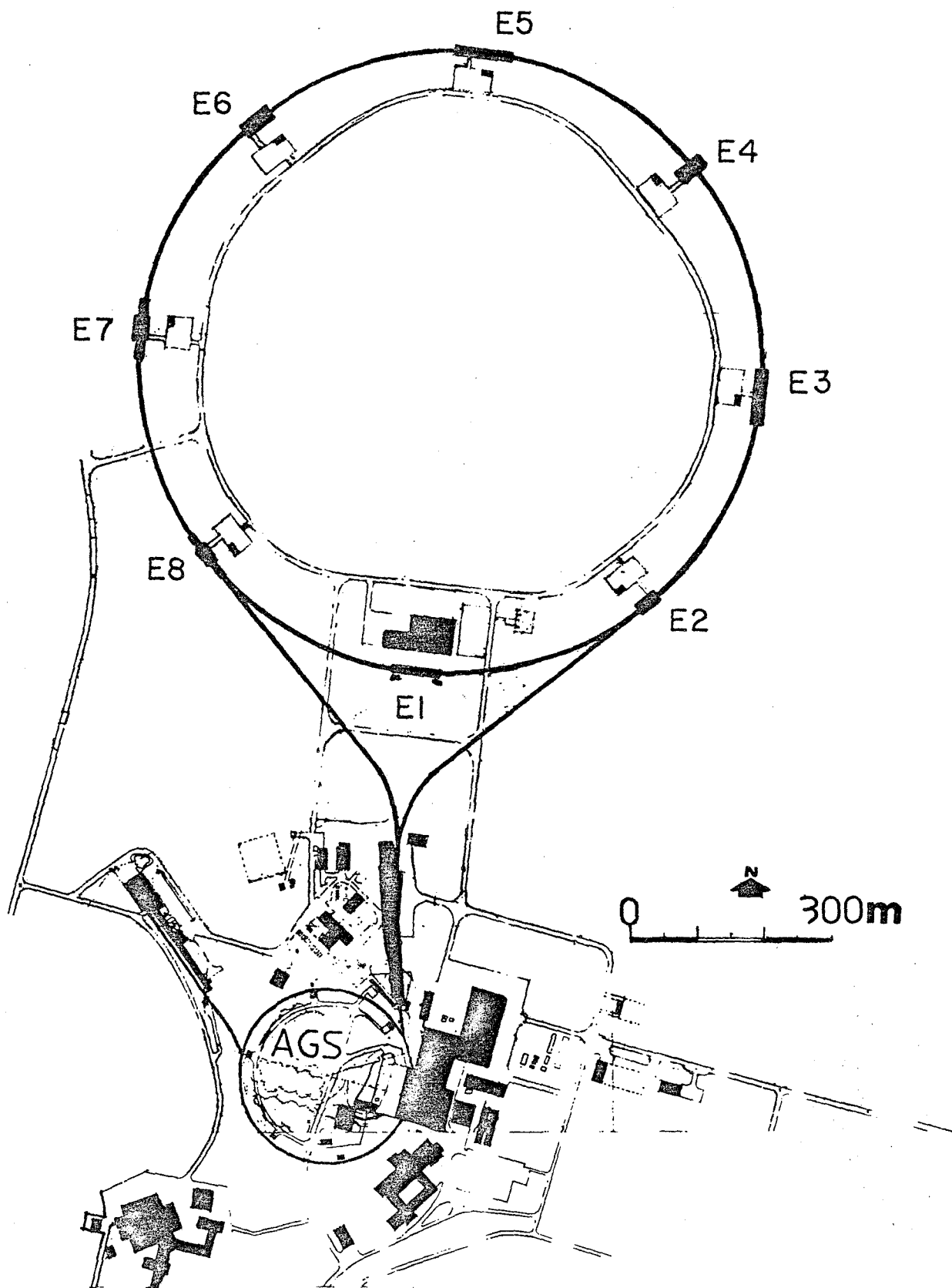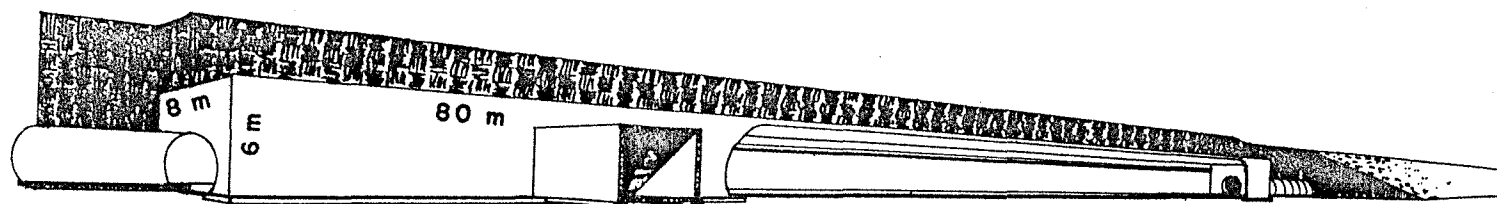
FIGURE 3

SMALL ANGLE HALL
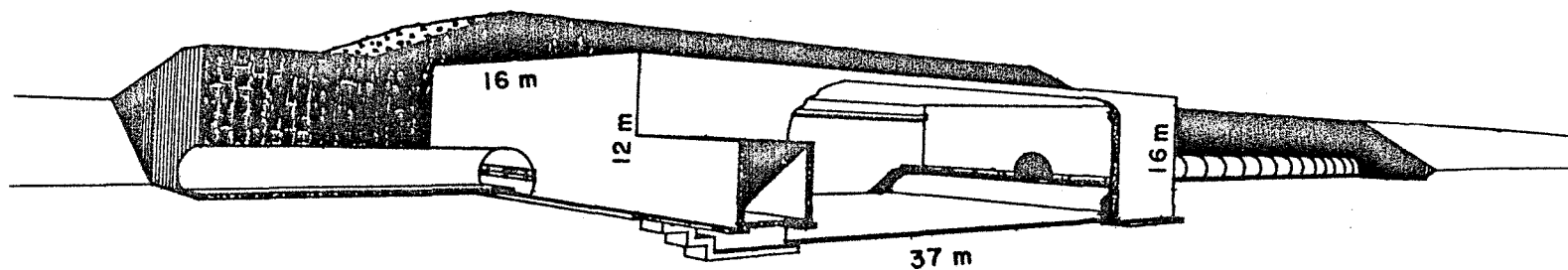
LEPTON HALL

HADRON HALL

FIGURE 4

EARTH SHIELDING

DEWAR

3.0

0.8

2.1

1.27

0.15

0.91
TYPICAL

4.57
TYPICAL

CABLE TRAYS — VACUUM & GAS HEADERS

0   1.0

METERS

4.8

FIGURE 5

INJECTED
BEAM AND
BEAM STACK

$\Delta p/p$

0.7%

7 | 10 | 22 | 14 | 10 | 10 | 7

DUMP PROFILE

57

SAGITTA

$\Delta p/p$

1.6%

BUNCHED
BEAM

7 | 15 | 36 | 15 | 7

80
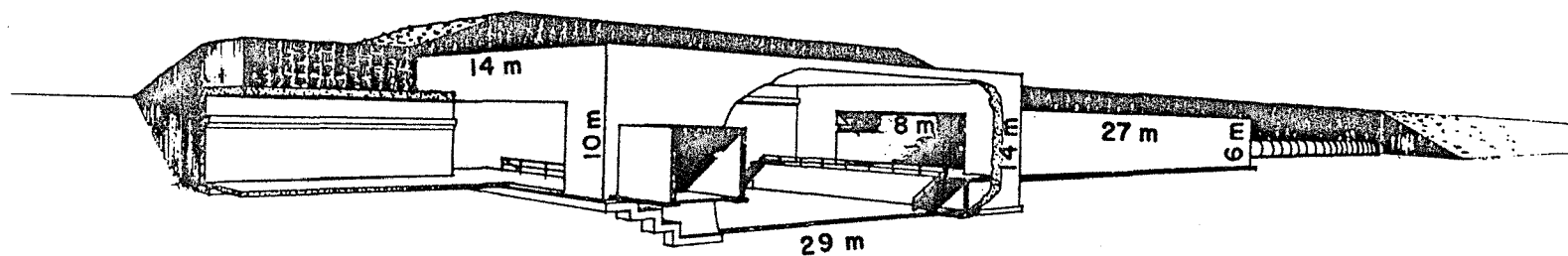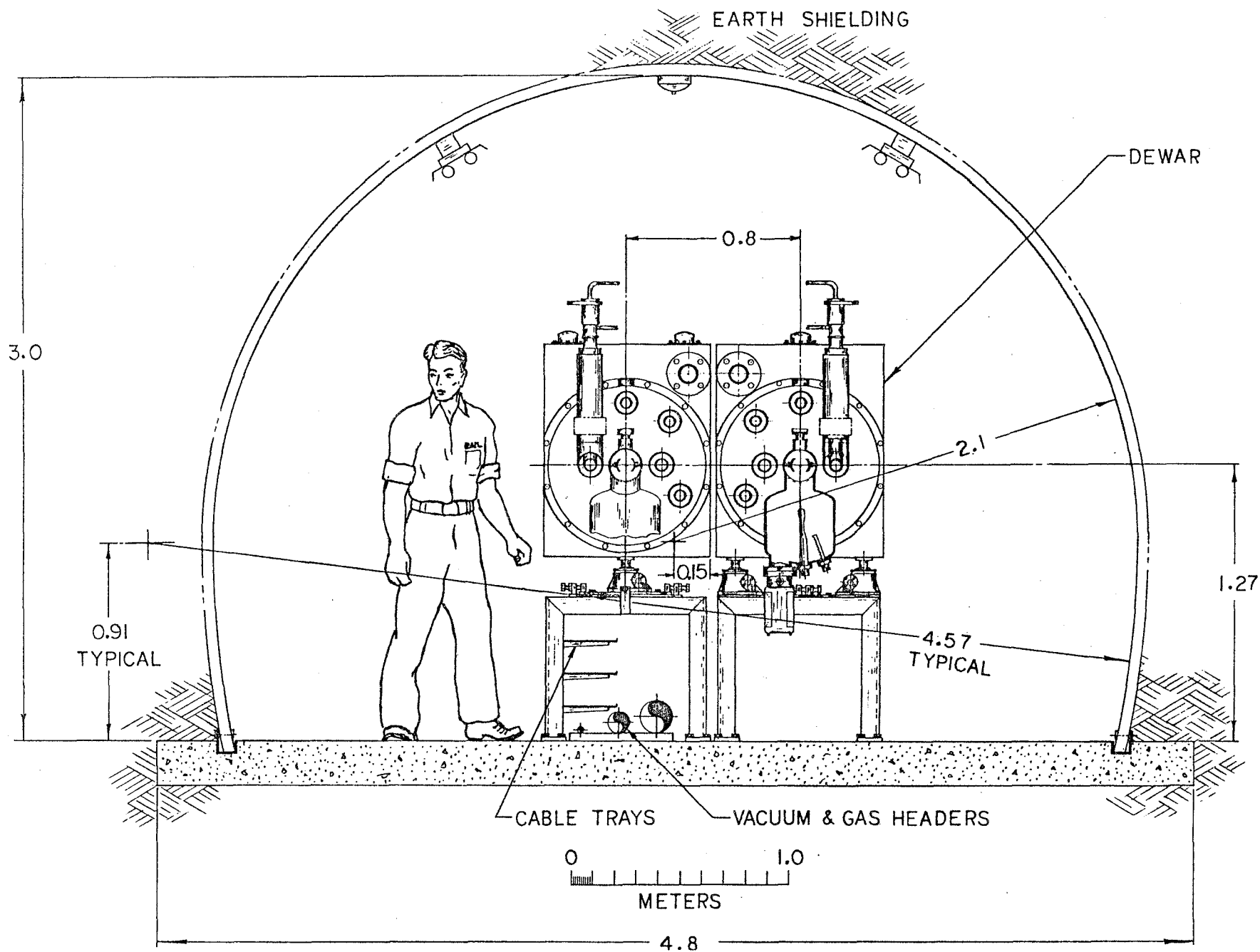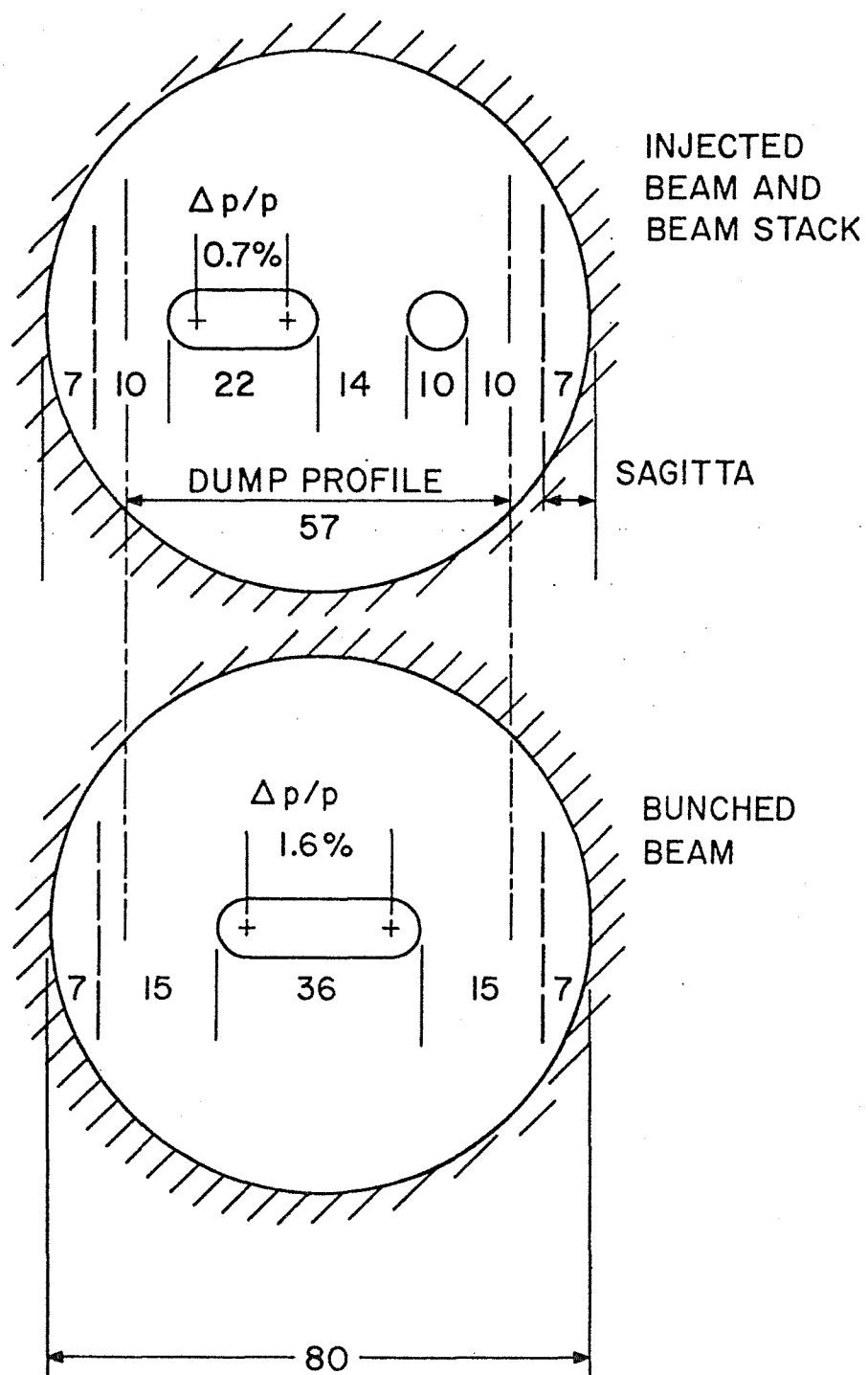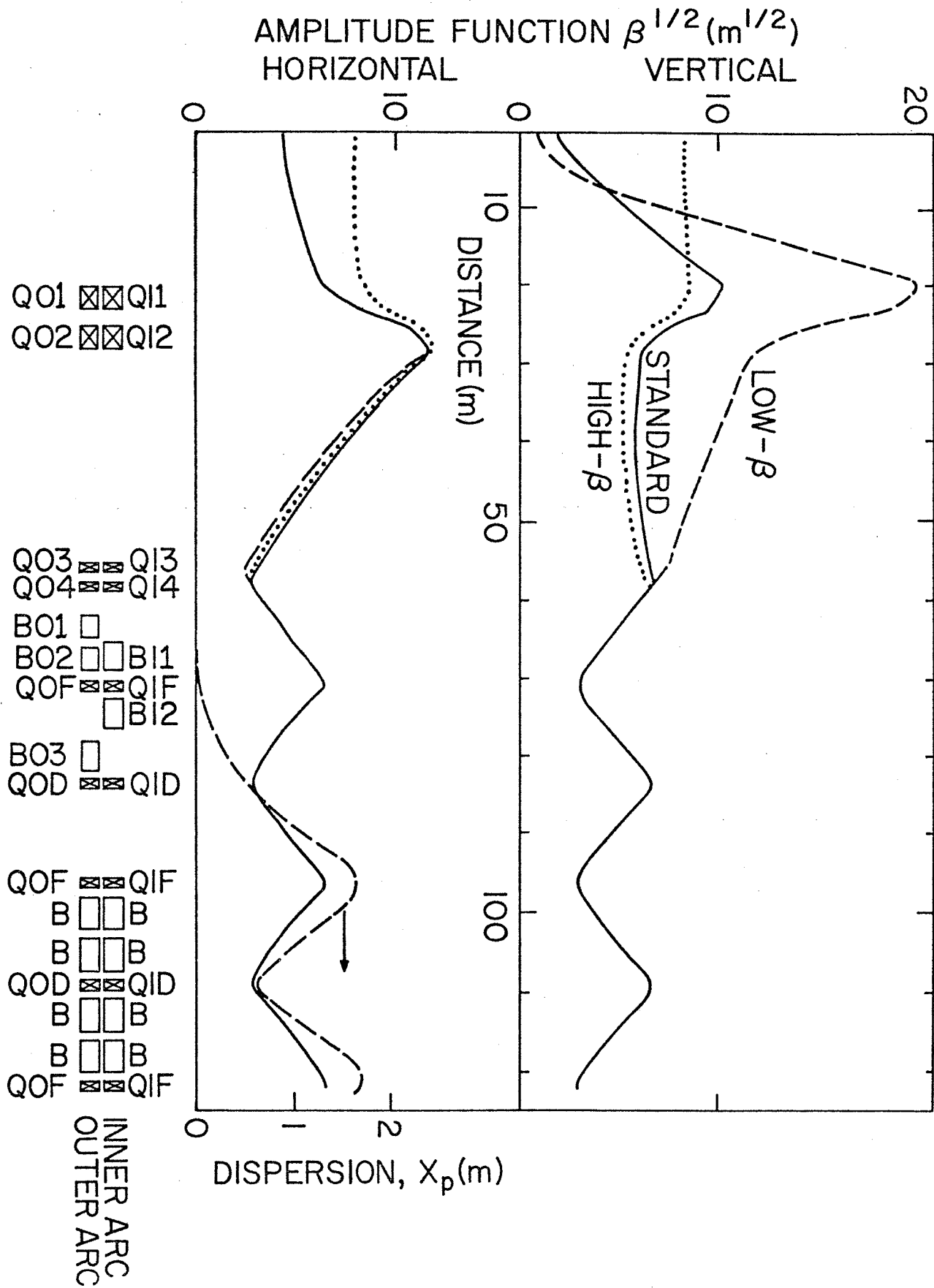
FIGURE 6

FIGURE 7

FIGURE 8

FIGURE 9

FIGURE 10

VACUUM TANK

SUPPORT CHAIN

STAINLESS STEEL HELIUM
VESSEL & SUPPORT TUBE

SUPERINSULATION

MAGNET STEEL
LAMINATIONS

FIGURE 11

16.5 cm O.D. Band

50.8 cm O.D. X 2.5 cm
Thick Wall Cast Tube

Super Insulation

He Cooling Slots

Warm Bore Tube
7.6 cm I.D. X 8.0 cm O.D.

Helical Cooling
Passages

0.3 cm Thick
Fiberglass / Epoxy

45.7cm Dia
Lamination

Cold Bore Tube
10.5 cm I.D. X 10.8 cm O.D.

Field Shaping Coils

12.15 cm I.D. X 1.7 cm
Thick Coil

DIPOLE MAGNET
CROSS SECTION

16.6 cm O.D. Band

43.2 cm O.D. X 2.5 cm
Thick Wall Cast Tube

Super Insulation

He Cooling Slots

Warm Bore Tube
7.6 cm I.D. X 8.0 cm O.D.

Cold Bore Tube
9.8 cm I.D. X 10.2 cm O.D.

38.1 cm Dia
Lamination

Field Shaping Coils

Gradient Trim Coil

12.0 cm I.D. x 1.7 cm
Thick Coil

QUADRUPOLE MAGNET
CROSS SECTION

0   10   20   30   40

CENTIMETERS

FIGURE 12

STAINLESS STEEL
SUPPORT TUBE

IRON LAMINATIONS

CORRECTION COILS

MAIN COILS

EPOXY SPACERS

FIBERGLASS-EPOXY WITH
HELIUM COOLING CHANNELS

COLD BORE TUBE

SPACE FOR
SUPER INSULATION

WARM BORE TUBE
(VACUUM CHAMBER)

EPOXY SPACERS

FIBERGLASS-EPOXY WITH
HELIUM COOLING CHANNELS

FIGURE 13

SPACERS

WEDGES AND POSTS

IRON SHIELD

CM

DIPOLE MAGNET CONDUCTOR ARRANGEMENT

SPACERS

WEDGES AND POSTS

IRON SHIELD

CM

QUADRUPOLE MAGNET CONDUCTOR ARRANGEMENT

FIGURE 14

HEAT SHIELD COOLING LOOP

SERIES COOLED MAGNETS IN ONE OCTANT

TEMPERATURE/FLOW CONTROL VALVE

RETURN HEADER
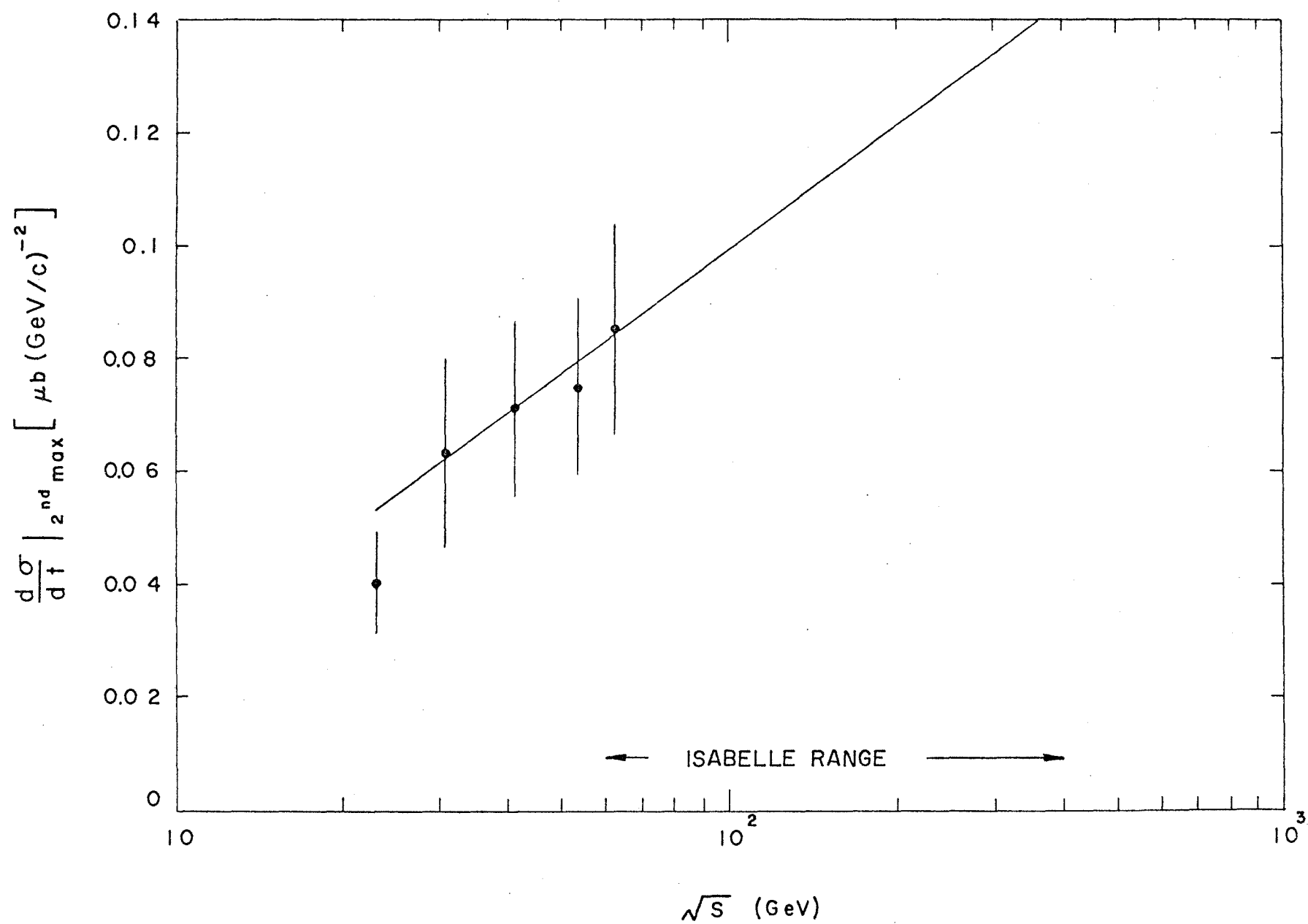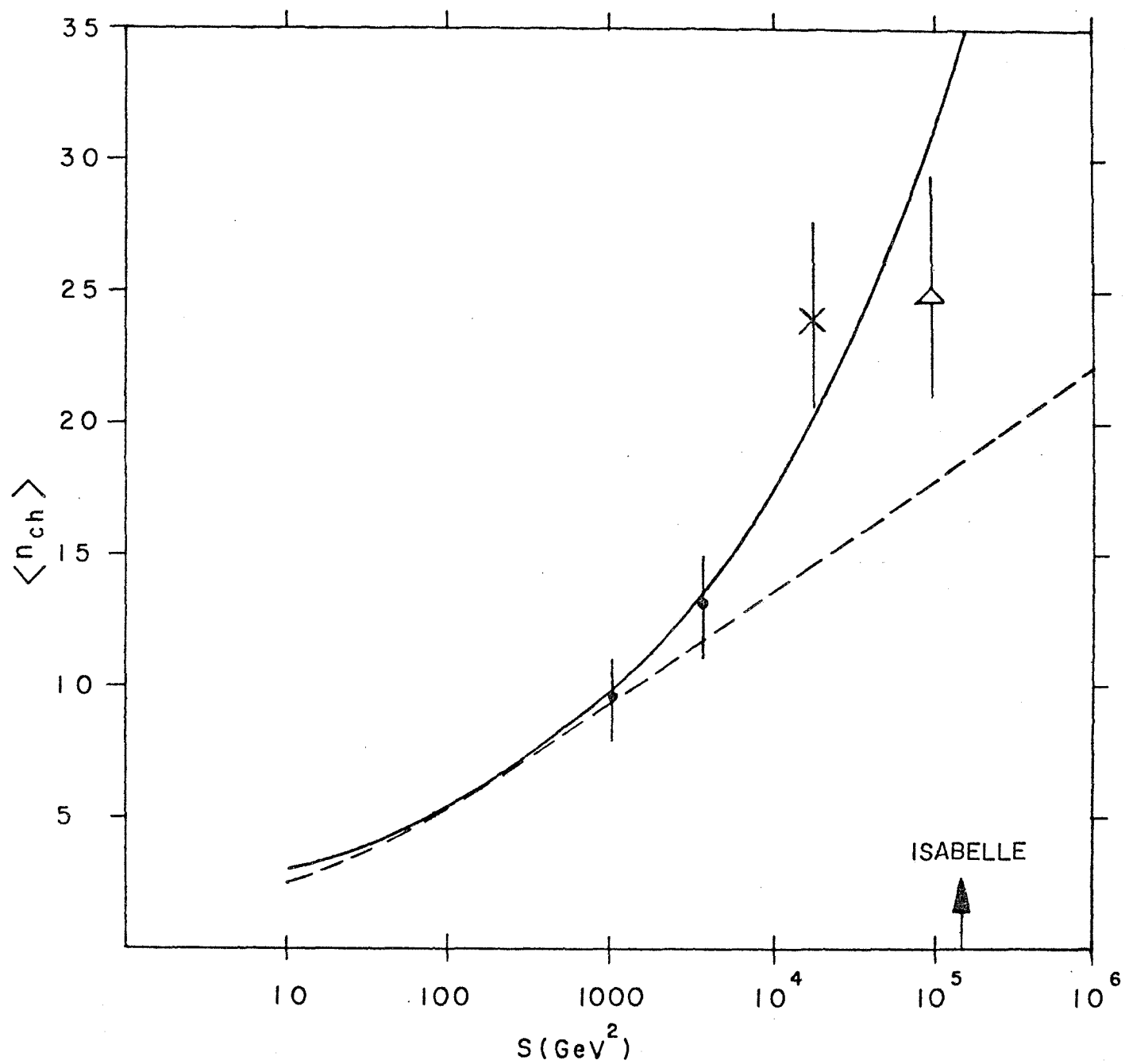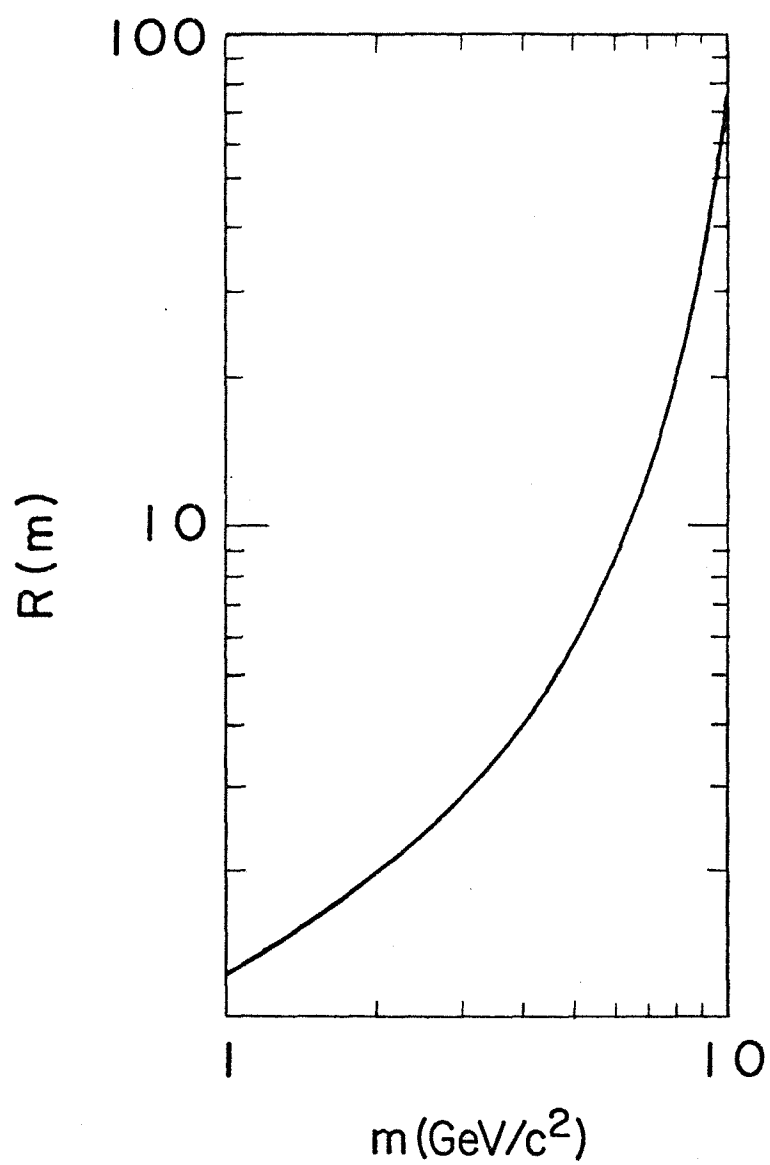
REFRIGERATOR (SUPPLIES COOLING FOR BOTH RINGS)

SUPPLY HEADER

FIGURE 15

FIGURE 16

FIGURE 17
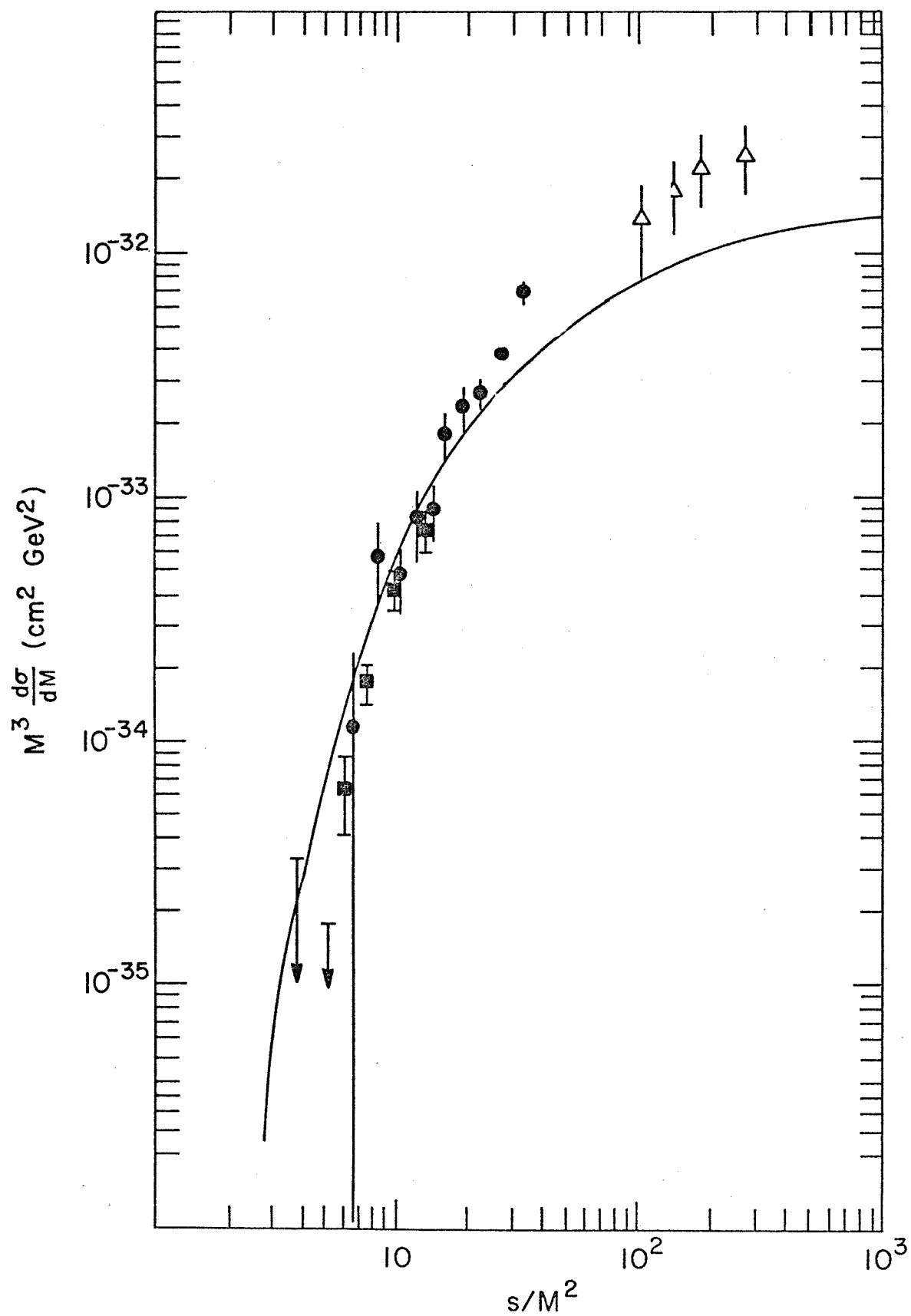
FIGURE 18
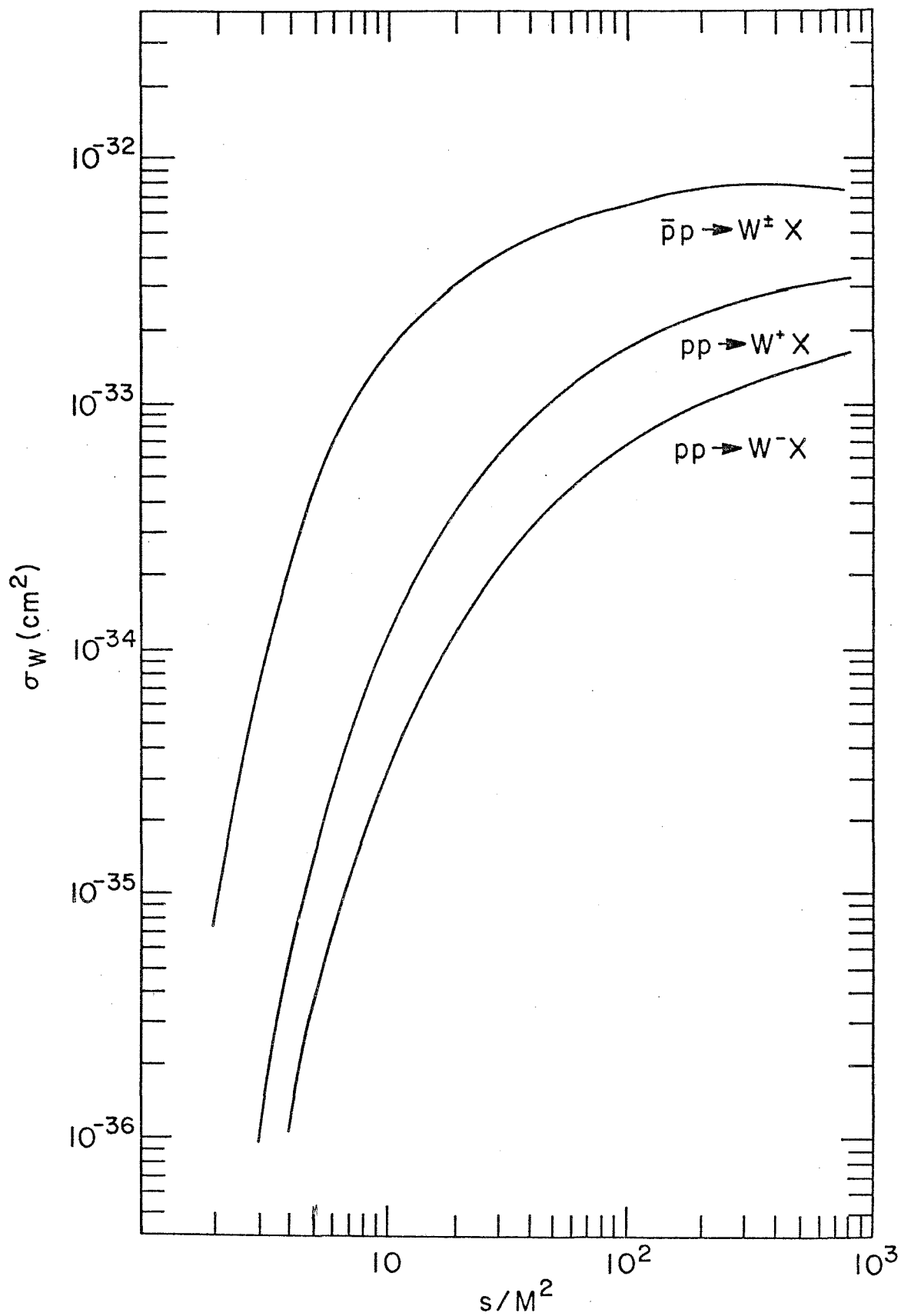
FIGURE 19
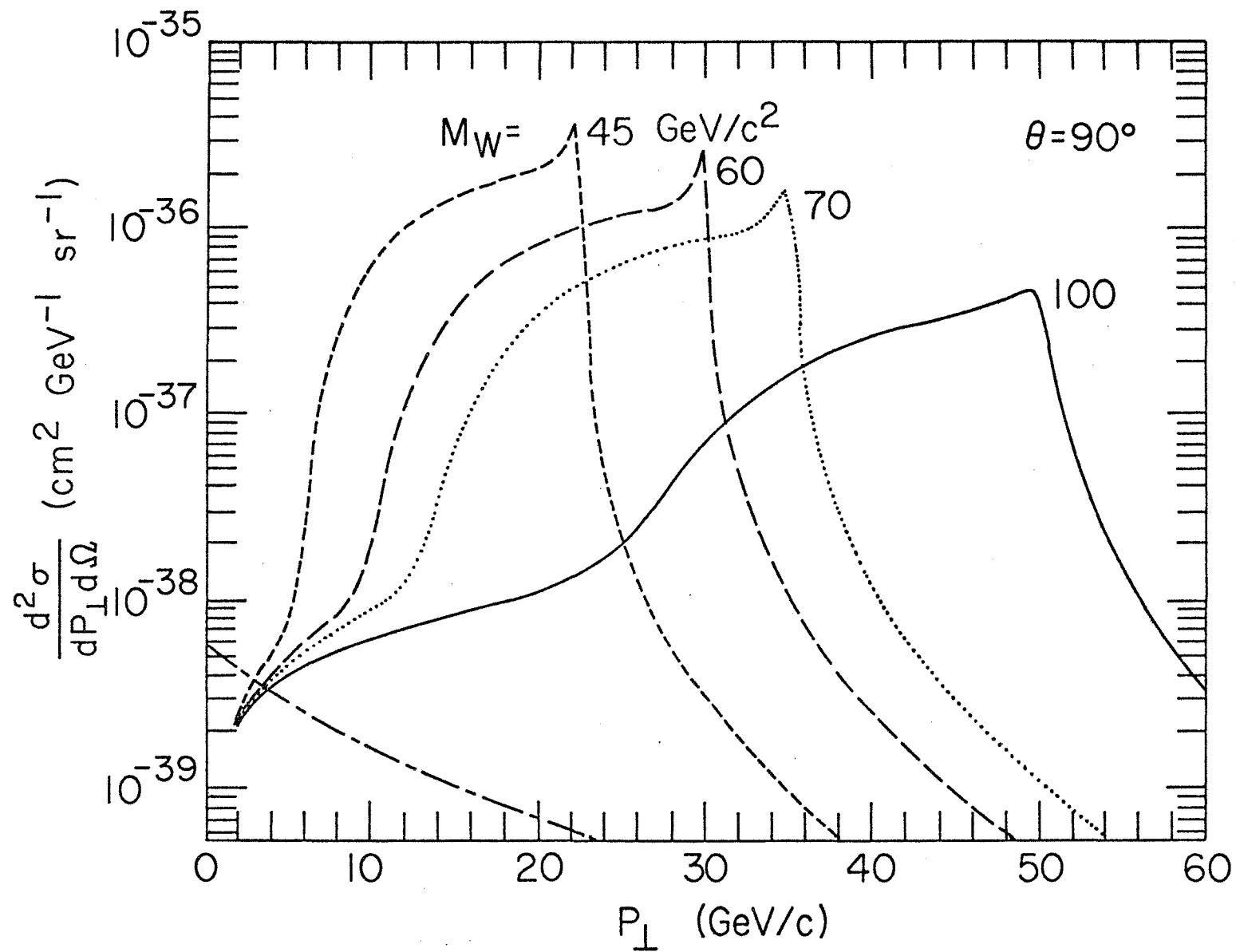
FIGURE 20
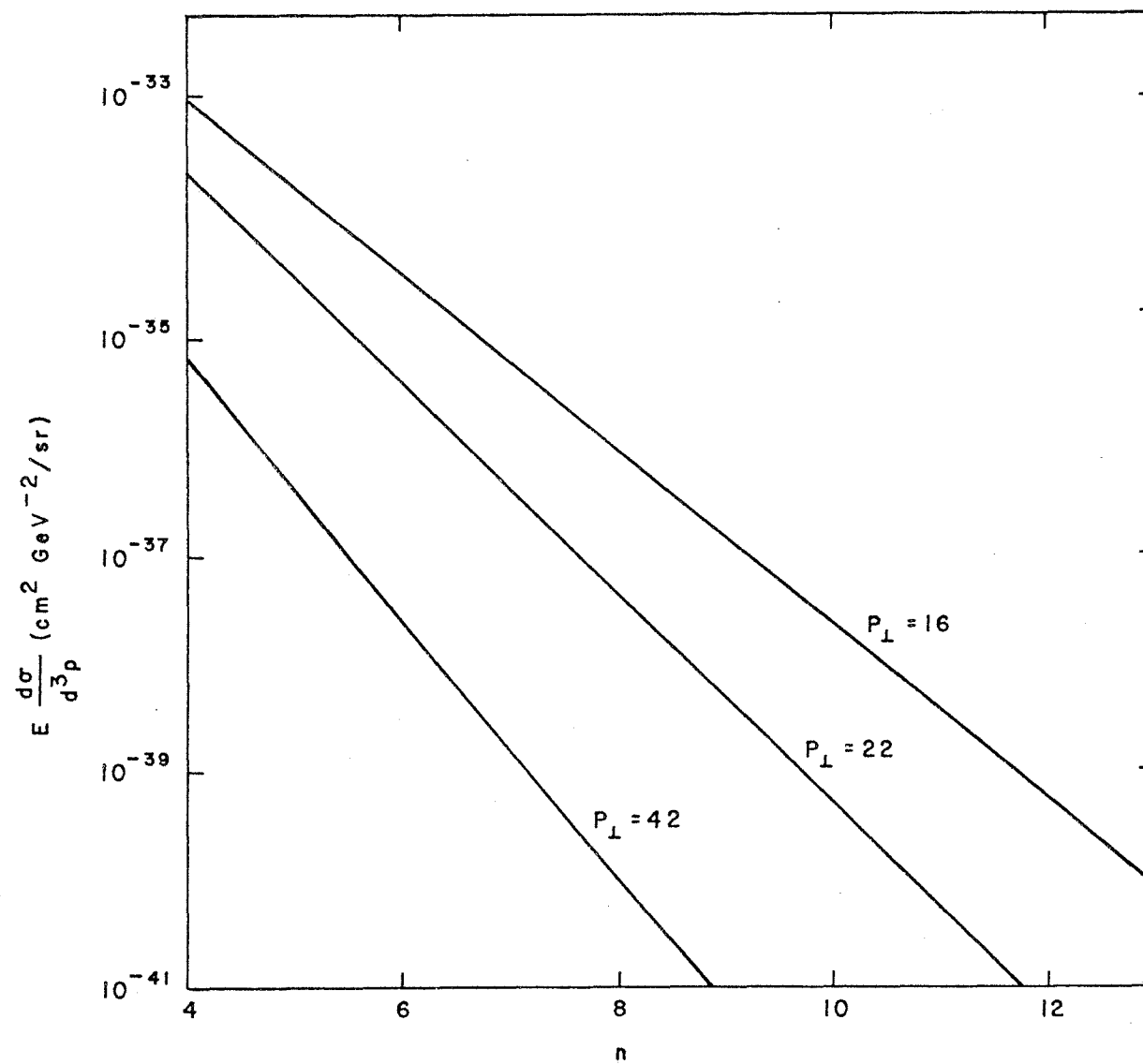
FIGURE 21 (a)
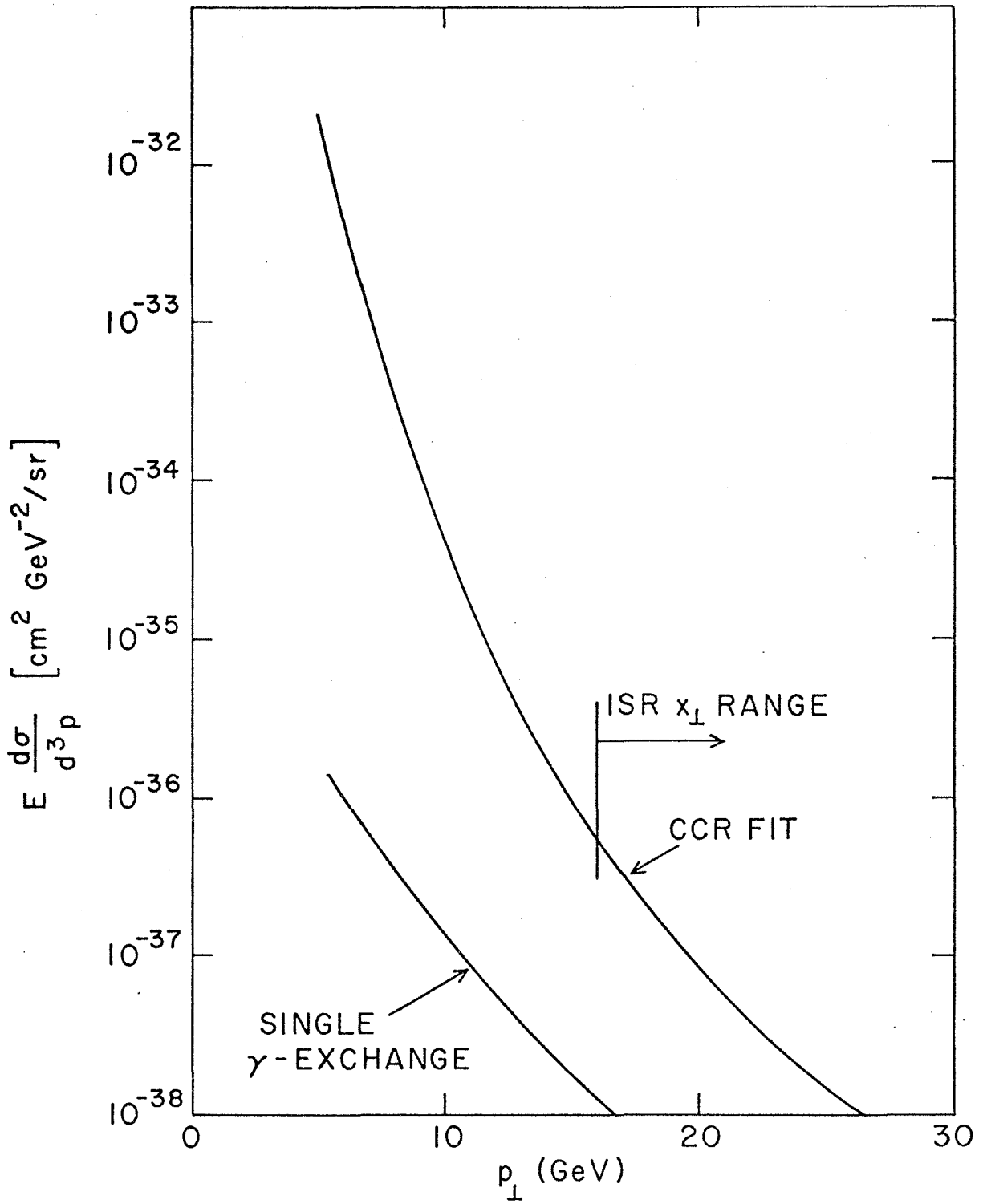
FIGURE 21 (b)
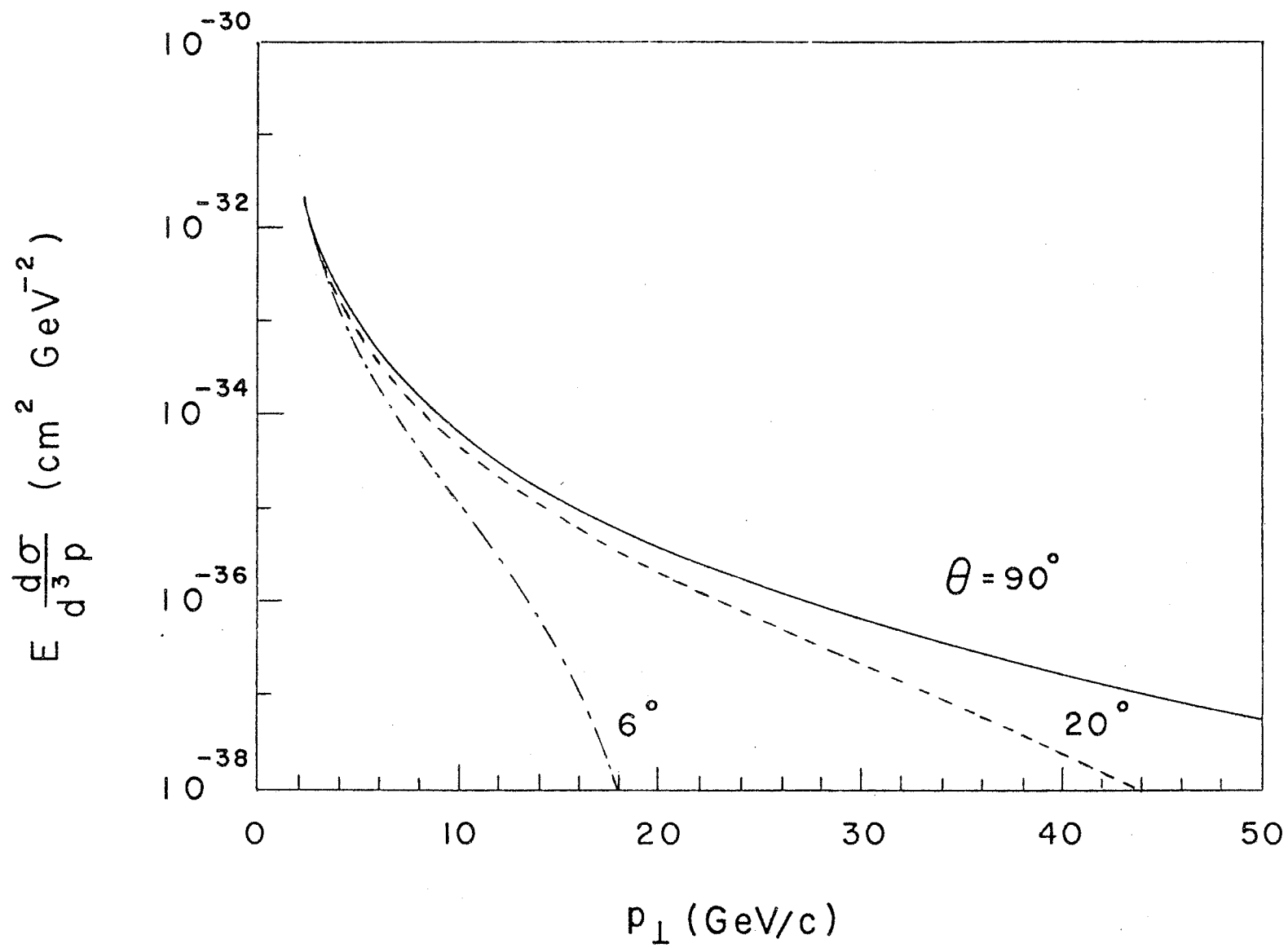
FIGURE 22
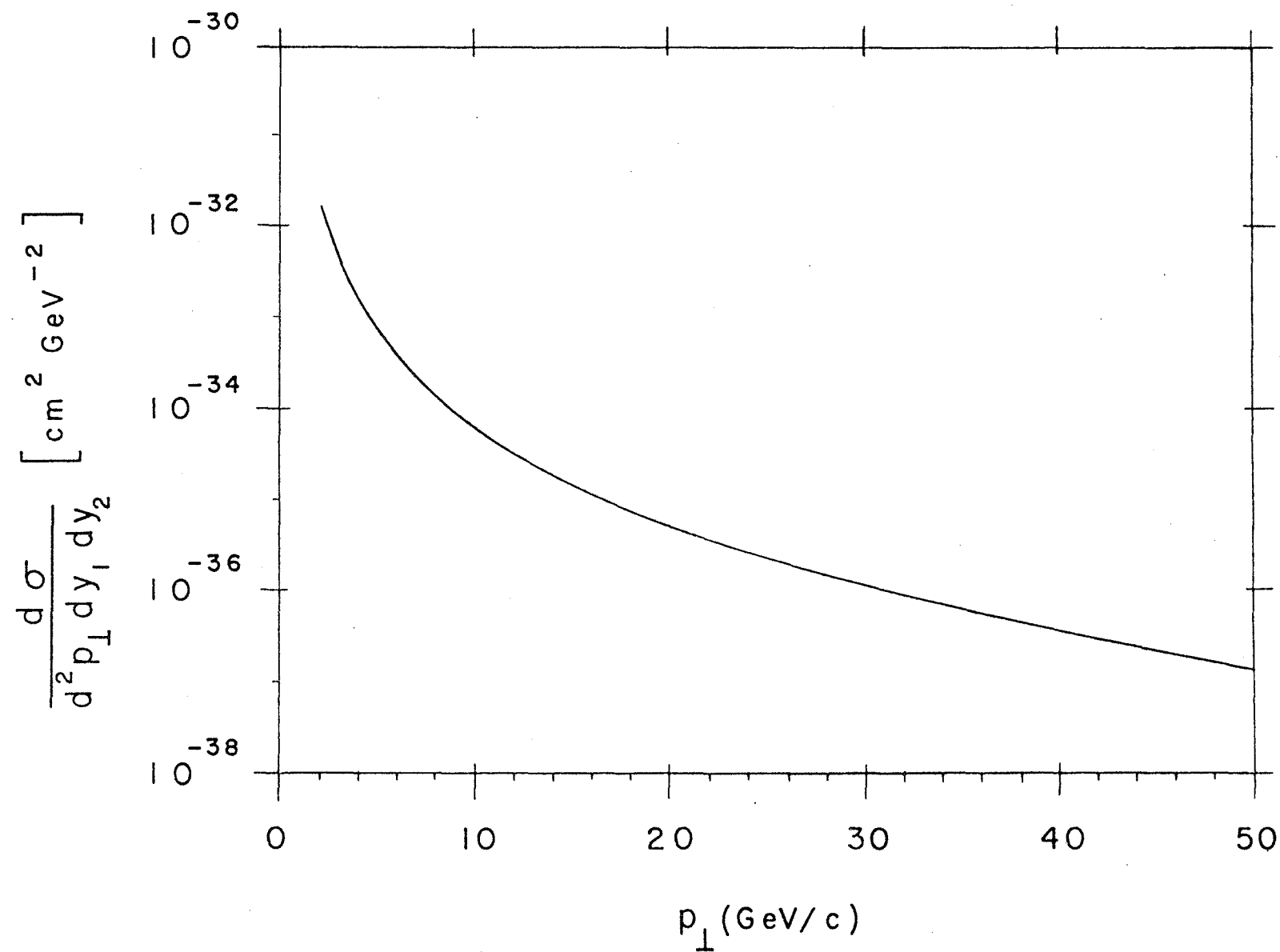
FIGURE 23 (a)
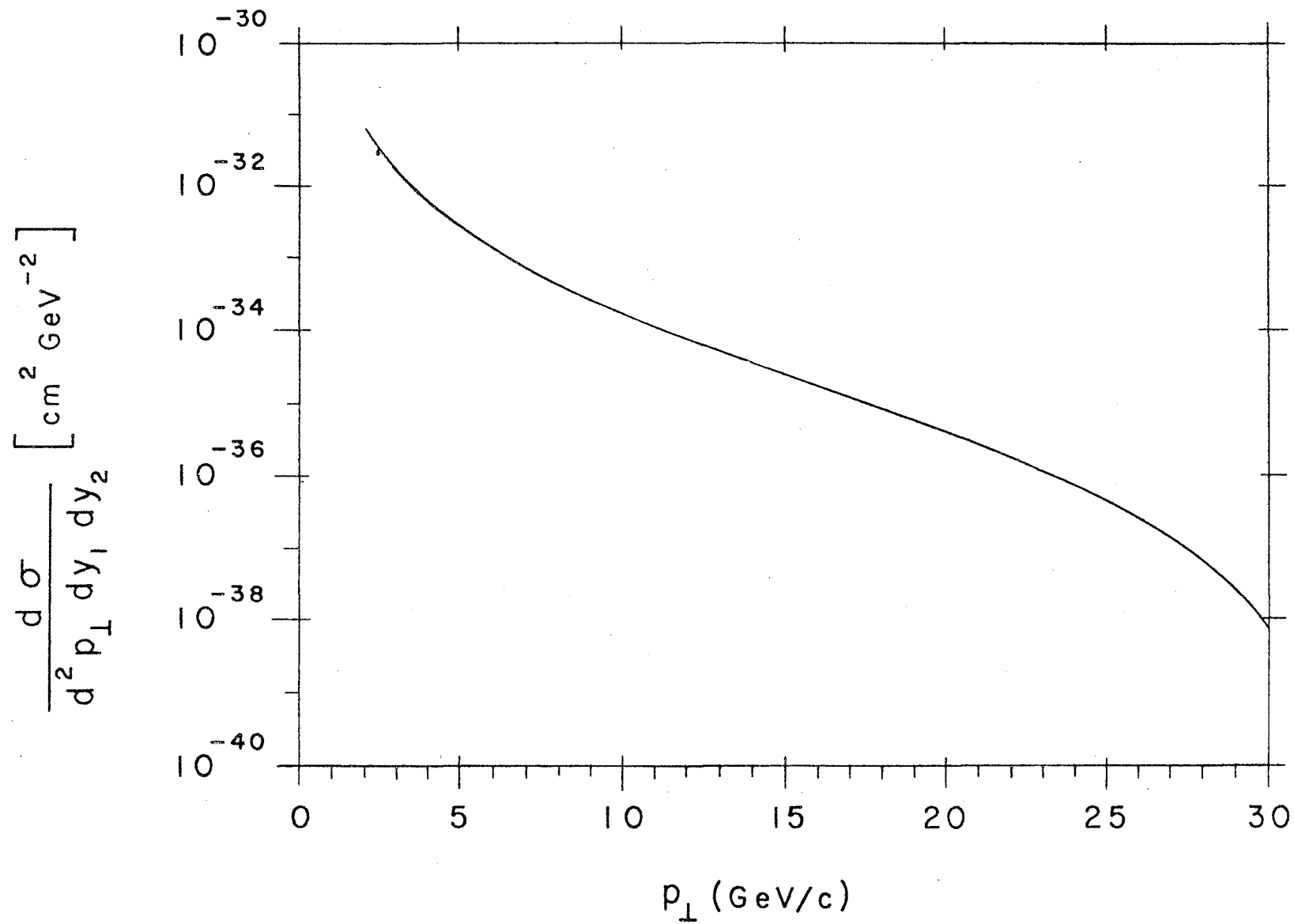
FIGURE 23 (b)

FIGURE 23 (c)

FIGURE 24 (a)

(p̄p) DATA
○ A.S. CARROLL (1974 b)
● GALBRAITH (1965)
△ DENISOV (1971)

$\sigma_T \, (\bar{p}p)$

$\sigma_T \, (pp)$

σ_T (mb)

(pp) DATA
○ DENISOV (1971)   ● AMALDI (1973 a)
□ BROMBERG (1973)   ▽ AMENDOLIA (1973 a,b)
◇ CHARLTON (1972)   ■ ISR (AMALDI, 1973 b;
△ DAO (1972)   AMENDOLIA, 1973 a)
× BARTENEV (1972,   ○ NAL (CARROLL, 1974 b)
         1973 a)

P_{lab} (GeV/c)

FIGURE 24 (b)

FIGURE 25 (a)

$$\rho = \frac{ReF(s,t=0)}{ImF(s,t=0)}$$

$\bar{p}\,p$

pp

$\bar{p}p$ pp

$\triangle$ AMALDI (1973a)

$\circ$ BARTENEV (1973b)

$\triangledown$ BEZNOGIKH (1972)

$\bullet$ $\circledcirc$ FOLEY (1965a, 1967)

$\square$ BELLETTINI (1965)

$\times$ WILLIS (1976)

S (GeV^2)
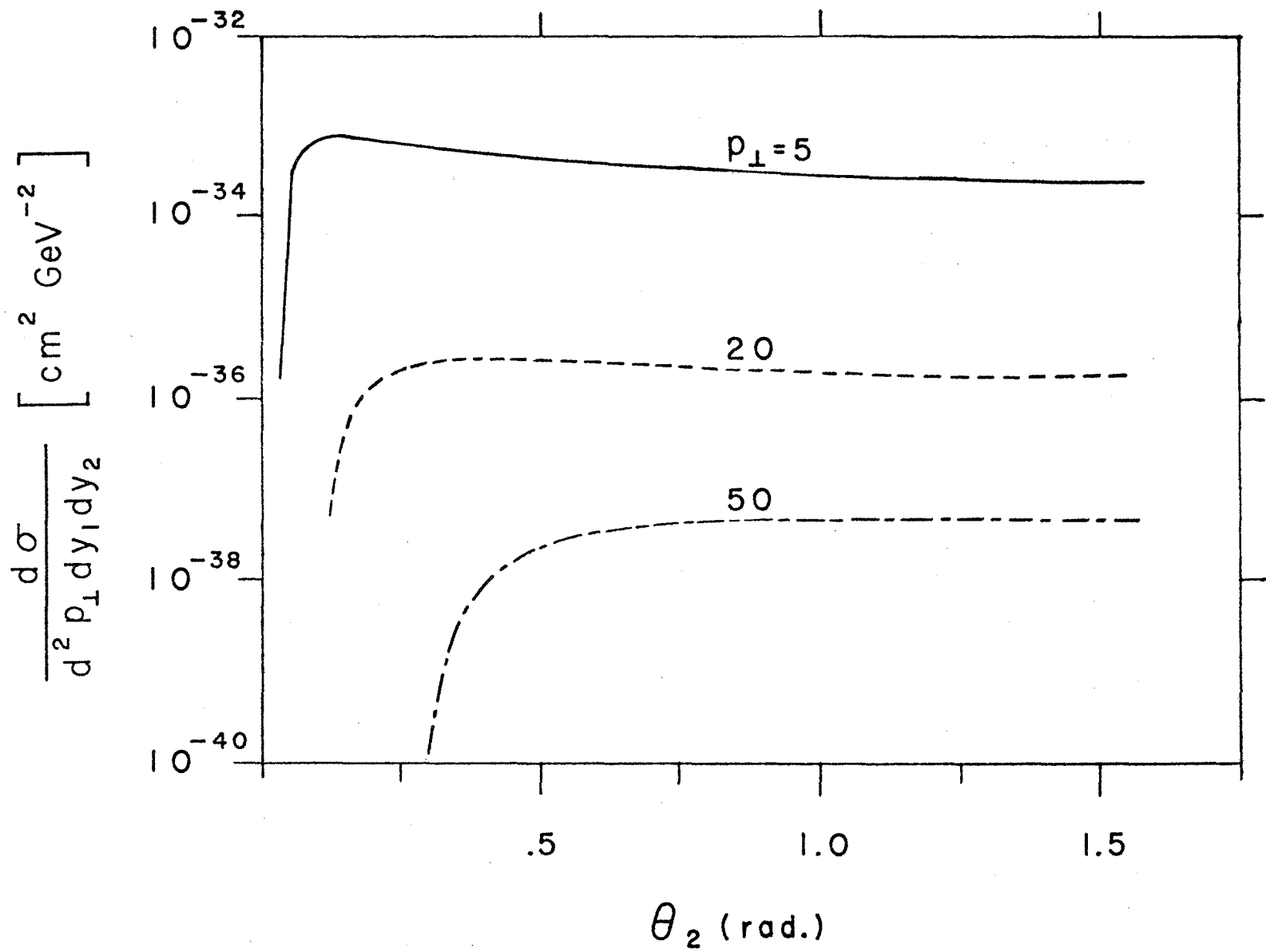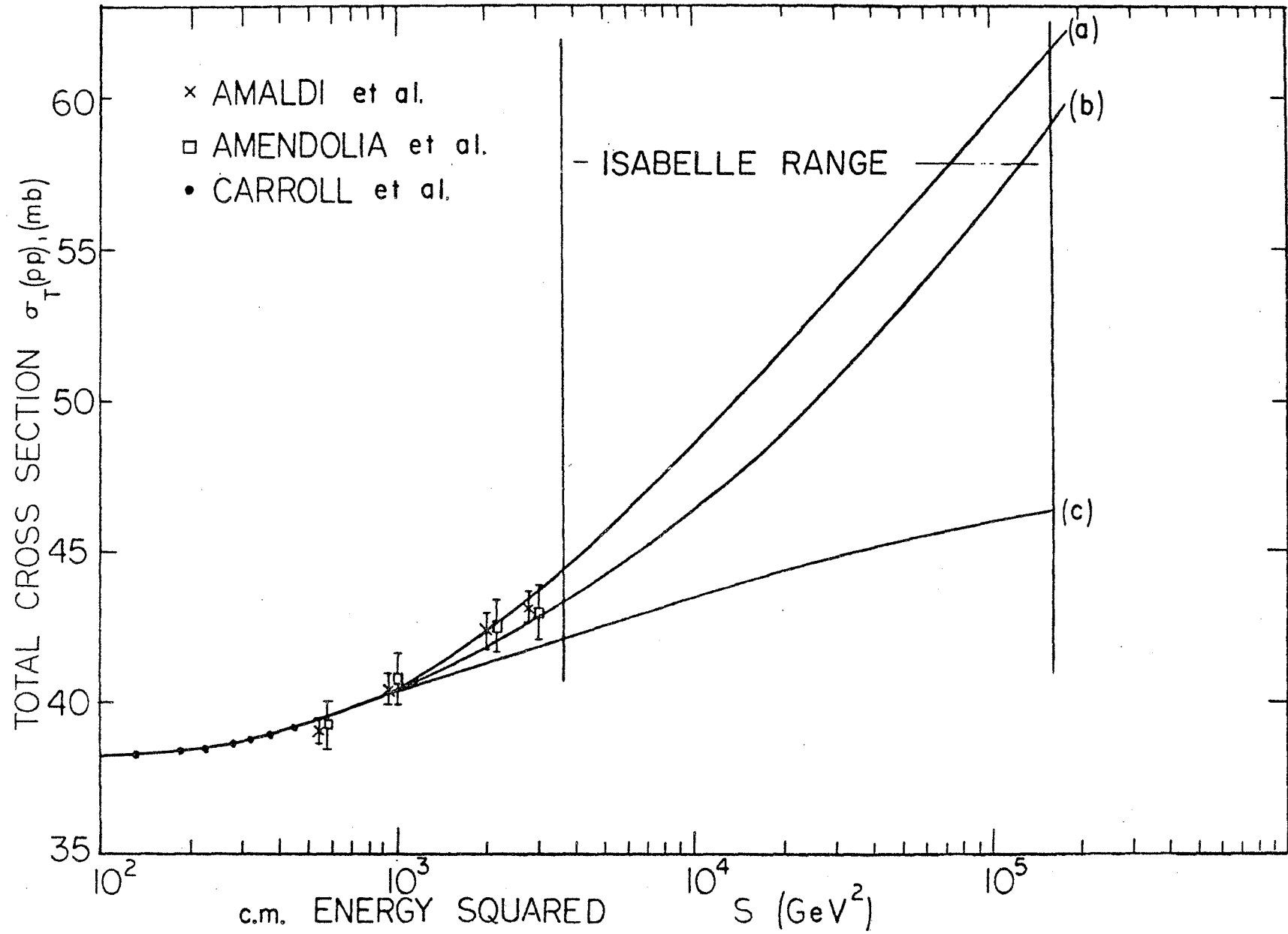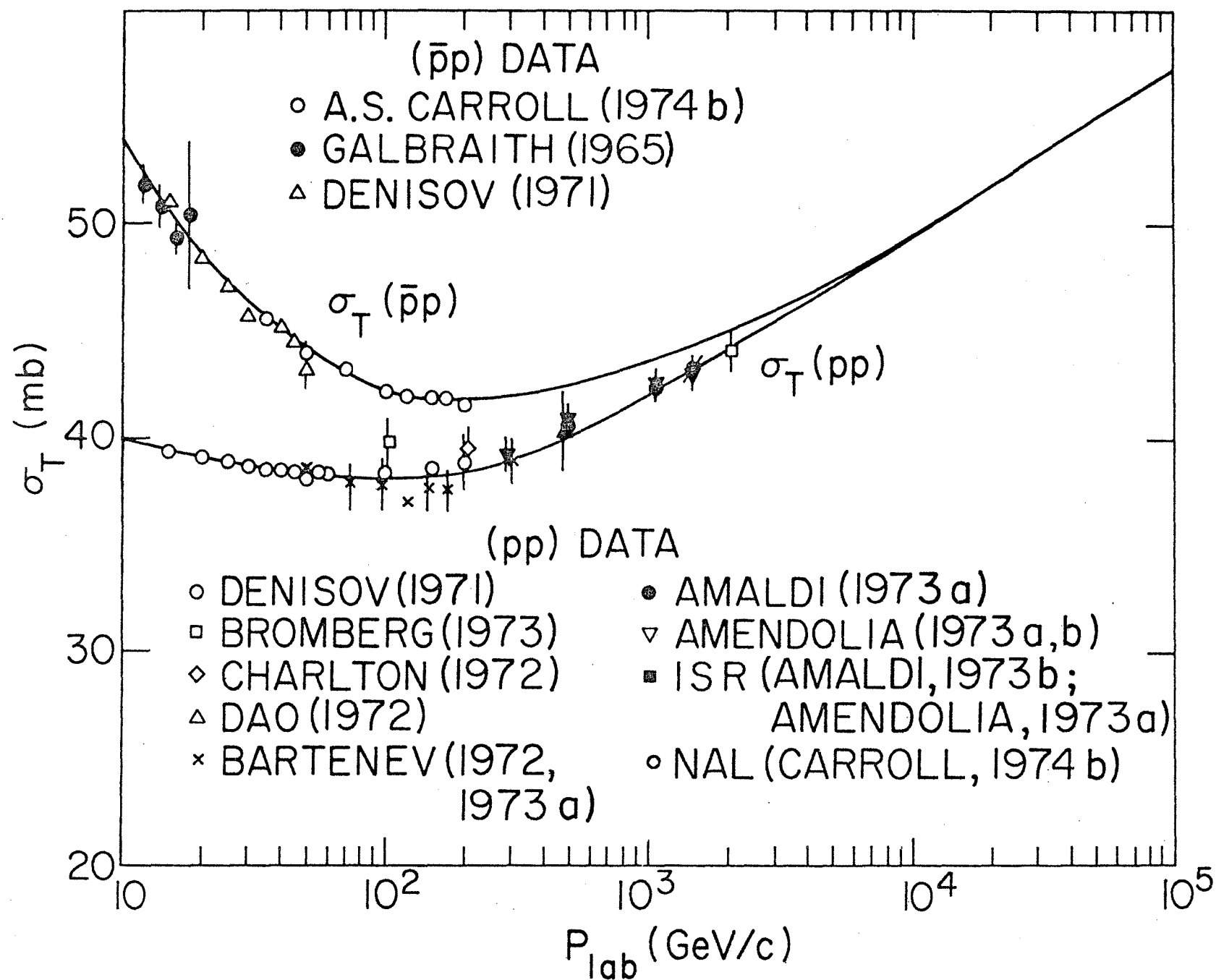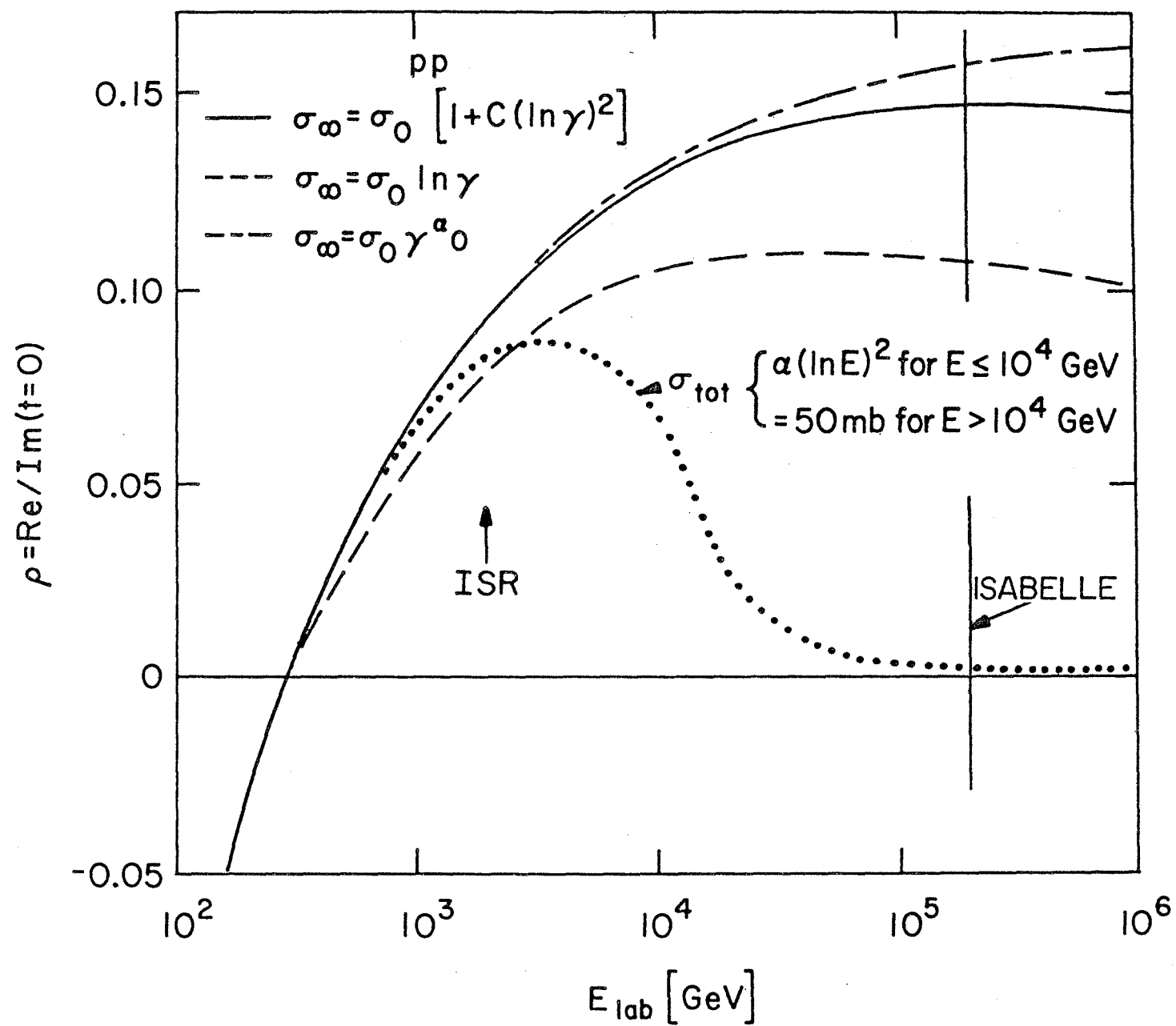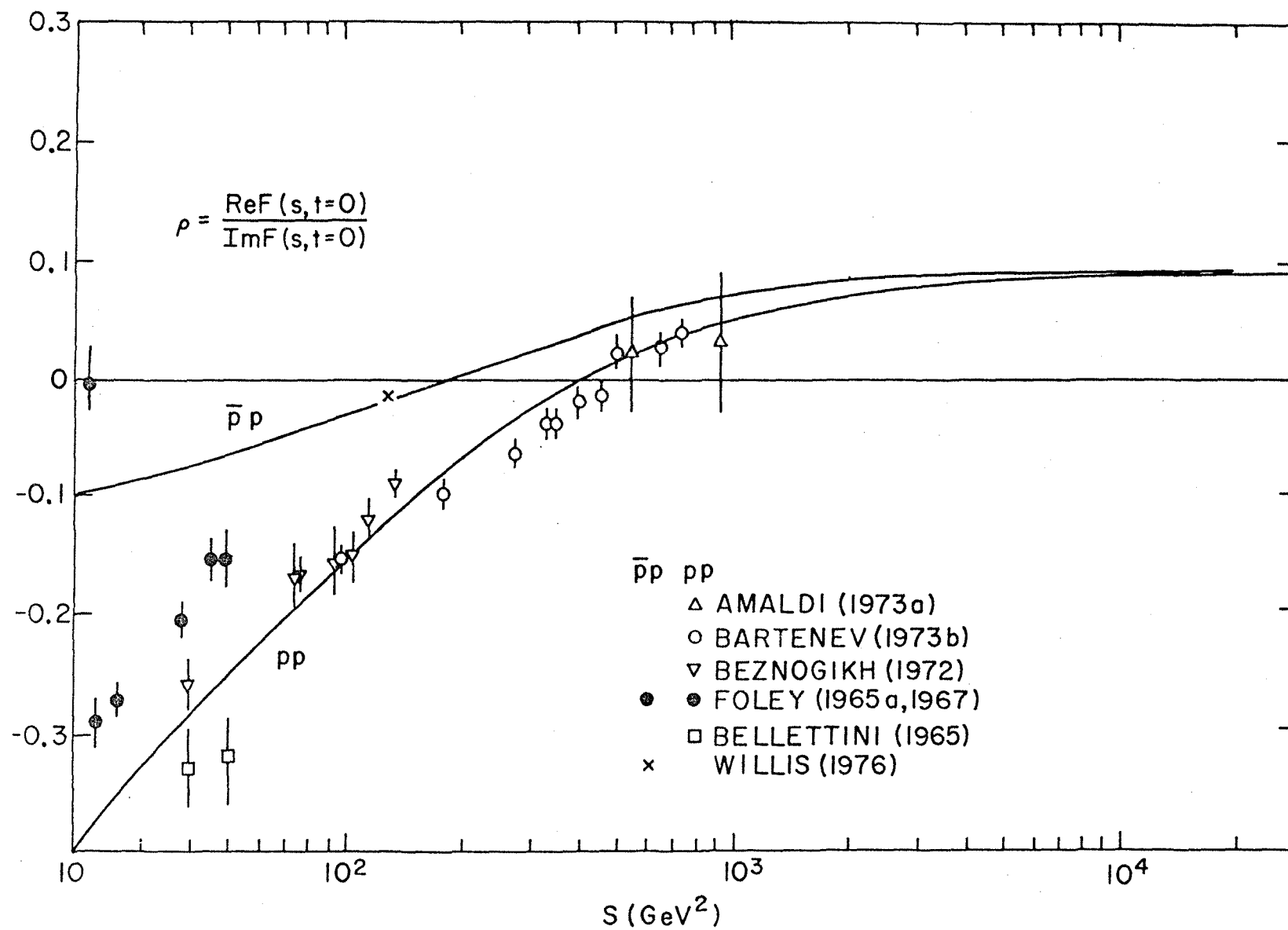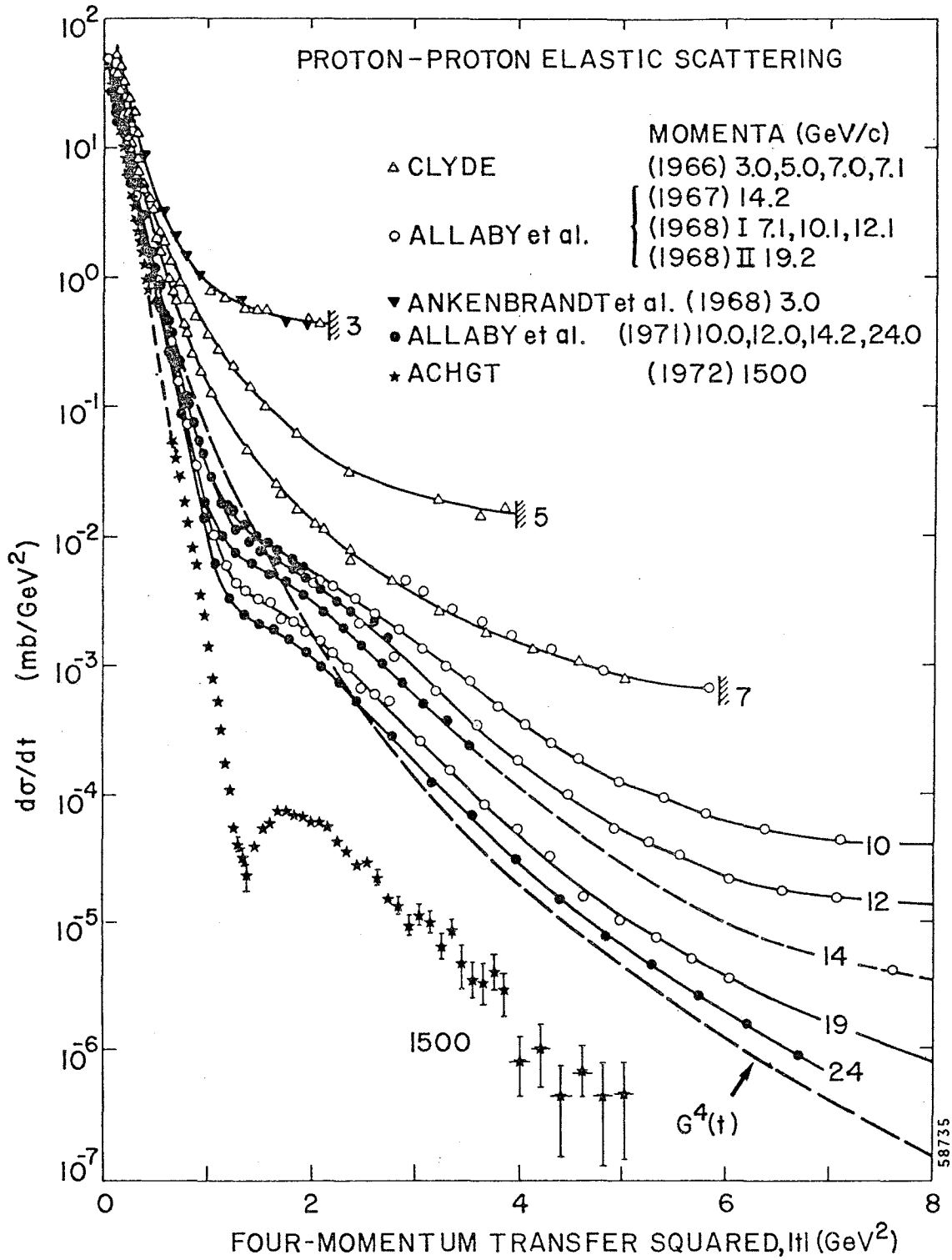
FIGURE 25 (b)
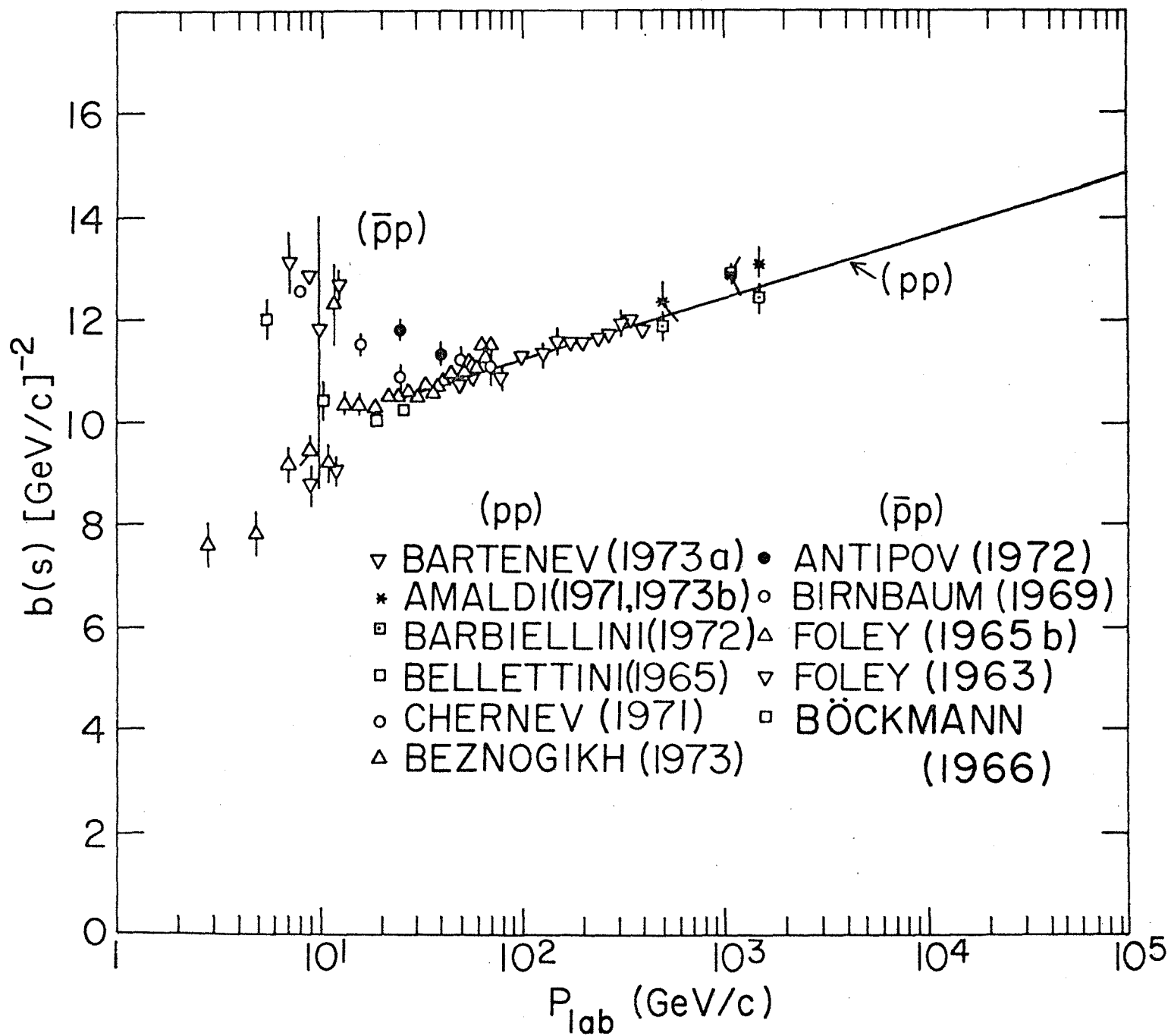
FIGURE 26

FIGURE 27
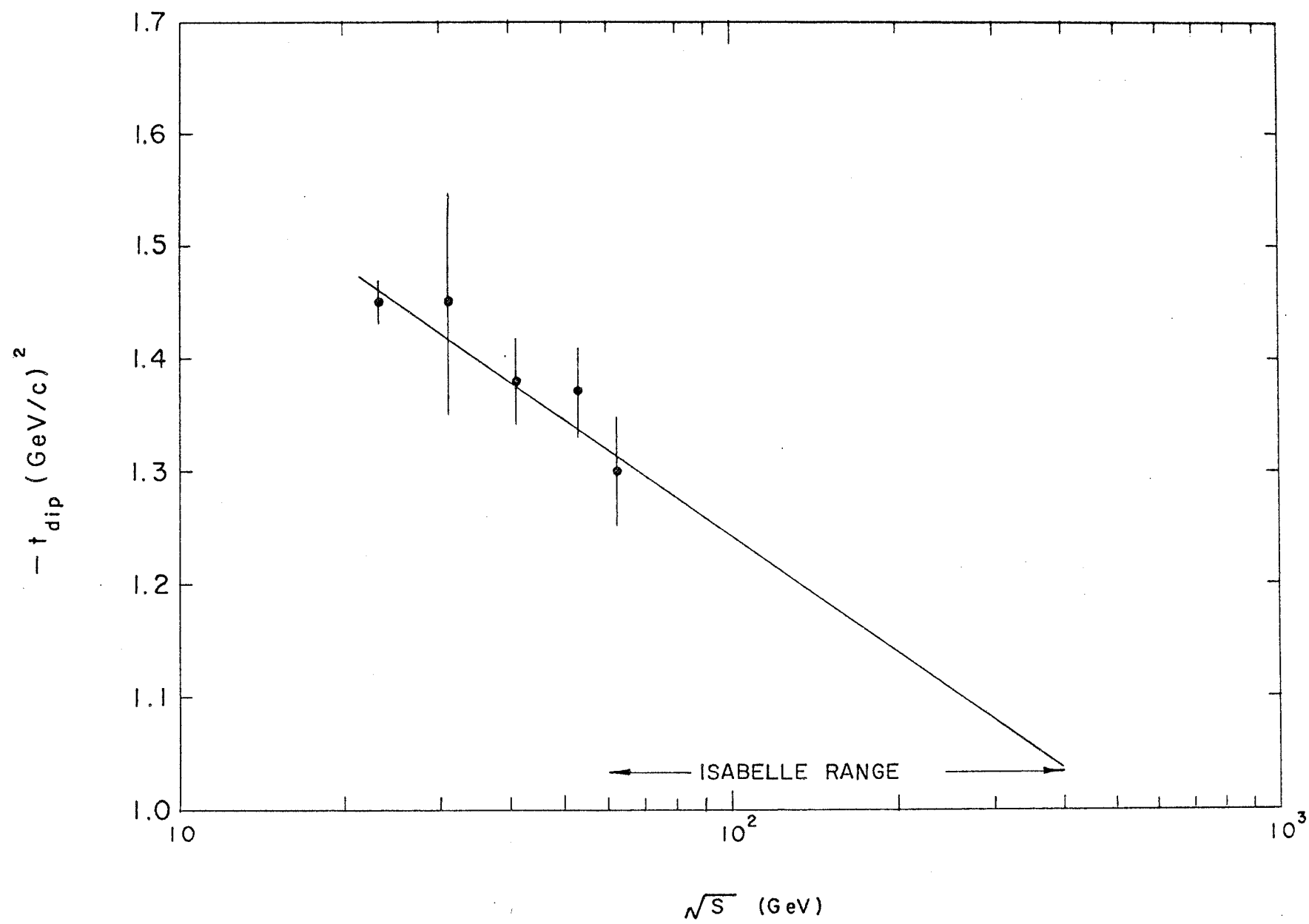
FIGURE 28 (a)

FIGURE 28 (b)

FIGURE 29

FIGURE 30

FIGURE 31

$\theta = 90°$

$$\left[E\frac{d^3\sigma}{dp^3}(\bar{p}p \to \pi) - E\frac{d^3\sigma}{dp^3}(pp \to \pi) \right] / E\frac{d^3\sigma}{dp^3}(pp \to \pi)$$
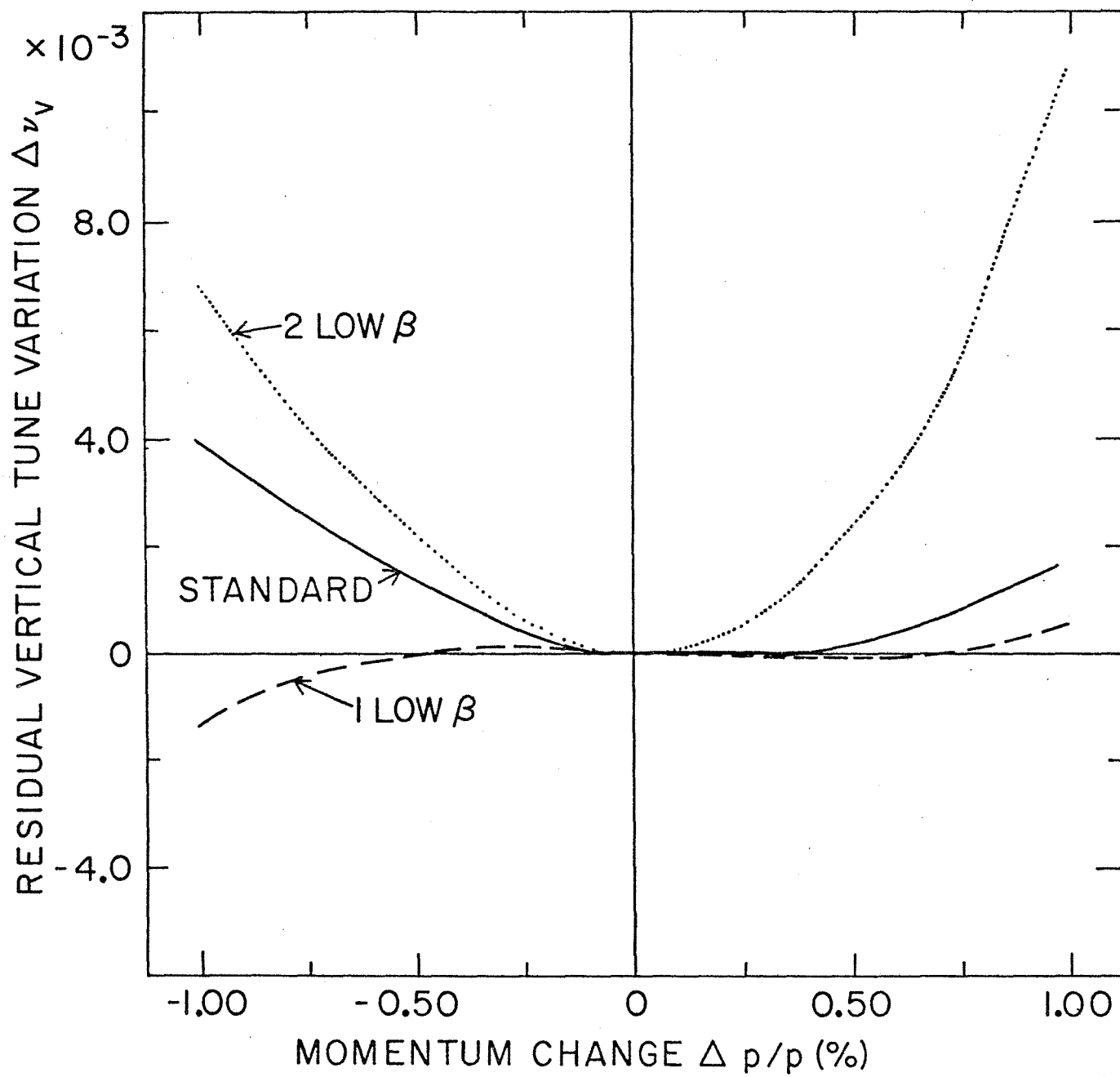
$x_\perp$
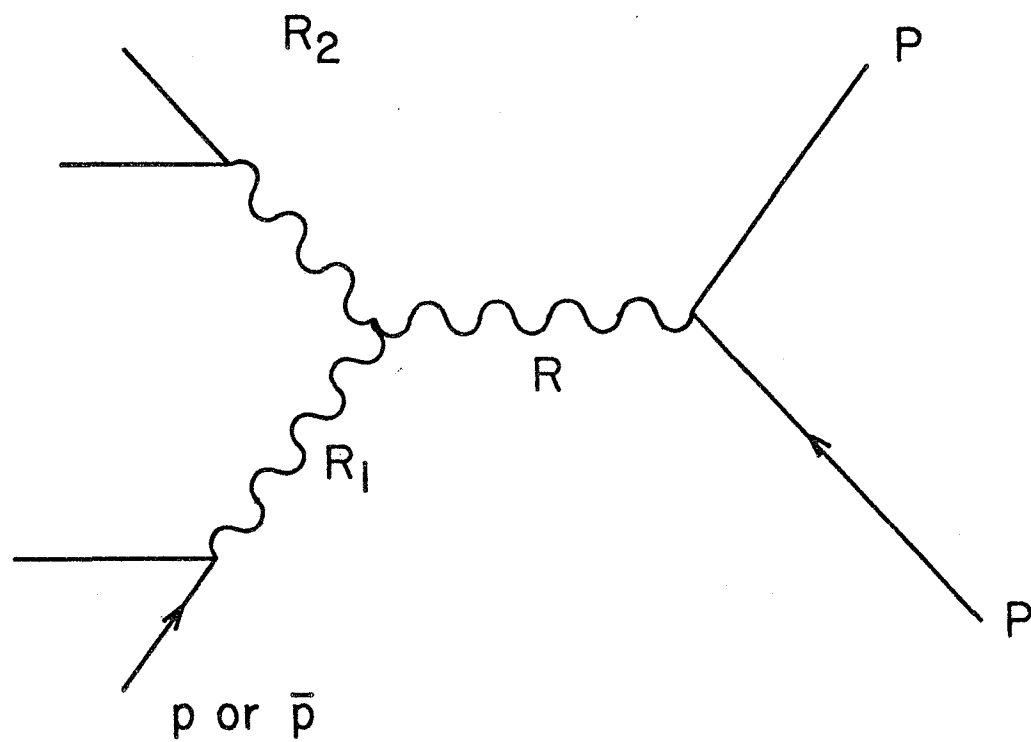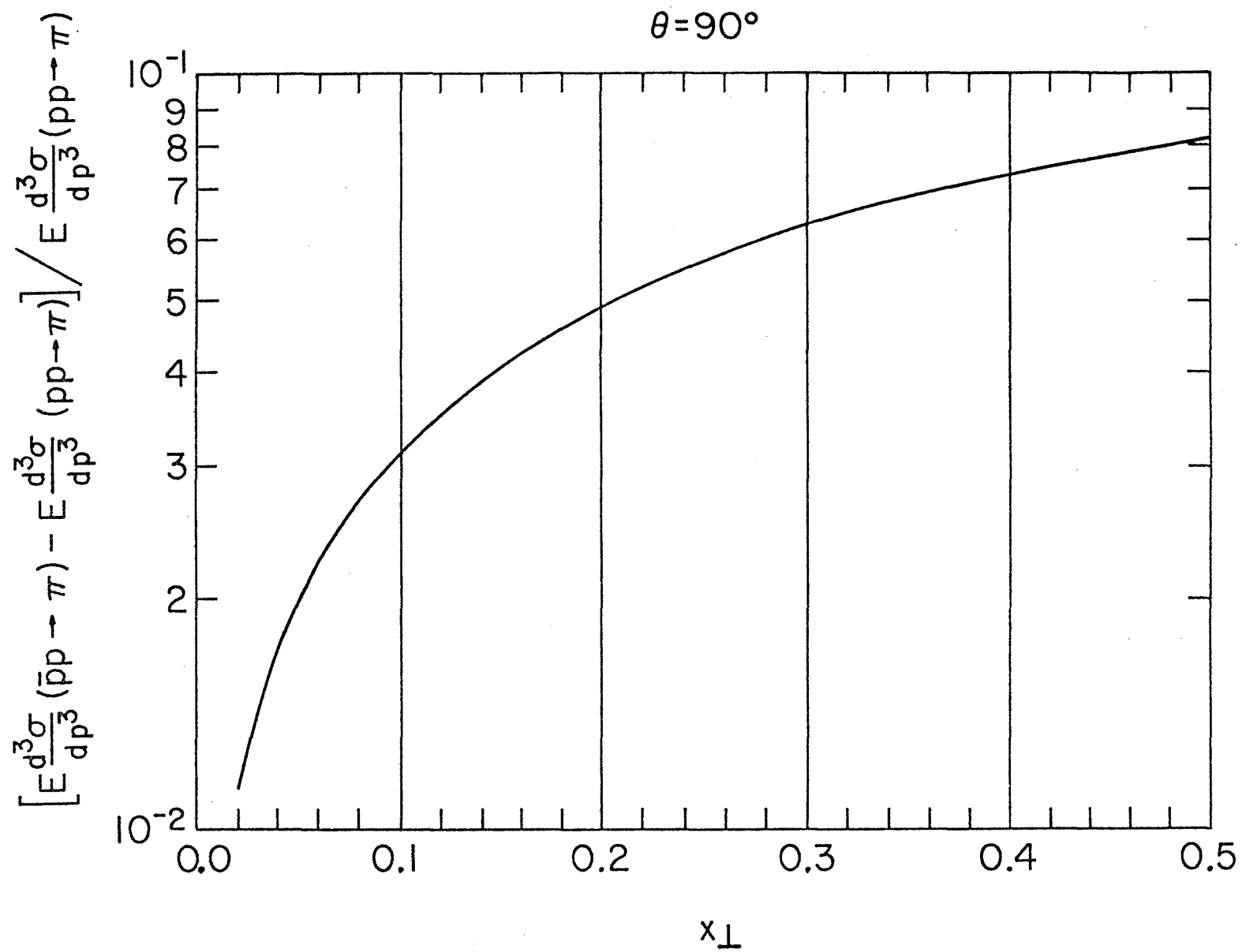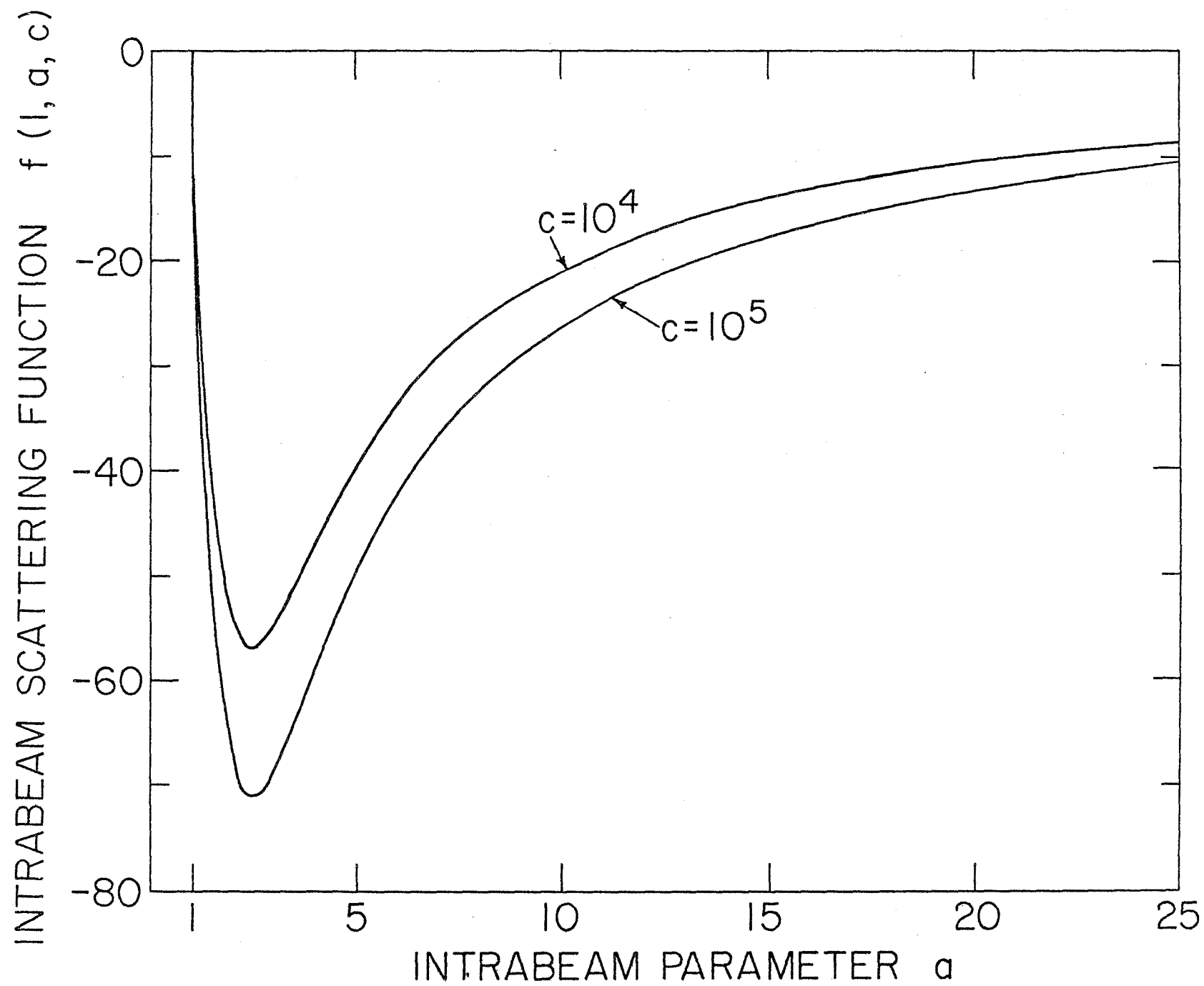
FIGURE 32

FIGURE 33

FIGURE 34

FIGURE 35

FIGURE 36